PEPPER-DERIVED PHYTOCHEMICALS MODULATE METASTATIC PROCESSES IN TRIPLE-NEGATIVE BREAST CANCER CELLS: A NANOPARTICLE-BASED DELIVERY APPROACH

By

Mohammad Javad Ghassemi Rad

Submitted in partial fulfillment of the requirements
for the degree of Master of Science

at

Dalhousie University
Halifax, Nova Scotia
May 2017

For my amazing parents Sedighe and Reza

“If you’re walking down the right path and you’re willing to keep walking, eventually you’ll make progress”

Barack Obama

Table of Contents

List of Tables

List of Figures

Abstract

Metastasis and disease relapse are the primary determinant of cancer prognosis. The process of epithelial to mesenchymal transition (EMT) plays a crucial role in the induction of metastasis. Novel therapeutics are urgently needed to decrease breast cancer mortality by preventing epithelial-to-mesenchymal transition (EMT)-associated metastasis. Transcription factors such as β-catenin, ZEB1, and Slug, along with epigenetic machinery including histone deacetylases (HDAC) and DNA methyltransferases (DNMT) are well-studied regulators of EMT. Piperine (PIP) and piperlongumine (PL), major alkaloids in pepper spices, inhibit breast cancer cell growth in vivo and in vitro; however, their lipophilicity has restricted possible clinical application. The purpose of this study was to increase the water solubility of PIP and PL using nanoparticles (NPs) as drug carrier and investigate the anti-metastatic potential of PIP- and PL-NPs in the context of EMT regulation in triple-negative breast cancer cells. The thin-film hydration method was used to encapsulate PIP and PL into biodegradable methoxy poly(ethylene glycol)-poly(lactic-co-glycolic) acid (mPEG-PLGA) copolymer. Colorimetric MTT and Annexin-V-FLUOS/propidium iodide staining assays were performed on MDA-MB-231 and MDA-MB-468 triple-negative breast cancer cells to determine the effect of PIP- and PL-NPs on cell growth and viability. The invasiveness of MDA-MB-231 cells was also tested in the presence of PL and PL-NPs, using gap closure and trans-well invasion assays. Western blotting and quantitative reverse transcription PCR (qRT-PCR) were used to evaluate the relative expression of EMT markers and associated transcription factors following treatment with PL and PL-NPs. At cytotoxic doses, PIP- and PL-NPs decreased the viability of MDA-MB-231, MDA-MB-468, and BT-549 breast cancer cells to a similar extent as free PIP and PL. Noncytotoxic doses of PL and PL-NPs inhibited breast cancer cell migration and invasion in vitro. Both free PL and PL-NPs inhibited the expression of EMT markers, ZEB1, β-catenin, and Slug, while increasing the expression of E-cadherin and NDRG1, inhibitors of EMT and metastasis, in MDA-MB-231 cells. Furthermore, PL and PL-NPs decreased the expression of HDAC1 and DNMT1, both of which are known transcriptional suppressors of E-cadherin and NDRG1. However, overexpression of HDAC-1 and DNMT-1 did not affect PL-induced E-cadherin expression in these cells. These results demonstrate that PL and PL-NPs inhibit metastatic properties of MDA-MB-231 breast cancer cells through inhibition of EMT-associated transcription factors. Ultimately, these findings indicate the potential use of NPs as phytochemical carriers for future in vivo studies to improve the bioavailability and serum solubility of PIP and PL.

List of Abbreviations and Symbols Used

℃	Degree Celsius
Ab	Antibody
ALDH	Aldehyde dehydrogenase
ANOVA	Analysis of variance
APC	Adenomatous polyposis coli
APS	Ammonium persulfate
ATCC	American Type Culture Collection
bFGF	Basic fibroblast growth factor
BSA	Bovine serum albumin
b.w.	body weight
$CaCl_2$	Calcium chloride
cDMEM	Complete Dulbecco's Modified Eagle Medium
cdk	Cyclin-dependent kinase
ChIP	Chromatin immunoprecipitation
CO_2	Carbon dioxide
C_q	Cycle value
CSC	Cancer stem cell
CYP450	Cytochrome P450
DCM	Dichloromethane
DDT	Dithiothreitol
dH_2O	Distilled water
DISC	Death-inducing signaling complex
DMEM	Dulbecco's Modified Eagle Medium
DMSO	Dimethyl sulfoxide
DNMT	DNA methyltransferase
ECM	Extracellular matrix
EDTA	Ethylene diamine tetraacetic acid
EGCG	Epigallocatechin-3-gallate
EGF	Epidermal growth factor
EGFR	Epidermal growth factor receptor
EGTA	Ethylene glycol tetraacetic acid
EMT	Epithelial-to-mesenchymal transition
EMT-TF	Epithelial-to-mesenchymal transition associated transcription factor
ER	Estrogen receptor
FBS	Fetal bovine serum
FGFR	Fibroblast growth factor receptor
FITC	Fluorescein isothiocyanate
GFP	Green fluorescent protein
GSK-3β	Glycogen synthase kinase-3 beta
HAT	Histone acetyltransferases
HCl	Hydrochloric acid
HDAC	Histone deacetylase
HDF	Human dermal fibroblast
HEPES	N-2-hydroxyethylpiperazine-N-2-ethane sulfonic acid

HER2	Human epidermal growth factor receptor 2
HMEC	Human mammary epithelial cell
HMLER	*Ras*-transformed human mammary epithelial cell
HPLC	High performance liquid chromatography
HRP	Horseradish peroxidase
Ig	Immunoglobulin
IL	Interleukin
LRP5/6	Low-density lipoprotein-related 5/6
MAPK	Mitogen-activated protein kinase
MET	Mesenchymal-to-epithelial transition
miRNA	MicroRNA
MMP	Matrix metalloproteinase
mPEG	Methoxy poly(ethylene glycol)
MTT	(3-(4,5-demethylthiazol-2-yl)-2,5-diphenyltetrazolium bromide)
NaCl	Sodium chloride
NaF	Sodium fluoride
NaOH	Sodium hydroxide
Na_3VO_4	Sodium orthovanadate
NDRG1	N-Myc downstream regulated gene 1
NF-κB	Nuclear factor-kappa B
NICD	Notch intracellular domain
NP	Nanoparticle
n.s.	Not significant
PAO	Phenylarsine oxide
PARP	Poly (ADP-ribose) polymerase
PCL	Poly(ε-caprolactone)
PCR	Polymerase chain reaction
PEG	Poly(ethylene glycol)
PGA	Poly(glycolic acid)
PI	Propidium iodide
PI3K	Phosphatidylinositol 3 kinase
PIP	Piperine
PL	Piperlongumine
PLA	Poly(lactic acid)
PLGA	Poly(lactic-co-glycolic) acid
PMSF	Phenylmethylsulfonyl fluoride
PR	Progesterone receptor
qRT-PCR	Quantitative reverse transcription polymerase chain reaction
rcf	Relative centrifugal force
ROS	Reactive oxygen species
rpm	Revolutions per minute
RTK	Receptor tyrosine kinase
SDS	Sodium dodecyl sulfate
SEM	Standard error of the mean
sf	Serum free
TEM	Transmission electron microscope

TEMED	Tetramethylethelyenediamide
TGF-β	Transforming growth factor-beta
TIMP	Tissue inhibitors of metalloproteinase
TNBC	Triple-negative breast cancer
TNF	Tumor necrosis factor
TSA	Trichostatin A
TTBS	Tween-20 Tris-buffered saline
uPA	Urokinase plasminogen activator
UV	Ultra-violet
v/v	Volume by volume
VEGF	Vascular endothelial growth factor
w/v	Weight by volume

Acknowledgments

I had the incredible opportunity to work with so many great people during my graduate studies. First and foremost, I would like to extend my profound gratitude and appreciation to my supervisor Dr. David W. Hoskin, for his limitless patience, skillful guidance, and encouraging support over the last four years. Thank you for believing in me and providing me with the opportunity to take on a project that may one day save human lives. The knowledge and wisdom you have imparted upon me have been a great help and support throughout my undergraduate and graduate studies, and has inspired me to pursue my goals with hard work and dedication, wherever life takes me. It has been an absolute pleasure studying in your lab during the day and star gazing with you during the night.

I would like to thank my supervisory committee, Dr. Karen Bedard and Dr. Robert Liwski, for their valuable input, great ideas, and numerous suggestions that helped shaping this project. Thank you to the Department of Pathology, and the administrative staff, especially Eileen Kaiser and Christine Anjowski, for their support throughout my graduate study.

My amazing lab members. Thank you for providing a supportive environment to work in, and making the lab like a second family to me. Thank you, Leanne Delaney, for always answering my questions with patients and keeping up with my insane ideas, and always being there for me as my go-to person, inside and outside of the lab. During your time in the lab, you taught me so many techniques and laboratory etiquettes, and for that, I am forever grateful. Amazing Wasundara Fernando, Alicia Malone, and Dr. Anna Greenshields thank you for all your support and keeping up with me all these years. Thank you for making my time in the lab an unforgettable experience with so many amazing memories. A huge thanks to Dr. Carolyn Doucette, Dr. Melanie Power Coombs, Dr. Laurence Madera, Dr. Jordan Warford, Andrea Rasmussen, Joe Loung, Emma MacLean, Allison Knickle, Dan Arsenault, Nathan Ryan, and Jasmine Boudreau, for creating a supportive lab environment and making the lab a great place to be during

happy times and not so happy times. I could not imagine a more supportive team to be a part of. I am deeply indebted to all your help and support.

I would like to thank Dr. Roberto de Antueno for sharing his knowledge of nanoparticles with me, and helping me optimize my nanoparticle formulation method. Thank you to members of Dr. McCormick's lab, especially Eric Pringle, for supporting and training me with the transfection studies. Also thanks to Mary Ann Trevors for taking the time to train me with flow cytometry and transmission electron microscopy. Thanks to Bruce Stewart for training me with using the lyophilizing machine. A shout-out to Jason McConnery for his initial contribution to the nanoparticle formulation protocol.

I huge thanks to the Beatrice Cancer Research Institute, for providing funds and opportunities for me to get training in cancer research. Also, thanks to the Canadian Breast Cancer Foundation (Atlantic Region), and Nova Scotia Graduate Scholarship, for providing funds necessary to make this project possible.

Last, but not least, thank you my amazing parents Sedighe and Reza, and my brothers, Saleh and Sadegh, for your constant support throughout my education, for being always by my side, and for encouraging me to continue to pursue my dreams. To my parents, thank you for believing in me and supporting me all the way. No words can express my heartfelt appreciation for everything that you have done and gone through to help us make a better future.

CHAPTER 1

INTRODUCTION

1.1 Cancer

Cancer is a collection of diseases arising from dynamic genomic changes that grant normal cells the ability to divide uncontrollably, and the potential to invade and spread to other parts of the body. Due to its complexity, cancer is a very difficult disease to treat and cure. It is estimated that about half of all Canadians will be diagnosed with cancer in their life-time and about one-quarter will succumb to the disease (1). Major types of cancers include lung, female breast, colorectal, and prostate (1, 2). Decades of research have improved our understanding of tumor biology, diagnostic strategies, and treatment capabilities, but to this day, cancer remains one of the leading causes of death in Canada (1). Cancer also poses a major burden to the Canadian economy with about $4.4 million cost to the healthcare system, which includes both the direct costs of hospitals, drugs, and physicians, as well as indirect cost due to loss of productivity (1). Cancer research in Canada and around the world has thus far created a complex body of scientific literature surrounding the disease. The process of translating this knowledge into patient care has been slow, but significant progress has been made in improving survival rates since the 1940s. Research shows that the complex heterogeneous nature of cancer requires the manifestation of several key essential alterations in cell physiology for malignant growth. In an effort to shed light on these essential alterations, Hanahan and Weinberg proposed the hallmarks of cancer as: sustaining proliferative signaling, replicating with limitless potential, evading growth suppressors, resisting cell death, inducing angiogenesis, deregulating cellular energetics, avoiding immune destruction, and activating invasion and metastasis (3, 4). Continued basic and clinical research will eventually resolve the complex biology of cancer, and further improve the survival and quality of life of cancer patients.

1.2 Breast Cancer

Breast cancer is the most common type of cancer diagnosed among women (2). Every year in Canada, about 2,500 new cases of breast cancer are diagnosed and about 5000 women will die from this disease (1). Breast cancers can arise from milk-producing lobules (lobular carcinoma) or from milk ducts (ductal carcinoma). Invasive ductal carcinoma, the most common type of breast cancer, as well as invasive lobular carcinoma, have the potential to invade the surrounding tissue and lymph nodes, and metastasize to distant organs (5). There are also other histological types of breast cancer described by the World Health Organization, but their prevalence is very low (5, 6).

Breast cancer is also a complex heterogeneous disease exhibiting different rates of incidence, survival and response to treatment. Treatment options include surgery, radiation therapy, chemotherapy, and some targeted therapies. Type of treatment depends on different clinical parameters such as tumor size, histological grade, lymph node involvement, and expression of estrogen receptor (ER), progesterone receptor (PR), and human epidermal growth factor receptor-2 (EGFR; HER2) biomarkers (7, 8).

The turning point in breast cancer research and treatment started with the identification of major molecular subtypes of breast cancer cells based on their distinct genomic signature (Table 1.1). Using cDNA microarray analysis, the laboratory of Perou and Sørlie classified gene expression characteristics of breast cancers from 38 patients into five distinct molecular subgroups: luminal A, luminal B, HER2-enriched, normal-like, and basal-like (9–11). This classification was later found to be a major predictor of response to treatment in breast cancer patients (10, 11). Luminal subtypes are cancers that express high levels of ER and PR, HER2 enriched overexpress HER2 while lacking ER/PR expression, and basal-like breast cancer lacks the expression of ER, PR and HER2, and are considered triple-negative breast cancer (TNBC) (7, 11). More recently, a new distinct molecular subtype of breast cancer cells was identified with characteristic low expression of tight junction and intercellular adhesion molecules like claudin-3, -4, -7, occludin and E-cadherin (12). This group of breast tumors are called claudin-low, despite their lack of ER/PR/HER2 expression and striking resemblance to basal-like breast cancer (12, 13).

1.2.1 Triple-Negative Breast Cancer (TNBC)

TNBC tumors cells make up about 20% of all breast cancer cases and are usually invasive ductal carcinoma in nature, with appearance at early age, especially in women of African origin and/or with BRCA1 mutations (11, 14, 15). Patients with these types of cancers do not benefit from targeted hormonal and antibody-mediated therapies like tamoxifen and trastuzumab, since these tumors lack the expression of ER, PR and HER2 (9, 16). Therefore, lack of targeted therapy along with the aggressive nature of TNBC tumors due to high chance of lymph node involvement, high rates of metastasis, high tumor grade and size at the time of diagnosis, and high rates of relapse, renders TNBC with the worst prognosis (17). These cancers, however, have a better response rate to chemotherapy if detected early, compared to ER-positive tumors (18).

Standard chemotherapy administered to TNBC patients includes doxorubicin, docetaxel and paclitaxel (19), sometimes combined with platinum DNA-damaging agents, like cisplatin and carboplatin, for added benefits (20). However, conventional chemotherapy is associated with severe side effects due to lack of selectivity toward malignant cells. Better treatment options are urgently needed to improve the survival and quality of life of TNBC patients.

Several attempts in generating targeted therapies against TNBC have shown minimal success at a clinical level. Given that most of TNBCs are BRCA1-deficient, it has been suggested that inhibition of poly (ADP-ribose) polymerase (PARP), which is a base excision DNA repair enzyme, would impair single-strand DNA repair in these tumors and renders them more susceptible to chemotherapy (21). Iniparib, a potent PARP inhibitor, has been tested in phase II and phase III clinical studies for patients with metastatic TNBC, in combination with gemcitabine and carboplatin (22, 23). However, the overall survival of patients was not improved compared to gemcitabine and carboplatin treatment (23). Other targeted therapeutics like the use of fibroblast growth factor receptor (FGFR) inhibitor in FGFR-amplified TNBC cells have shown some success in pre-clinical studies (24). In addition, monoclonal antibodies that target vascular endothelial growth factor (VEGF), and tyrosine kinase inhibitors against VEGF receptors are at early stages of clinical trial for inhibiting angiogenesis and metastasis of TNBC tumors (25). Ultimately, a combinational therapeutic approach that includes both

chemotherapy and targeted therapy will probably improve the outcome for TNBC patients.

Another factor that contributes to the aggressive phenotype and poor prognosis associated with TNBC is the high rate of p53 mutation seen in these tumors. In their earlier work, Sørlie and colleagues (2001) found that 82% of basal-like tumors had mutations in the p53 gene, compared to 71% of HER2-positive and 13% of luminal A tumors (10). p53 is a tumor suppressor that prevents cell cycle progression and promotes apoptotic cell death in response to stress signals like genotoxic damage, reactivation of oncogenes, loss of intercellular contact, and hypoxia, therefore preventing the malignant progression of cells (26). Recently, several studies have tried to use the p53 status of TNBC as a targetable approach for this form of breast cancer. Using small molecules library screening, PRIMA-1 was identified as an activator of mutant p53 function (27). PIRMA-1 restored mutant p53 DNA binding ability, expression of p53 target genes like MDM-2 and p21, as well as p53-dependent apoptosis in a variety of human tumors, including TNBC (27, 28). A methylated derivative of PRIMA-1 with stronger apoptosis-inducing effect has been tested in a phase I clinical trial for patients with hematological malignancies or prostate tumors with minimal side effects (29). p53 upregulates the expression of pro-apoptotic proteins like Bax and PUMA (30, 31), and inhibits anti-apoptotic B-cell lymphoma-2 (Bcl-2) protein (32), which stimulate the release of mitochondrial cytochrome c that initiates apoptosis.

1.2.2 Cancer Cell Death (Apoptosis and Necrosis)

Intrinsic to all cells is the process of programmed cell death that is activated to eradicate damaged or unhealthy cells. On the other hand, acquiring abilities to avoid cell death is an essential hallmark for all types of cancers (3, 4). Therefore, the ultimate goal of cancer therapy is to induce cancer cell death while sparing the normal cells.

First described by Kerr and colleagues in 1972, apoptosis is a form of programmed cell death that is distinct from necrotic cell death and acts as a barrier to cancer development (33). The process of apoptosis is characterized by cellular shrinkage, DNA fragmentation and condensation, membrane blebbing, and separation of cellular components into apoptotic bodies (33). Transfer of phosphatidylserine from the inner

leaflet to the other leaflet of plasma membrane was later identified as a way of removing apoptotic bodies by the phagocytes (34, 35). Intracellular signals that result from DNA damage, oncogene activation, hypoxia, or lack of survival signal, and extracellular signals including the binding of tumor necrosis factor (TNF) superfamily ligands to death receptors result in activation of death-inducing caspases through intrinsic and extrinsic pathways, respectively (36, 37).

The external death signals are mediated through binding of the TNF superfamily ligands to their respective receptors leading to the assembly of death-inducing signaling complex (DISC), which then activates caspase-8 (37, 38). Activated caspase-8 relays the death signal to caspases-3, -6, and -7, either directly, or indirectly through activation of Bid, Bak, and Bax, which facilitate the release of mitochondrial cytochrome c by permeabilizing the mitochondrial outer membrane (37–39). Similarly, the intrinsic stimuli described above also leads to mitochondrial outer membrane permeabilization and the release of cytochrome c (40), which forms the apoptosome via Apaf-1 and caspase-9 that will eventually activate caspases-3, -6, and -7 (37, 41). Caspases-3, -6, and -7 are apoptosis executioners that dismantle the cell through degradation of cellular components (37, 38).

Contrary to the regulated nature of apoptosis, necrosis is believed to be poorly regulated. Necrosis results from physical and/or chemical insults to the cells that lead to immediate permeabilization of the plasma membrane, swelling and rupture of the cell, and degradation of cellular components using lysosomal acid hydrolases (37, 42). Recently, a programmed version of necrosis, necroptosis, was discovered that involves activation of receptor-interacting protein kinase-1 and -3, and inhibition of apoptosis using cellular inhibitors of apoptosis (cIAP1 and cIAP2) (42). Necroptosis, serve as suitable target to destroy apoptosis-deficient cancers.

Several mechanisms that would allow cancer cells to mitigate apoptosis include upregulation of anti-apoptotic protein Bcl-2 (43–45), mutations in the apoptotic regulator p53 (26, 46), downregulation or mutation of pro-apoptotic proteins like Bak, Bax, and caspases (47, 48), as well as interruption of death signaling circuitry (49). Therapeutic targeting of the cell death pathway is currently being evaluated in clinical trials for effective killing of cancer cells. The use of Bcl-2 mimetics, which antagonize Bcl-2,

shows promising results in hematological malignancies, as well as lung and breast tumors (50, 51).

Today, several different therapeutics are available for breast cancer patients, and together, with early detection capabilities, like mammography; and gene signature diagnostic platforms, like OncotypeDX® and intrinsic subtyping to determine the best course of treatment; the mortality of breast cancer patients has reduced by 44%, and the five-year survival rate has increased to 87% (1). Yet, despite these latest developments, breast cancer remains as the second leading cause of cancer-related deaths among Canadian women (1). About 30% of women who are diagnosed with early stage breast cancer will go on to develop metastatic disease (52). As mentioned earlier, TNBC is associates with higher rates of metastasis within 5 years of diagnosis and lower survival, compared to other forms of breast cancer (17, 52). Conventional therapy fails to prevent metastasis and metastatic cancer remains incurable. Treatments are only used to control the disease, extend the period of good quality life, and alleviate the pain as the patients' remaining days are numbered.

1.3 Molecular Mechanism of Breast Cancer Metastasis

One of the hallmarks of cancer, proposed by Hanahan and Weinberg in 2000, is the ability of cancer cells to invade adjacent tissue and metastasize into distant organs (3). Despite advances in treatment strategies and early detection capabilities, metastases remain as the primary cause of cancer-related deaths in the world (53). Metastasis is a complex multi-step process involving genetic and/or epigenetic alterations that allow individual cancer cells to leave the primary tumor site, degrade and migrate through the extracellular matrix (ECM), intravasate into nearby blood and lymphatic vessels, then leave the circulation into the parenchyma of distant tissue to form a metastatic lesion, and finally colonize at the new metastatic site (54). Breast cancer primarily metastasizes to bone, brain, lung, and liver (52). While the anatomical architecture of blood flow between primary and secondary tumor sites may play a role in metastasis, in breast cancer expression of certain genes as well as the organ-specific microenvironment dictate the site of metastatic colonization (55).

The role of the microenvironment and stromal cells in modulating the ECM and assisting cancer cells with metastasis from primary site to distant secondary sites is well established (56). Tumor stroma may include fibroblasts, myofibroblasts, endothelial cells, adipocytes, mesenchymal stem cells, and immune cells like macrophages, neutrophils, and mast cells (57). The first step to metastasis is the formation of new blood vessels (angiogenesis). Due to dysregulated nature of tumor growth, solid tumors experience significant oxygen deprivation or hypoxia (58). As a result, tumor cells and the surrounding stromal cells secrete inflammatory and pro-angiogenic cytokines, such as TNF-α, VEGF, basic fibroblast growth factor (bFGF), and interleukin-8 (IL-8) (58, 59). The in-depth contribution of each type of stromal cell to angiogenesis is beyond the scope of this review; however, factors produced by these cells will induce proliferation, migration, and assembly of endothelial cells through autocrine and paracrine routes. Matrix metalloproteinases (MMPs), serine proteases like urokinase plasminogen activator (uPA)/plasmin, and cysteine proteases like cathepsins produced by the endothelial cells and cancer cells will begin degrading and remodeling the ECM to allow for the migration of endothelial cells and the formation of new blood vessels (58, 60, 61). Breast cancer is associated with high levels of VEGF expression, which acts in an autocrine fashion and increases the invasiveness and migration of tumor cells through activation of receptor tyrosine kinase (RTK) phosphatidylinositol 3 kinase (PI3K)/Akt signaling (62, 63). In contrast to blood vessel formation in normal tissue, tumor vasculature is often deformed and leaky due to the unregulated process of tumor angiogenesis (55, 58). However, tumor vasculature provides cancer cells with nutrients and facilitates their intravasation during metastasis.

The dissemination of cancer cells from primary tumor requires the loss of contact with basement membrane, as well as loss of cell-to-cell adhesion. Epithelial cell connections to the components of the basement membrane and ECM are largely mediated through α- and β- chains of integrins (64), while intercellular adhesion interactions include cadherins associated with cytosolic α-, β-, γ-catenins, and actin cytoskeleton (65). Altered expression of integrins and integrin-mediated intracellular signaling for proliferation, separation from the basement membrane, and migration within the ECM are common features of most cancers (58).

Altered expression of cadherins and catenins is also essential to cancer progression. Normally, inappropriate or loss of cell-to-cell adhesion activate anoikis, which is a specialized type of apoptosis (66). Consequently, suppression of anoikis is a prerequisite to successful metastatic dissemination of cancer cells. Loss of E-cadherin is associated with the metastatic phenotype in a variety of cancers including breast, lung, gastric, pancreatic, kidney and prostate (58). In fact, Onder and colleagues (2008) showed that loss of E-cadherin results in the induction of anoikis resistance, invasiveness, and a metastatic phenotype in breast cancer (67). Meanwhile, upregulation of N-cadherin is associated with increased invasiveness and migration of breast cancer cells (68, 69). Reduction or loss of E-cadherin expression is mediated through somatic mutation (70), proteolytic cleavage (71), and/or silencing of the E-cadherin (*CDH1*) promoter via epigenetic modification (70, 72–75). Loss of E-cadherin and gain of N-cadherin, a process known as cadherin switch, can be mediated by transcription factors such as Slug, Snail, Twist, and ZEB1 (76, 77). These transcription factors are part of a broader process known as epithelial-to-mesenchymal transition (EMT), which is described in more detail in section 1.4.

The local invasion of metastatic tumor cells also requires the loss of basement membrane and ECM. Several classes of proteases involved in degrading basement membrane and ECM include MMPs, uPA/plasmin, and cathepsins (58, 61, 78). MMPs constitute the principle proteases involved in remodeling basement membrane and ECM during invasion and metastasis. MMPs such as MMP-1, MMP-2, MMP-3, MMP-9, and MMP-13 are involved in metastatic progression of breast cancer (79, 80).

1.3.1 MMPs in Breast Cancer Progression and Metastasis

MMPs are a family of 23 zinc-dependent endopeptidases, whose primary function is to degrade various components of the ECM (81). Based on their specificity, MMPs can target collagen (collagenases), gelatin (gelatinases), or a broad spectrum of ECM proteins (stromelysins) (81). In addition, membrane-type MMPs possess a transmembrane domain, and function as an activator of gelatinases and fibrinolytic enzymes (82). The substrate-binding domain and the catalytic domain of MMPs can be inhibited by tissue inhibitors of metalloproteinases (TIMPs) (83), as well as by small molecules and

synthetic pharmacological inhibitors (84). Apart from their ECM-degrading properties, MMPs can also affect cell migration, proliferation, differentiation, apoptosis, and angiogenesis (83). As mentioned earlier, cancer cells rely on the matrix-degrading properties of MMPs to successfully execute invasion and metastasis.

Like many other MMPs, MMP-1 expression is induced in response to inflammatory cytokines, such as TNF and IL-2, through the mitogen-activated protein kinase (MAPK) or nuclear factor-kappa B (NF-κB) signaling pathways (85). MMP-1 is activated by MMP-3 (stromelysin-1) prior to cleaving a broad range of matrix proteins that includes, but is not limited to, collagen type I and fibronectin (83, 85). MMP-1 derived from fibroblasts increases the migration and invasiveness of breast carcinoma cells, in vitro and in vivo (86). Higher levels of MMP-1 and MMP-3 have been observed in metastatic MDA-MB-231 cells compared to less invasive, ER-positive MCF-7 cells (80). Interestingly, knockdown of MMP-1 in MDA-MB-231 TNBC cells impairs their metastatic potential in nude mice (87).

MMP-2 and MMP-9, also known and gelatinase A and gelatinase B, respectively, are able to degrade collagen type IV, a major component of ECM, as well as gelatin (denatured collagen) fibronectin (MMP-2 only), and plasminogen (MMP-9 only) (83). These proteases are largely regulated by the PI3K/Akt signaling pathway (88, 89). High expression of MMP-2 and MMP-9 in murine mammary carcinoma cells is associated with higher rates of invasion in vitro (79). Similarly, MMP-2, MMP-3, and MMP-9 are highly expressed in brain metastases of breast cancer (90). MMP-13 (Collagenase III), also expressed in the presence of inflammatory cytokines and NF-κB signaling (85), is associated with poor prognosis and an invasive phenotype in breast cancer. High expression of MMP-13 is observed in cancer cells and stromal fibroblasts, and is correlated with high levels of lymph node metastasis, as determined by immunohistochemistry (91). Balduyck and colleagues (2000) showed higher expression of MMP-13 in MDA-MB-231 TNBC cells, compared to MCF-7 breast cancer cells (80).

Unlike the other MMPs involved in cancer progression, MMP-3 (stromelysin-1) is the least studied. MMP-3 activates other MMPs such as MMP-1, and MMP-9 (85, 92). Expression of MMP-3 is increased in the presence of matrigel, and this protease is required for matrigel invasion by mammary tumor cells (93). Overexpression of MMP-3

in mouse mammary epithelial cells increases cellular reactive oxygen species (ROS), which in turn results in the expression of Snail, loss of epithelial marker E-cadherin, gain of mesenchymal marker vimentin, and the execution of EMT (94). More importantly, MMP-3 is considered a stromal enzyme in many breast cancers (94), which further highlights the role of the tumor microenvironment in cancer cell plasticity and malignant transformation.

These results confirm the roles of MMP-1, -2, -3, -9, and -13 in breast cancer metastasis and highlight their potential use as prognostic biomarkers. Production of MMPs by both tumor and stromal cells allows for angiogenesis and cancer cell migration. The acquisition of a mesenchymal phenotype by epithelial carcinoma cells characterized by migration and invasiveness is dependent on the process of oncogenic EMT, which is now widely accepted as the mechanism underlying metastasis (95).

1.4 EMT in Cancer Progression and Metastasis

EMT is a natural developmental process that is characterized by the genomic changes that lead to the loss of epithelial phenotype, such as disruption of cell junctions and cell polarity, and the gain of mesenchymal phenotype, such as fibroblast morphology, resistance to apoptosis, and invasive/migratory properties (76, 95, 96). EMT is important during embryonic development and tissue repair, at which time epithelial cells must change their plasticity to a mesenchymal state, migrate, and settle in a new location (95). These mesenchymal cells then serve as progenitors to generate epithelial tissue and new structures via the process of mesenchymal-to-epithelial transition (MET) (95). In cancer, EMT enables carcinoma cells to acquire cellular motility, invade through the underlying ECM, and metastasize to distant organs, where mesenchymal tumor cells would undergo MET to form a carcinoma metastasis that displays the same degree of growth and differentiation as the primary tumor.

Signaling pathways such as transforming growth factor-beta (TGF-β)/Smad and Wnt/β-catenin, as well as a variety of EMT-associated transcription factors (EMT-TFs) such as Snail (*Snail1*), Slug (*Snail2*), Twist1/2, and ZEB1/2 are involved in transcriptional reprogramming during EMT (76, 95). These transcription factors result in the loss of the epithelial marker E-cadherin, which is the hallmark of EMT, and gain of

mesenchymal markers such as N-cadherin, fibronectin, and vimentin, in various human carcinoma cell lines, including immortalized human mammary epithelial cells (HMECs) (76, 97–100). Indeed, expression of these EMT-TFs and mesenchymal markers have been observed in circulating tumor cells of metastatic breast cancer patients (101, 102). Apart from their invasive phenotype, mesenchymal tumor cells expressing EMT-TFs are associated with cancer stem cell (CSCs)-like characteristics such as limitless proliferative potential, self-renewal, differentiation capability, and resistance to chemotherapy and radiation therapy (99, 100, 103).

CSCs, or tumor initiating cells, were initially described in hematological malignancies in 1972, but have recently been identified in solid tumors, including cancers of the breast, colon, skin, lung, head and neck, pancreas, ovarian, and prostate (104). Breast CSCs have a characteristic $CD44^{high}/CD24^{low}$ surface marker expression (105), high aldehyde dehydrogenase (ALDH) activity (106, 107), and mammosphere-forming ability in vitro that is indicative of self-renewal potential (108). Mani and colleagues (2008) found that mesenchymal cells generated from ectopic expression of EMT-TFs, Twist or Snail, in immortalized HMECs, have a $CD44^{high}/CD24^{low}$ surface marker expression and significantly higher mammosphere-forming ability compared to control HMECs (99). Interestingly, expression of ZEB1 is not only essential for the $CD44^{low}$-to$CD44^{high}$ conversion, but is also required for the maintenance of CD44 expression and mammosphere formation by $CD44^{high}$ breast cancer cells (109). Other studies also confirm that the overexpression of EMT-TFs and the induction of EMT are associated with increased stemness, self-renewal, and tumorigenecity in breast (100), ovarian (103), and colorectal cancers (110). Interference with the conversion of non-CSCs to CSCs or elimination of CSCs, which exhibit chemotherapy and radiotherapy resistance, would prevent the relapse of the disease and improve the therapeutic outcome for cancer patients. Therefore, a thorough understanding of the interconnected regulatory networks that are the driving force of EMT during tumor progression and metastasis (Figure 1.1) may allow for the development of effective anti-metastatic therapies.

1.4.1 TGF-β/Smad Pathway Induces EMT in Cancer

TGF-β is a secreted or membrane-bound protein cytokine that plays an essential role during embryogenesis and maintains adult tissue homeostasis (111). TGF-β exerts its cellular effect by binding to the serine/threonine kinase receptor types I and II (TGF-βRI and TGF-βRII), leading to heterotetramerization of the receptor (111–113). Following receptor activation, TGF-βRI is phosphorylated by TGF-βRII, which creates the binding site for the Smad2/3 protein complex (112, 113). Following interaction with Smad4, the Smad2/3/4 complex translocates into nucleus and regulates the transcription of a variety of genes involved in cell proliferation, motility and invasion, and apoptosis through interaction with co-factors and DNA-binding proteins (Figure 1.1) (111). TGF-β also plays a dynamic role during development and progression of cancer.

TGF-β is a multi-functional cytokine that has both positive and negative effects on tumor progression. During early stages of tumor growth, TGF-β acts as a tumor suppressor by inducing growth arrest and apoptosis (113). TGF-βRII inactivation or mutations in Smad3 or Smad4 are known to cause malignant transformation of intestinal neoplasm in adenomatous polyposis coli (APC)-deficient mice (114–116). Similarly, TGF-βRII mRNA is downregulated in E7-induced murine cervical cancer (117), suggesting that TGF-β is important in preventing malignant transformation. Also, TGF-β signaling is found to arrest cell cycle progression through expression of cyclin-dependent kinase (cdk) inhibitors such as p51 and p21, as well as repressing the expression of c-*Myc* oncogene (113, 117). However, tumors may acquire resistance to the tumor suppressive arm of TGF-β as a result of mutations within the TGF-β signaling pathway or downstream cell cycle regulators (111, 118). For instance, stable expression of oncogenic Ki-ras^{G12V} is essential to allow the growth-promoting effect of TGF-β on TGF-β-insensitive HD6-4 colon cancer cells (119). Increasing evidence suggests that TGF-β also acts as a positive regulator of tumor progression. During later stages of tumor growth, TGF-β signaling induces cancer growth and metastasis (76). Up-regulation of TGF-β is associated with poor outcomes in breast, lung, gastric, pancreatic, and hepatocellular cancers (120). TGF-β treatment of invasive MDA-MB-231 human breast carcinoma cells, results in cell proliferation and EMT-like morphological changes (121).

TGF-β is the primary mediator of EMT. Following TGF-β signaling, Smad2/3/4 forms a complex with Snail, which now targets the E-cadherin (*CDH1*) promoter during TGF-β-induced EMT in breast epithelial cells (122). Elevated levels of mesenchymal markers such as N-cadherin and fibronectin, as well as MMP-2 and MMP-9, have been observed in MDA-MB-231 cells following 48 hours of treatment with TGF-β (121). Moreover, transcription of EMT-TFs such as Snail and Slug are upregulated by TGF-β in MDA-MB-231 breast (121) and DLD1 colon (97) adenocarcinoma cells. ZEB1 expression is also increased in the presence of TGF-β in NMuMG mouse mammary epithelial cells and is required for the silencing of E-cadherin expression (123). Increased expression of these transcription factors induces various hallmarks of metastatic cancer, including increased migratory and invasive potential, angiogenesis, chemo/radiotherapy resistance, and anoikis resistance in variety of human tumors (76).

In addition to the canonical TGF-β signaling, which is dependent on Smad proteins, the non-canonical pathway (Smad-independent) induces EMT through activation of the RTK-PI3K /Akt pathway (124), which in turn activates the NF-κB pathway (125). Both PI3K/Akt and NF-κB signaling pathways have major roles in inflammation, proliferation, survival, and invasion of cells. PI3K/Akt-mediated expression of Snail and ZEB, and suppression of E-cadherin, is dependent on the p65 subunit of active NF-κB signaling (125). Similarly, constitutive activation of NF-κB in MCF-10A human breast epithelial cells, using stable expression of p65, increases the expression of ZEB, as well as fibronectin and vimentin, while suppressing E-cadherin expression by these cells (126). In contrast, inhibition of NF-κB signaling completely represses TGF-β- and TNF-α-induced EMT in non-small cell lung cancer (127). These findings confirm the dual effect of TGF-β on cancer cells, and demonstrate the complexity of TGF-β signaling and its collaboration with other signaling pathways. Ultimately, the complex nature of TGF-β signaling in promoting EMT and cancer progression requires a cautious approach when TGF-β is used as a therapeutic target.

1.4.2 Regulation of Wnt/β-catenin Signaling in EMT

Like the TGF-β signaling pathway, the Wnt signaling pathway is also essential for embryonic development and tissue homeostasis, and can be activated through both

canonical and non-canonical means. Wnt signaling, first identified in fruit flies, is initiated with the binding of Wnt ligand (there are 19 isoforms in humans) to the frizzled transmembrane receptors and low-density lipoprotein-related 5/6 (LRP5/6) (Figure 1.1) (128).

Activation of the canonical pathway leads to the cytoplasmic stability of a proto-oncogene, β-catenin (128), which is normally associated with E-cadherin at the cell membrane but tightly regulated in the cytoplasm through phosphorylation and ubiquitination by a complex containing APC, axin, glycogen synthase kinase-3 beta (GSK-3β), and casein kinase-1α (CK1a), and subsequent degradation by proteasomes (128). Upon Wnt signaling, GSK-3β is inhibited by disheveled, which prevents the phosphorylation and degradation of β-catenin (128). Stabilized β-catenin translocates into the nucleus and interacts with T-cell factor/lymphocyte enhancer factor and other co-factors to induce the expression of genes associated with cellular proliferation such as *cyclin D1* and *c-Myc*, as well as *VEGF* for controlling blood vessel formation during cancer progression and metastasis (128). Dysregulation of Wnt signaling and the overexpression of Wnt factors is reported in several human malignancies including breast, ovarian, head and neck, and colorectal cancers.

The evidence for the link between the Wnt/β-catenin signaling pathway and the induction of EMT for cancer progression is compelling. A study conducted by Onder and colleagues (2008) revealed that shRNA-mediated loss of E-cadherin expression in *ras*-transformed human mammary epithelial cells (HMLERs) not only induces EMT by up-regulation of mesenchymal markers such as N-cadherin and vimentin, but also increases the nuclear localization of β-catenin (67). Moreover, GSK-3β is mainly unphosphorylated in HMLERs lacking E-cadherin, thereby allowing β-catenin to escape cytoplasmic degradation (67). Alternatively, downregulation of β-catenin decreases the expression of N-cadherin, vimentin, and fibronectin, while promoting a more epithelial phenotype through reduction of motility and invasiveness, as well as increasing the susceptibility to anoikis, in HMLERs (67).

The effect of Wnt/β-catenin pathway on regulation of EMT-TFs has been studied extensively. Current data suggest that Snail is also targeted for proteasomal degradation by GSK-3β through phosphorylation (129). Co-immunoprecipitation data of colorectal

cancer cells indicate that Snail interacts with β-catenin, which further enhances β-catenin-dependent transcription (130). Similarly, loss of E-cadherin and the increased β-catenin stability in HMLERs is associated with up-regulation of Twist (67). In addition, the RTK-PI3K/Akt pathway can also stimulate β-catenin signaling through inhibition of GSK-3β, in response to EGFR signaling, resulting in a synergistic effect on the induction of tumorigenesis (131, 132). It is likely that these pathways activate different target genes that interact cooperatively to promote tumor formation and progression.

Although β-catenin-mediated oncogenesis is primarily caused by activation of canonical Wnt pathway, there is a strong evidence that the non-canonical Wnt pathway is also involved in EMT and cancer progression. Wnt5a, a non-canonical Wnt ligand, signals through activation of protein kinase C (PKC), nuclear factor associated with T-cells (NFAT), and calmodulin-dependent protein kinase II (CamKII) (133, 134). Interestingly, human oral squamous cell carcinomas show increased expression of Wnt5a ligand, which is associated with increased expression of Snail and suppression of E-cadherin in these cell lines (133). In contrast to mammary epithelial and uroepithelial carcinomas, where Wnt5a functions as a tumor suppressor, Wnt5a is a well-established marker of metastatic melanoma (133, 134). However, future studies are needed to further determine the specifics of Wnt5a signaling before using targeted therapy against this ligand.

1.4.3 Role of Notch and Hedgehog Pathways in EMT

Similar to the other EMT-inducing pathways mentioned above, the Notch pathway is also important in regulating normal cellular processes involved in cell proliferation, survival, and differentiation (135). Recent studies have provided solid evidence for the potential effect of the Notch pathway in the induction of EMT, causing tumor invasiveness and metastasis. In mammals, four receptors (Notch1-4) and five ligands (Jagged1,2 and Delta-like1,3,4) have been identified for the Notch signaling pathway (135). Notch ligands are transmembrane proteins that bind to Notch receptors on adjacent cells. Following this initiation of signaling, the intracellular domain of Notch receptor (NICD) is cleaved by γ-secretase and translocates to the nucleus where it interacts with a variety of other cofactors and transcriptional regulators such as histone transacetylase p300/CBP,

mastermind-like 1, and CSL (135). Although Notch signaling is not sufficient to induce EMT, it enhances transcription of several genes involved in cell cycle, differentiation, and survival.

One of the effects of Notch on EMT is through TGF-β signaling. Inhibition of Notch3 interferes with TGF-β-induced EMT and metastasis of non-small cell lung cancer cells (136). Notch 3 is also responsible for cell invasion and migration, and the expression of IL-6 required for metastasis of non-small cell lung cancer cells to the bone (136). In fact, the contribution of Notch3 to TGF-β-induced EMT is mediated through ZEB1 (136). Another study suggested that Slug (*Snail2*) is the direct target of Jagged1-mediated Notch signaling, resulting in suppression of E-cadherin expression and induction of EMT in MCF-10A (137). Interestingly, Notch-mediated activation of Slug and suppression of E-cadherin leads to Wnt-independent activation and nuclear localization of β-catenin, as well as anoikis resistance in breast cells (137). The Notch pathway is also involved in promoting stemness phenotype in cancer cells, which makes it a promising therapeutic target (135).

Hedgehog signaling pathway is one of the key regulators of embryonic development, organogenesis and maintenance of stem-cell characteristics (76, 138). Binding of Hedgehog ligands (Sonic, Desert, Indian) to the twelve-transmembrane receptor, PTCH1, activates transcription factor GLI-1/-2 to induce expression of Hedgehog target genes (138). Ultimately, mutations that lead to constitutive activation of this pathway result in human malignancies such basal cell carcinoma, medulloblastoma, pancreatic and colorectal cancers (138–140).

The effects of the Hedgehog pathway in human cancers was initially reported as a PTCH1 mutation that resulted in constitutive activation of this receptor in patients with basal cell carcinomas (138). Metastatic pancreatic tissue samples show an upregulation and constitutive activation of GLI-1 compared to primary tumor samples (139). Blocking of the Hedgehog pathway using cyclopamine in pancreatic cancer cells abolishes their metastatic potential through significant downregulation of Snail and E-cadherin mRNA transcripts (139). Constitutively active Hedgehog-GLI-1 pathway and the subsequent induction of EMT and metastasis is also reported in sporadic human colon carcinoma and

colon cancer stem cells (140). These results highlight the induction of EMT following dysregulation of Hedgehog signaling.

Figure 1.1 illustrates a summary of these main signaling events in the induction of EMT. Understanding these signaling pathways that lead to EMT and cancer progression is essential for the development of novel anti-cancer therapies for incurable human malignancies. Currently, small-molecule inhibitors like kinase inhibitors, compounds like metformin and curcumin, as well as microRNA (miRNA)-based therapy like antagomirs, are being evaluated to target key components of the EMT in cancer therapy (141). These therapeutic interventions have shown some promising results in pre-clinical and clinical experiments (141).

1.4.4 Effects of NDRG1 on EMT

N-Myc downstream regulated gene 1 (NDRG1) is a tumor metastasis suppressor, initially identified in colon cancer (142), which is also downregulated in other cancers such as prostate and breast (143, 144). NDRG1 expression is regulated by a variety of stimuli, such as nickel (145), and epigenetic modification, including DNA methylation and histone deacetylation (146, 147). However, as suggested by the name, NDRG1 is primarily regulated by oncogenes, N-Myc, and c-Myc (148), which are transcriptional targets of Wnt/β-catenin pathway; hence, NDRG1 could be linked to the Wnt/β-catenin pathway and EMT.

To identify the link between NDRG1 and the Wnt pathway, Liu and colleagues (2012) took advantage of the yeast two-hybrid screening of a normal human prostate cDNA library and found a strong interaction between NDRG1 and the Wnt co-receptor LRP6 (149). Overexpression of NDRG1 in prostate and breast cancer cells prevents Wnt signaling by inhibiting LRP6 and disheveled, which reactivates GSK-3β, and blocks β-catenin translocation into nucleus (Figure 1.1) (149). Similarly, overexpression of NDRG1 inhibits TGF-β-induced EMT in colon and prostate cancer cells (150). NDRG1 significantly reduces the protein levels of Smad2 and phosphoSmad3 (Figure 1.1) (150). Interestingly, depletion of iron using iron chelator, Dp44mT, is shown to re-express NDRG1 through mechanisms are that not fully elucidated, and attenuate Wnt and TGF-β

signaling in prostate colon and breast cancer cells (149, 150). These findings could have huge implications for the therapeutic intervention of EMT.

1.4.5 EMT-independent Regulation of Metastasis

Despite the compelling evidence for the involvement of EMT in tumor progression, there is still debate about the relevance of EMT in cancer cell invasion and metastasis. The argument is that the majority of studies on EMT are based on in vitro experiments with limited clinical significance, which not only fails to resemble the three-dimensional tumor growth in situ, but also does not take into account the effects of the tumor microenvironment. The challenge associated with studying EMT in vivo is that both the primary and the secondary tumors are epithelial in nature and at the same differentiation state (53). Recently, two research groups sought to examines the role of EMT on metastasis in vivo, using genetically engineered mouse models of breast and pancreatic cancers (151, 152).

In one of the studies, Zheng and colleagues (2015) used a transgenic mouse model bearing genetic deletions in *Snail1* or *Twist1* genes and spontaneous pancreatic cancer (151). As expected, loss of Snail and Twist increased E-cadherin expression in cancer cells while decreasing the expression of ZEB and Slug. Surprisingly, tumor burden and the number of circulating tumor cells was not affected by the absence of EMT, compared to the control mice. In fact, a similar frequency of liver, lung, and spleen metastases was observed in EMT-suppressed and EMT-positive pancreatic tumor-bearing mice. When tumors were treated with gemcitabine, however, absence of EMT rendered these cells more susceptible to chemotherapy. In the second study, Frischer and colleagues (2015), designed a Cre-mediated switch strategy that would allow for the formation of green fluorescent protein (GFP) upon expression of fibroblast specific protein 1 or vimentin, two critical EMT markers, in mouse models of metastatic breast cancers (152). Lung metastases of these animals lacked the expression of GFP; however, when these tumors were treated with cyclophosphamide, GFP-negative cells died by apoptosis whereas GFP-positive cells remained relatively resistant to chemotherapy. These results imply that while EMT is essential for chemotherapy resistance, it is not required for the process of metastasis.

Despite their brilliant study design, these authors did not consider the complexity of EMT, which involves multiple signaling molecules and transcription factors, and mechanisms of action that are not yet fully elucidated. Cancer cells must accumulate multiple genetic and epigenetic changes for each step of the EMT. Apart from these two studies, the evidence for the role of EMT in cancer metastasis found in in vitro studies, in vivo mouse models of human cancers, and circulating tumor cells of cancer patients are compelling (53, 101, 102, 153). Therefore, it is critical to continue investigate the role of EMT in metastatic diseases, and develop new therapeutics that target cellular processes essential to metastasis and drug resistance. Ultimately, factors such as intratumoral heterogeneity, as well as complexity and redundancy that exist within EMT must be considered when studying this process in vivo (153).

1.5 Epigenetics

Epigenetics involves the cellular and physiological traits that are not caused by changes in the DNA sequence. Instead, DNA methylation, histone tail modification, chromatin remodeling, and miRNA-mediated multi-gene silencing are the driving forces of epigenetics (154). Global DNA hypomethylation, which leads to activation of silent genomic regions, as well as promoter hypermethylation of tumor suppressor genes are prevalent initiators of carcinogenesis (154). The growing interest in studying epigenetics is due to the reversibility of the changes in gene expression that can occur without any alterations in genomic sequences, which can be restored to a normal state using epigenetic therapeutics. Ultimately, targeting the major epigenetic modifiers might be promising for cancer prevention and therapy.

Among these epigenetic modifications, DNA methylation is done by DNA methyl-transferases (DNMT-1, -3A, and -3B) that result in transcriptional silencing the tumor suppressors (155). DNA methylation occurs at CpG islands, found primarily in or near the promoter regions of the genes, where a methyl group, donated by S-adenosyl methionine, is covalently linked to the cysteine ring (154–156). DNMT-1 is used for maintenance of the methylation while DNMT-3A and -3B are used as *de novo* enzymes to establish new methylation patterns (154). In a normal cell, most CpG sites, especially those present in DNA transposable elements and the non-coding regions of DNA, are

methylated to prevent genomic instability. However, depending on the type of cell and tissue, the majority of CpG islands of promoters are hypomethylated to allow access of the transcriptional machinery (154, 157). Malignant transformation involves global DNA hypomethylation, which allows for genomic instability that is essential for tumor development and growth, and hypermethylation of promoter regions of genes that are barriers to unlimited growth (154, 157). Cancer cells rely on both DNMT-1 and DNMT-3B for maintenance of their methylation status (158). Unfortunately, the mechanisms that fuel the aberrant DNA methylation patterns in cancer are largely unknown. Along with DNA methylation, post-translational modification of histone N-terminal tails using methylation, acetylation, ubiquitination, sumoylation, and phosphorylation can alter the transcriptional landscape of the genome (154). Histone deacetylases (HDACs) remove the acetyl groups from lysine residues of histone proteins to induce chromatin compaction and reduce the accessibility of transcriptional machinery (154). On contrast, the acetylation of histone H3 on lysine 4, 36, and 79, and histone H4 on lysine 20 residue by histone acetyltransferases (HATs) results in abundance of euchromatin and transcription activation (154). The effects of histone methylation however, depend on the site of methylation. Mono-, di-, or tri-methylation of histone H3 on lysine 9 and 27 (H3K9me3; H3K27me3) results in transcription repression, while methylation of lysine 4 on histone H3 (H3K4me3) allows for activation of transcription (154). Other histone modifications are associated with a more dynamic effect and are far less studied (159).

As mentioned earlier, aberrant DNA methylation patterns can lead to genomic instability and tumorigenesis. For instance, exposure of mouse skin to ultra-violet (UV) B radiation results in increased DNMT activity, along with hypermethylation and transcriptional inactivation of tumor suppressor genes (160). Furthermore, histone deacetylation also affects the expression of numerous genes involved in cancer initiation and metastasis. Overexpression of HDAC-1 and HDAC-2 is associated with decreased expression of anti-proliferative p21 in prostate, gastric, colorectal, and cervical tumors (161). HDAC inhibition in TNBC cell lines, significantly reduces their proliferation and survival in vitro, and their tumorigenesis in vivo (162).

1.5.1 Epigenetic Regulation of EMT and Metastasis

Several studies have explored the links between EMT and the chromatin remodeling in metastasis. As mentioned earlier, downregulation of E-cadherin, directly mediated by EMT-TFs, is the key event in activation of EMT program. Snail-mediated repression of E-cadherin is reversed in the presence of the HDAC inhibitor, trichostatin A (TSA) (74). In fact, chromatin immunoprecipitation (ChIP) assay reveals that TSA treatment results in a strong increase in histone acetylation of the E-cadherin promoter (74). More importantly, in vivo results confirm that Snail interacts with the E-cadherin promoter to recruit HDACs (74). ZEB1 is also implicated in the recruitment of HDAC-1 and HDAC-2 in human pancreatic cancer (75). A similar study also reports the importance of HDAC-1, -6 and -8 for breast cancer cell invasion and migration through the regulation of MMP-9, using MDA-MB-231 and MCF-7 cell lines (163). E-cadherin promoter methylation has also been recognized as part of the epigenetic program that suppresses E-cadherin expression during EMT in invasive breast and prostate cancer cells (72, 164).

Epigenetic regulation of miRNAs, in terms of DNA methylation and histone modification, have gained interest for the study of normal and cancerous cells. Microarrays conducted on cells before and after the induction of EMT have identified the miR200 family of tumor suppressive miRNAs as a inhibitors of EMT (165, 166). In contrast to normal HMECs, in which the promoter sequence CpG islands of miR-200c and miR-141 (miR-200 family members) lack methylation, breast cancer cell lines MDA-MB-231, MDA-MB-157 and BT-549, as well as prostate cancer cell line, PC3, show high levels of DNA methylation for both of these miRNAs (167). ChIP assays show that the miR-200c and miR-141 CpG islands of normal HMECs have transcriptionally competent histones (H3K4me3), while the cancer cells have repressive histones (H3K9me2) associated with these miRNAs (167).

Members of the miR-200 family and ZEB1 tightly regulate the expression of each other in a reciprocal manner (168, 169). Induction of miR-200b and miR-200c in MDA-MB-231 and BT-549 TNBC cells results in increased histone acetylation of E-cadherin promoter (166). These effects are the result of transcriptional repression of ZEB1 by miRNAs followed by the disruption of ZEB1-HDAC complex in MDA-MB-231 and BT-549 cells (166). Chaffer and colleagues (2013) suggested that the ZEB1 promoter in

basal-like $CD44^{low}$ breast cancer cells is associated with both permissive (H3K4me3) and suppressive (H3K27me3) histone markers (109). While TGF-β signaling results in a noticeable decrease in repressive (H3K27me3) marker at ZEB1 promoter, the presence of miR-200 family members has the opposite effect in basal-like breast cancer cells (109). These results, along with the importance of miR-200 family in EMT, confirm that epigenetic forces contribute to the phenotypic changes observed in cancer cells.

1.5.2 Targeting Epigenetic Machinery in Cancer Therapy

DNMT inhibitors 5'-azacytidine, and 5'-aza-2'-deoxycitidine, were among the first epigenetic drugs approved by the Food and Drug Administration (FDA) for cancer therapy (154). Both inhibitors are nucleoside analogs which get incorporated into DNA during replication and trap DNMT on the DNA, thereby preventing DNA methylation (170). These DNMT inhibitors are currently being used for the treatment of hematological malignancies (170, 171).

HDAC inhibitors are also well-studied, FDA-approved, anti-cancer treatments. For instance, treatment of leukemia cells with TSA or a DNMT inhibitor show impressive results in halting leukemia progression (172). TSA also results in a synergistic upregulation of ER expression in TNBC cells, when combined with 5'-aza-2'-deoxycytidine (173, 174). Among the approved HDAC inhibitors, valproic acid has shown potent inhibitory effects on cancer cell growth, survival, angiogenesis, and metastasis in a variety of solid and hematological malignancies (175). The use of small-molecule inhibitors that target other members of the epigenetic machinery also holds great promise as a cancer therapeutic (176).

Today, combination therapy is under investigation to lower the emergence of resistance to chemotherapy and improve response rates (170, 171). Unfortunately, a combination of epigenetic drugs may result in functional antagonism or insignificant benefits compared to single therapy (177, 178). Long-term effects of these drugs are also still under investigation. Moreover, in contrast to the hematological tumors, solid tumors seem to have limited response to HDAC inhibitors. Surprisingly, recent data indicates that cancers of the prostate or nasopharynx are more prone to EMT induction following treatment with HDAC or DNMT inhibitors (179–181). Ultimately, a more detailed

understanding of the molecular links between epigenetic regulators and the epithelial-mesenchymal plasticity may reveal new targets for therapeutic interventions. One exciting class of therapeutics with possible effects on the epigenetic modulation, as well as possessing anti-tumorigenesis and anti-metastatic properties are dietary phytochemicals.

1.6 Pepper-derived Phytochemicals: Piperlongumine and Piperine

Natural-source bioactive compounds, known as phytochemicals, have attracted huge research interest over the past few decades, as an alternative therapeutic approach for cancer prevention and treatment. These compounds exhibit a broad range of pharmacological activity, high therapeutic potential, good availability and lower cost, and lower toxicity compared to conventional treatments (182). Historically, phytochemicals have been used as a remedy for a diverse range of diseases, including cancer, without a thorough understanding of their mechanism of action. Various cultures around the world incorporate herbs and spices in their cuisine, not only for their taste, but also for their health-promoting and disease-preventing effects. The antioxidant activity of some of these natural products results in protective effects against cardiovascular diseases, chronic inflammation, and cancer (183–185). Major classes of phytochemicals includes carotenoids, alkaloid/nitrogen-containing, polyphenols/flavonoids, organosulfur compounds, and vitamins (182). Flavonoids such as curcumin from turmeric root (186, 187), resveratrol from the skin of grapes (188–190), and epigallocatechin-3-gallate (EGCG) from green tea (191) are among the most studied phytochemicals for their chemoprevention and anti-cancer properties.

Phytochemicals inhibit the growth and metastatic potential of tumors through inhibition of key signaling pathways such as Wnt/β-catenin, EGFR, JAK-STAT, PI3K/Akt, and NF-κB, involved in cancer cell survival and metastasis, modulation of anti-apoptotic, and pro-apoptotic genes, and regulation of epigenetic machinery (miRNAs, HDACs, HATs, DNMTs) (192, 193). For instance, curcumin inhibits NF-κB signaling and expression of MMP-2 and MMP-9, while increasing the expression of TIMPs; thereby preventing the invasive phenotype of TNBC in vitro and in vivo (183, 194). Similarly, thymoquinone (from black cumin), targets EMT in TNBC and inhibits

the metastasis of xenografted tumors in mice (195). EGCG and resveratrol, can also inhibit metastasis through modulation of HDACs, DNMTs, and oncogenic miRNAs (192, 193).

Most relevant to this project are the nitrogen-containing compounds called alkaloids. Medical used of alkaloid-containing plants dates back several centuries with noteworthy examples of caffeine as a stimulant, and codeine and morphine as analgesic compounds. Well-known examples of this group of compounds with anti-cancer effects are vinca alkaloids. Discovered from the leaves of periwinkle plants in 1950s, the vinca alkaloids vincristine and vinblastin were identified as inhibitors of microtubule-polymerizing agents, and were among the first anti-cancer phytochemicals approved for use in therapy, despite their neurotoxicity (196). A decade later, the discovery of taxanes (paclitaxel, docetaxel), also tubulin modulators, was a major breakthrough in the use phytochemicals in cancer therapy (196). Similarly, pepper-derived alkaloids piperlongumine (PL) and piperine (PIP) (see Figure 1.2 for structures) have shed light on the anti-cancer effects of pepper, which is a spice with universal use in cuisines.

1.6.1 Piperlongumine (PL)

PL is an alkaloid found in the fruits of long pepper plants (*Piper longum*), with a variety of pharmacological activities that include anti-microbial (197), anti-diabetic (198), anti-depressant (199), and anti-atherosclerotic (200) effects. The anti-cancer effects of PL have been studied much more extensively against a variety of human tumors including leukemia, melanoma, colon, breast, lung and prostate (197). PL induces cell cycle arrest and apoptosis in cancer cells through up-regulation of pro-apoptotic proteins (p53, caspase 3, PUMA, Bim), and downregulation anti-apoptotic and cell cycle proteins (Bcl-2, survivin, cyclin D1) (197).

A recent publication by Raj and colleagues (2010) showed that as little as 10 μM of PL selectively reduces the viability of TNBC, ER/PR/HER2-positive breast, pancreatic, ovarian, colon, and lung cancer cells, independent of their p53 status, while leaving normal cells such as human dermal fibroblasts (HDF) and MCF-10A breast epithelial cells unaffected (201). The cytotoxic effects of PL are mediated through direct inhibition of cellular glutathione, and generation of ROS, as these cytotoxic effects are reversible in

the presence of ROS scavenger, N-acetyl-L-cysteine. In fact, ROS generation by PL is only seen in cancer cells and oncogene-transformed cells, but not in normal cells. PL, administered at 2.4 mg/kg body weight (b.w.), also decreases the in vivo growth of cancer in transgenic or xenografted mice. Tumor blood vessel formation and expression of VEGF is also decreased by PL in vivo. Furthermore, hematological and histopathological analysis indicates that PL is not toxic in mice. This study provoked further research on PL to evaluate its anti-cancer mechanism.

Understanding the mechanism by which PL decreases the growth of cancer cells and induces cell-cycle arrest has been a top priority due to its potential clinical application. Earlier studies have shown that PL decreases kinases involved in cell proliferation like cdk2, and the major cell cycle regulator, cyclin D1 (202). Further analysis has revealed that PL has inhibitory effects on PI3K/Akt and NF-κB signaling axes that are crucial to cell proliferation and survival (203–205). Phosphorylation and activation of Akt is significantly inhibited in PL-treated MDA-MB-231 TNBC cells, which is accompanied by a decrease in the expression of cyclin D1 and increase in the expression of p21 (203). The apoptosis-inducing effects of PL could be mediated through autophagy followed by ROS-induced inhibition of Akt signaling (204). Suppression of anti-apoptotic Bcl-2, induction of Bax, and release of mitochondrial cytochrome c followed by the generation of ROS and inhibition of NF-κB (203, 205, 206) could also explain PL-mediated apoptosis. Consistent with these findings, Ginzburg and colleagues (2014) reported that PL-mediated inhibition of NF-κB signaling suppresses the expression of NF-κB target genes IL-6, IL-8, MMP-9 that are essential for invasive phenotype of prostate cancer cells (206). However, the anti-metastatic potential of PL has not been thoroughly investigated.

Despite the potential anti-tumor effects of PL, its use in a clinical setting has been delayed due to limited toxicity and low bioavailability. PL is mainly eliminated through hepatic metabolism by the cytochrome (CY)P450 family of liver enzymes that mediate demethylation, epoxidation, and oxidation, resulting in four different metabolites (207). Inhibition of CYP1A2 enzyme, and its 93% plasma protein-binding ability suggests a low hepatic clearance rate for this phytochemical (207). However, the half-life of PL in mice plasma is 1.6 hours (201), which is strikingly lower than that of vinblastine and

vincristine, which are 7.5 and 14.3 hours, respectively, as measured in rats (208). Higher plasma protein-binding ability could hinder the ability of a drug to exhibit pharmacological activity. Oral administration and intestinal degradation and metabolism, as well as clearance from kidney could also be responsible for low bioavailability of PL. Also, some studies have hinted at a potential genotoxic effect of PL (197) since ROS induced by PL could result in DNA damage, despite lack of obvious clinical complications in mice treated with 2.4 mg/kg b.w. of PL for 6 days (201). Nevertheless, low bioavailability, minor toxicity, and the hydrophobic nature of PL makes it desirable for development of novel drug delivery systems.

1.6.2 Piperine (PIP)

PIP is the principle active component and major alkaloid extracted from black pepper (*Piper nigrum*) and long pepper (209, 210) plants. PIP exhibits a broad range of pharmacological activity, including anti-inflammatory (211–213), cardio-protective (214), neuroprotective (215), chemoprevention and anti-cancer (216–218), as well as anti-oxidant properties (219). PIP is also well known for enhancing the bioavailability of other phytochemicals, such as curcumin (220), and as a treatment option for vitiligo (221), a condition caused by T lymphocyte-mediated destruction of skin melanocytes.

The chemopreventative effects of PIP have been studied in a variety of carcinogenesis models. In vivo studies show that oral administration of PIP (50 mg/kg b.w.), prior to and during exposure to the carcinogen dimethyl benza[a]anthracene, prevents the development of skin tumors in mice and hamsters (222, 223). PIP also mitigates the toxicity associated with other carcinogens such as cadmium (224). The mechanism of PIP chemoprevention is mainly through ROS scavenging (223, 224), and inhibition of NF-κB signaling (213, 225).

PIP exhibits dose-dependent anti-proliferative and cytotoxic effects on a variety of human cancer cell lines, albeit PIP is less potent than PL. PIP induces cell-cycle arrest through modulation of cell cycle proteins such inhibition of cdk1 phosphorylation and activation, as well as downregulation of cyclin B1 in U2OS human osteosarcoma cells (226). Activation of caspases, decreased levels of anti-apoptotic Bcl-2, and increased expression of Bax are seen in PIP-treated A549 lung cancer cells (227). Non-cytotoxic

doses of PIP show growth inhibitory effect by increasing the expression of p21, and decreasing cell-cycle dependent cyclin proteins in prostate (228) and TNBC breast cancer cells (218). At higher doses (>100 μM), however, PIP triggers caspase-dependent apoptosis in TNBC cells and ER-positive breast cancer cells, while leaving normal cells like HMECs unaffected, even at 150 μM (218). A recent study by Greenshields and colleagues (2015) shows that three intra-tumoral injection of PIP (0.2 mg/kg b.w.) significantly suppresses TNBC growth in a xenografted mouse model of breast cancer (218). PIP also boosts the cytotoxic effects of conventional therapies such as 5-fluorouracil, paclitaxel, and ionizing radiation on cancer cells (218, 229, 230).

The anti-metastatic properties of PIP have also been studied to some extent. Low doses of PIP decrease the expression of MMPs in fibrosarcoma, mouse mammary carcinoma, and TNBC cells (218, 231–233). As a result, a decrease in tumor cell invasion and migration is seen following PIP treatment (218, 233). In endothelial cells, PIP-mediated inhibition of PI3K/Akt and NF-κB signaling is believed to be responsible for the loss of MMP expression (231, 234). Interestingly, 100 μM of PIP reduces endothelial cells proliferation and migration, suggesting a possible inhibitory mechanism of PIP on angiogenesis (234). In vivo studies also show that PIP (5 mg/kg b.w.) interferes with the lung metastasis of 4T1 mouse mammary carcinoma cells to the lungs (233). The inhibitory effects of PIP on mammosphere-forming ability of breast cancer cells have also been shown in vitro (218, 235). These findings show that PIP may be effective in cancer therapy.

Similar to PL, the lipophilic nature of PIP also produces solubility challenges in pre-clinical and clinical studies. PIP is also processed by liver to various metabolites, which are mainly extracted by the kidney (236). PIP exhibits a plasma concentration half-life of 8.5 hours (237). Although PIP is well tolerated in animal studies, high doses of PIP can lead to hemorrhagic necrosis, gastrointestinal complications, and reproductive toxicity (210). However, nanoparticle-based drug delivery has shown great potential in improving the bioavailability and efficacy of candidate drugs, while reducing drug toxicity and increasing tumor selectivity (238). In fact, encapsulation of PIP into liposomes has improved the pharmacokinetic parameters of the phytochemical (237).

1.7 Nanoparticles (NPs)

Today, patients receiving high dose chemotherapy face severe side effects due to drug toxicities and inefficient delivery to the tumor. The application of nanomedicine in cancer therapy shows great promise in improving the potency and efficacy of existing anti-cancer compounds, while providing opportunities for targeted delivery. Nanomedicine may include the use of viral vectors, drug conjugates, organic NPs, and inorganic NPs (239). Organic NPs can be synthesized from lipids (i.e. liposomes), natural polymers (e.g. albumin), and synthetic polymers (e.g. polylactide), while inorganic NPs are often made with metals or silica (239). Encapsulation of hydrophobic anti-cancer drugs into NPs improves their solubility and in vivo stability (238–240). NPs can also improve the circulation time of drugs in blood. Surface modification of NPs with hydrophilic poly(ethylene glycol) (PEG) not only improves NP solubility but also prevents rapid opsonization by serum proteins and elimination by phagocytic cells of spleen and liver (241–243). However, one of the most convincing arguments for the use of NPs in cancer therapy is the potential for selective delivery of anti-cancer compounds to the tumor microenvironment. This phenomenon can be achieved by taking advantage of the distinct physiology of tumor vasculature (passive targeting) or coating NPs with ligands that bind to receptors found on tumor cells (active targeting) (238, 239).

During passive targeting, the leaky vasculature and impaired lymphatic drainage of tumors allows for the accumulation of NPs at the tumor site rather than in normal tissues (238, 239). Indeed, the distance between endothelial cells in tumor vasculature is ~380-780 nm and can reach up to 1 μm in diameter (244), while the vasculature of normal tissue is only permeable to molecules smaller than 11.5 nm (245). This is also known as the enhanced permeability and retention effect (238, 239). NPs with average size range of 40-100 nm therefore preferentially concentrate in the tumor microenvironment and are also protected from retention in or rapid clearance by liver, spleen, and kidneys (246). Smaller particles (<~5) are more likely to undergo renal clearance (247), and larger particles (> 200 nm) are more prone to opsonization and retention in liver/spleen (248). Doxil® and Caelyx® are PEGylated liposomal doxorubicin and first generation FDA-approved NPs used for drug delivery based on passive targeting (239, 249). Active targeting relies on the interaction between ligands on NPs and receptors found

specifically on tumor cells, in order to minimize binding to healthy cells (239). Doxorubicin-immunoliposomes designed to target EGFR have been tested in clinical trials for advanced solid tumors (250), and are now under investigation for EGFR-positive TNBC patients (clinicaltrial.gov; NCT02833766).

However, the type of NP also determines its effectiveness in therapeutic delivery. Liposomes, which can be made from phospholipids and cholesterol, exhibit high cellular affinity and biodegradability, while lacking any immunogenicity. However, liposomes are associated with low encapsulation efficiency, limited control on drug release, and difficulty with storage and mass production (238, 251). Meanwhile, synthetic polymer and co-polymers are biodegradable FDA-approved alternatives with a higher chemical versatility, and a more sustained drug release (240, 251). Synthetic polymers such as poly(lactic acid) (PLA), poly(glycolic acid) (PGA), poly(lactic-co-glycolic) acid (PLGA), and poly(ε-caprolactone) (PCL) are among the most studied compounds used for polymeric NPs. The use of PEGylated synthetic polymers in the delivery of docetaxel (BIND-014), cisplatin (Nanoplatin), paclitaxel (NK-105), doxorubicin (NK-911) has been reported at various phases of clinical trials against a broad range of human malignancies (239). Nab-paclitaxel, also known as Abraxane®, are paclitaxel-bound albumin NPs approved for treatment of breast cancer, pancreatic cancer, and non-small cell lung cancer, which not only improved the response rate of patients, but also eliminated the allergy-based side effects of solvent-based paclitaxel (239, 252). These results illustrate the great potential of NPs in delivery of cancer therapeutics.

1.7.1 NP Delivery of Phytochemicals for Cancer Therapy

The lack of therapeutic use of many phytochemicals with promising anti-cancer properties is due to their metabolism, absorption, distribution, and excretion of these compounds in human body. Given that NPs show great potential in improving the pharmacokinetics and pharmacodynamics of different anti-cancer drugs, several studies sought to investigate the anti-cancer effects of phytochemicals using NPs as a drug delivery approach. As mentioned earlier, curcumin shows great anti-cancer potential (186, 187); however, its hydrophobic nature results in limited bioavailability as well as rapid metabolism and elimination (253, 254). A recent study by Khalil and colleagues

(2013) shows that encapsulation of curcumin in PEG-PLGA NPs significantly improves the plasma concentration and half-life of this compound, following oral administration (50 mg/kg b.w.) in rats (243). Encapsulation of curcumin into magnetic NPs also shows improved bioavailability and anti-cancer effects in pancreatic tumor-bearing mice (255).

PEG-PLA NPs containing luteolin, a flavonoid found in green vegetables (e.g. broccoli and cabbage) with well-established anti-cancer properties but poor pharmacokinetics, exhibit significant tumor growth inhibitory effects in vivo compared to free luteolin (256). Encapsulation of other anti-cancer compounds such as paclitaxel, fisetin, and oridonin into synthetic polymers has also been investigated (257–259); however, only a few studies have reported on the encapsulate PIP or PL into NPs. Veerareddy and Vobalaboina (2007) show improved plasma half-life and tissue distribution of PIP using PEGylated liposomes (237), while encapsulation of PL into methoxy (m) PEG-PCL NPs prevents endothelial cell migration and tubule formation in vitro, as well as subcutaneous tumor growth in vivo (260).

1.8 Rationale and Objectives

The objectives of this study were to optimize a feasible method for the preparation of PIP- and PL-NPs, and to investigate the mechanism by which PIP- and PL-NPs inhibit the metastatic potential of TNBC cells. Treatment options for TNBC patients are invasive with undesirable toxicities, and fail to prevent EMT-induced metastatic relapse of the disease. Therefore, alternative therapeutics are urgently needed to improve the clinical outcome of TNBC patients. Phytochemicals show great potential in targeting cancer associated signaling pathways and epigenetic machinery involved in cancer cell proliferation, survival, and invasion. Pepper derived phytochemicals, PIP and PL, show impressive anti-cancer effects in vitro and in vivo. However, their anti-metastatic potential, especially that of PL, is still not yet fully elucidated. The focus of this investigation is on the anti-metastatic potential of PIP and PL in the context of cell migration, invasion, and EMT/epigenetic regulation of TNBC cells. This study was also set to improve the solubility of these phytochemicals and provide opportunity for targeted delivery in vivo, by encapsulating PIP and PL into NPs made from mPEG-PLGA polymer.

Table 1.1 Molecular profiling of breast cancer cells

Molecular subtypes	Gene expression profiling	Current treatment	Prevalence	Prognosis
Luminal A	ER+ and PR+	HT* (Tamoxifen, Anastrozole) Chemotherapy	50 – 60%	Excellent
Luminal B	ER+/- and PR+/- HER2-/+	HT*+Anti-HER2 Chemotherapy	10-20%	Intermediate
HER2-enriched	HER2+ and ER-	Anti-HER2 (Trastuzumab) Chemotherapy	15-20%	Poor
Basal-like	TNBC	Chemotherapy	10-20%	Worst
Claudin-low	TNBC	Chemotherapy	12-14%	Poor-Worst
Normal-like	TNBC	Chemotherapy	5-10%	Intermediate

* HT: Hormonal therapy

Figure 1.1 Illustration of the main signaling pathways that lead to the induction of EMT.

TGF-β, Wnt, Hedgehog, TNF-α, RTK-PI3K/Akt and Notch are the main embryonic signaling events that lead to the activation of EMT in primary cancer cells. These pathways result in the activation of downstream signaling molecules that promote the expression of EMT-TFs. EMT-TFs such as Snail, Slug, Twist1/2, and ZEB1/2 downregulate the expression of epithelial markers, and promote the expression of mesenchymal and stemness makers, which results in cancer progression and metastasis. NDRG1, an inhibitor of TGF-β and Wnt pathways, along with miR-200 family, which inhibit EMT-TFs, serve as potential targets for the inhibition of EMT.

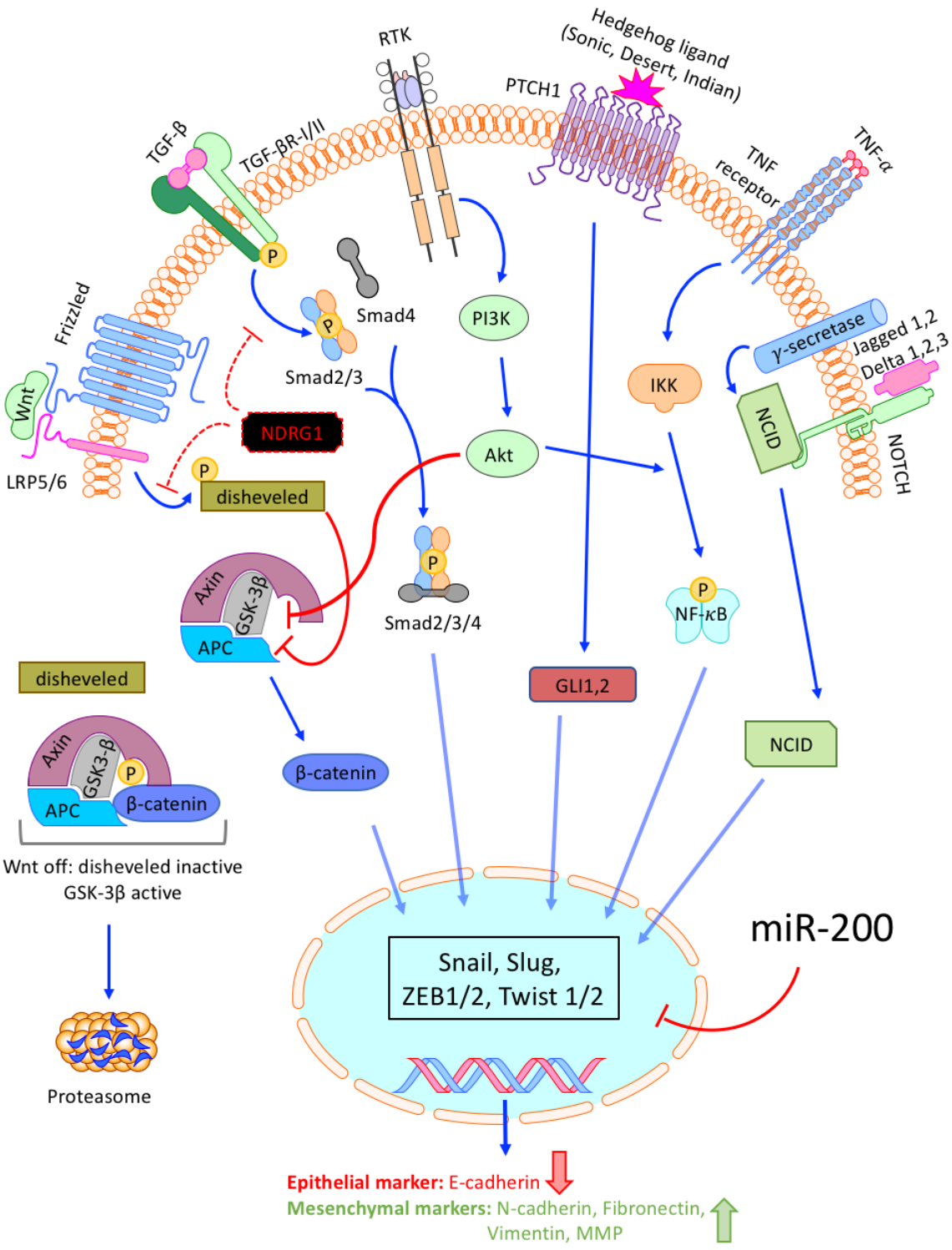
RTK
Hedgehog ligand
(Sonic, Desert, Indian)
PTCH1
TGF-β
TGF-βR-I/II
TNF
receptor
TNF-α
Frizzled
Wnt
LRP5/6
Smad4
Smad2/3
PI3K
γ-secretase
Jagged 1,2
Delta 1,2,3
IKK
NCID
NOTCH
NDRG1
Akt
disheveled
Axin
GSK-3β
APC
Smad2/3/4
NF-κB
GLI1,2
NCID
β-catenin
Wnt off: disheveled inactive
GSK-3β active
Proteasome
Snail, Slug,
ZEB1/2, Twist 1/2
miR-200
Epithelial marker: E-cadherin
Mesenchymal markers: N-cadherin, Fibronectin,
Vimentin, MMP

Figure 1.1

Figure 1.2 Piperlongumine (PL) and Piperine (PIP) chemical structures.

(A) PL: 5,6- dihydro-1-[(2E)-1-oxo-3-(3,4,5-trimethxyphenyl)-2-propenyl]-2(1H)-pyridinone; (B) PIP: 1-[5-(1,3-Benzodioxol-5-yl)-1-oxo-2,4-pentadienyl] piperidine.

(A)

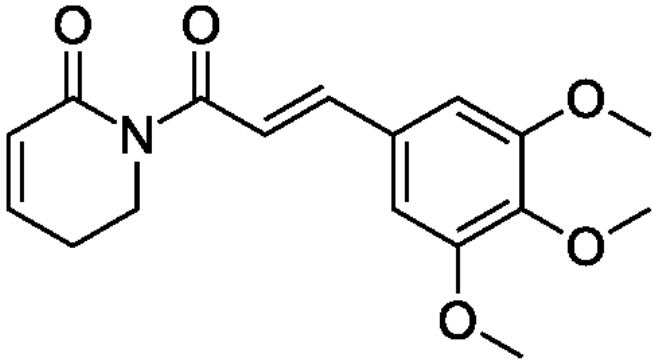

(B)

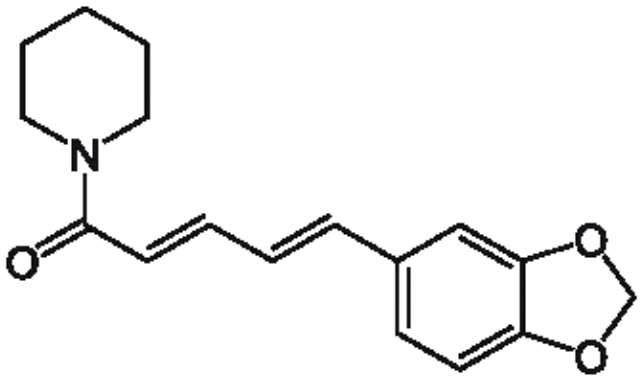

Figure 1.2

CHAPTER 2

MATERIALS AND METHODS

2.1 Chemicals and Reagents

PIP, dimethyl sulfoxide (DMSO), dichloromethane (DCM), Lutrol® F68, MTT (3-(4,5-demethylthiazol-2-yl)-2,5-diphenyltetrazolium bromide), β-mercaptoethanol, phosphate buffered saline (PBS), phenylmethylsulfonyl fluoride (PMSF), Triton X-100, bovine serum albumin (BSA), sodium acetate, sodium deoxycholate, aprotinin, leupeptin, sodium fluoride (NaF), pepstatin A, dithiothreitol (DTT), phenylarsine oxide (PAO), phosphatase substrate, gelatin, insulin, hydrocortisone, and mitomycin C were all purchased from Sigma-Aldrich (Oakville, ON). Trypan blue dye solution, L-glutamine, 10,000 units/mL penicillin/ 10,000 µg/mL streptomycin solution, 1M N-2-hydroxyethylpiperazine-N-2-ethane sulfonic acid (HEPES) buffer solution, fetal bovine serum (FBS), horse serum, B27 serum-free supplement, 0.25% trypsin-EDTA or TrypLE™ Express, Lipofectamine® 2000, carbenicillin (disodium salt), propidium iodide (PI), Dulbecco's Modified Eagle Medium (DMEM), DMEM/F-12 medium, Opti-MEM™ medium, F-12 medium, and appropriate supplements were all purchased from Invitrogen Canada Inc. (Burlington, ON). Methoxy poly (ethylene glycol)-b-poly (D,L) lactic-co-glycolic acid (mPEG-PLGA; 5,000-10,000 Da) was purchased from Akina Inc. (West Lafayette, IN). Sodium hydroxide (NaOH), and hydrochloric acid (HCl) were purchased from Fisher Scientific (Ottawa, ON). Ethylene diamine tetraacetic acid (EDTA) was purchased from EM 46 Industries Inc. (Hawthorne, NY). Annexin-V-FLUOS was purchased from Roche Diagnostics (Laval, QC). Sodium chloride (NaCl), acrylamide/bis-acrylamide (29:1, 30% solution), ammonium persulfate (APS), sodium dodecyl sulfate (SDS), Tris-base, Tween-20, tetramethylethelyenediamide (TEMED), glycine, agarose, ethylene glycol tetraacetic acid (EGTA), and sucrose were purchased from BioShop Canada Inc. (Burlington, ON). Bio-Rad protein assay dye reagent concentrate and SsoFast EvaGreen™ Supermix® were purchased from Bio-Rad (Hercules, CA). Human TGF-β-1 (derived from HEC 293 cells), bFGF, and epidermal growth factor (EGF) were purchased from PeproTech (Dollard des Ormeaux, QC). PL,

Luminata™ Forte Western horseradish peroxidase (HRP) substrate, fibronectin, ARP 100 (selective MMP-2 inhibitor), sodium orthovanadate (Na_3VO_4), and calcium chloride ($CaCl_2$) were all purchased from EMD Millipore (Etobicoke, ON).

DMSO was the primary vehicle for both PIP and PL. PIP and PL stocks were made up at 150 mM and 20 mM in DMSO, respectively, and stored at -80 ℃ until use.

2.2 Antibodies

Anti-human ZEB1, β-catenin, Slug, Pan-cadherin, NDRG1, phospho (P)-Smad-2, Smad-3, Vimentin, DYKDDDK (Flag)-tag, Myc-tag, HDAC-1, HDAC-4, HDAC-6, and DNMT-1 immunoglobulin G (IgG) rabbit monoclonal antibodies (Abs), as well as HDAC-2 and HDAC-3 IgG mouse monoclonal Abs were all purchased from Cell Signaling Technology Inc. (Beverly, MA). Goat anti-mouse and donkey anti-rabbit HRP-conjugated secondary Abs were purchased from Santa Cruz Biotechnology Inc. (Santa Cruz, CA). β-actin IgG rabbit monoclonal Ab (HRP conjugate) was purchased from Cell Signaling Technology Inc. (Beverly, MA). All Abs were made in 5% w/v fat-free milk or 5% w/v BSA, in TTBS (20 mM Tris-HCl [pH 7.6], 200 mM NaCl, 0.05% Tween-20).

2.3 Cell Lines and Culture Conditions

MDA-MB-231 human breast adenocarcinoma cells were kindly provided by Dr. S. Drover (Memorial University of Newfoundland, St. John's, NL). MDA-MB-468 human breast adenocarcinoma cells were a generous gift from Dr. P. Lee (Dalhousie University, Halifax, NS). BT-549 human breast ductal carcinoma cells and MCF-10A immortalized human mammary epithelial cells were generously provided by Dr. P. Marcato (Dalhousie University, Halifax, NS). MCF-7 human breast carcinoma cells were generously provided by Dr. K. Goralski (Dalhousie University, Halifax, NS). Normal HDF cells were purchased from Lonza Inc. (Walkersville, MD). All breast cancer cell lines were authenticated by the American Type Culture Collection (ATCC) using the short tandem repeat method prior to use.

Breast cancer cell lines MDA-MB-231, MDA-MB-468, BT-549, MCF-7, as well as HDFs were cultured in DMEM that was supplemented with 10% heat-inactivated FBS, 100 U/mL penicillin, 100 μg/mL streptomycin, 2 mM of L-glutamine, and 5 mM of

HEPES; henceforth, known as complete DMEM (cDMEM). Serum free (sf) DMEM lacked FBS. These cells were propagated as required in T-75 mm^2 tissue culture flasks using 0.25% trypsin-EDTA and cDMEM, and maintained at 37 °C in a humidified 10% CO_2 incubator during culture and treatment periods.

MCF-10A cells were cultured in DMEM/F-12 medium supplemented with 10% horse serum, 100 U/mL penicillin, 100 µg/mL streptomycin, 20 ng/mL EGF, 0.5 mg/mL hydrocortisone, and 10 µg/mL insulin, referred to as cDMEM/F-12. MCF-10A were also propagated in T-75 mm^2 tissue culture flask maintained at maintained at 37 °C in a humidified 5% CO_2 incubator during culture; but transferred to cDMEM and maintained at 37 °C and humidified 10% CO_2 incubator during treatment periods.

2.4 Formulation of NPs

2.4.1 Single Emulsion Solvent Extraction

A modified Fessi method (261) was employed for the formulation of these NPs. In brief, the organic phase was made by dissolving 8.5 mg PIP or 5 mg PL, and 100 mg mPEG-PLGA in 10 mL DCM. The aqueous phase consisted of 150 mL distilled water (dH_2O) and 0.1% Lutrol® F68 used as a surfactant to stabilize the emulsion droplets. The organic phase was added drop-wise to the aqueous phase under magnetic stirring at high speed for 2 hours. The emulsion was heated to ~40 °C under vacuum to remove DCM by evaporation, using a rotary evaporator (Büchi, Switzerland). The solution was then ultracentrifuged at 27,000 rcf for 15 minutes to remove any residual DCM or unencapsulated drugs. Finally, the NP pellet was dissolved in 10 mL dH_2O containing 5% sucrose as a cryoprotectant, flash-frozen, and lyophilized into NP powder.

2.4.2 Thin-Film Hydration

As previously described by Lim Soo et al. (2006) (262), the drug (PIP or PL) and the copolymer (mPEG-PLGA) were co-dissolved with a ratio of 1:9 in 5 mL of DCM and transferred to a 250 mL round-bottom flask. The mixture was evaporated under vacuum using a rotary evaporator (Büchi, Switzerland) at 60 °C. The co-evaporation of the phytochemical and the polymer was obtained as a homogenous mixture in a form of a thin film coating the inner surface of the flask. The thin-film material was re-dissolved in

5 mL normal saline (0.9% NaCl) and stirred at 60 °C to allow the self-assembly on polymers into micro- and nano-sized micelles with PIP or PL encapsulated inside. The mixture was placed in dialysis membrane with 14 kDa cut-off (Viskase, USA) against 0.9% NaCl buffer at room temperature, to remove any encapsulated phytochemical. Buffer solution was replaced at 30 minute, 2 hour, and 4 hour intervals, to further facilitate the removal of free PIP or PL. The sample was then flash-frozen in liquid nitrogen and ultimately lyophilized into NP powder. Prior to use, these NPs were reconstituted in sterile water at a desired concentration, and sonicated with an ultrasonic probe at 50W output (40% of 125 W Q125 sonicator, QSonica, USA), for 5 minutes, to obtain a desired size of particles and further improve the entrapment of PIP or PL into NPs.

In both methods, NPs were dissolved in sterile water at the desired concentration and filter sterilized using a 0.20 μm syringe filter (Sarstedt, Germany) prior to use, to remove polymer aggregates and crystal particles of free drugs. NP powder was stored at room temperature; however, reconstituted samples were stored at -80°C. Empty NPs were prepared and handled according to the same procedures except that PIP or PL were not added.

2.5 Characterization of NPs

2.5.1 Transmission Electron Microscopy (TEM)

NPs were dissolved in sterile water, and a drop of the solution was places on a Formvar/Carbon-coated grid and allowed to settle for 15 minutes. Then, the drop was gently removed with a stream of dH_2O, and the grid was stained with a drop of 0.2 % uranyl acetate for 30 seconds. Following staining, the grid was left to dry and then examined using a JEOL JEM 1230 Transmission Electron Microscope (JEOL, Japan). The images were captured using a Hamamatsu ORCA-HR digital camera (Hamamatsu, Japan). Particle size was measured using AMT Image Capture Engine (version 602, AMT Crop. USA), and the measurements of 90 randomly selected NPs were used to report an average NP size.

2.5.2 Encapsulation Efficiency

The drug encapsulation efficiency of nanoparticles was determined using the spectrophotometric technique. Initially PIP or PL were dissolved in DMSO at the concentration ranges of 10-80 μg/mL, and the absorbance was measured at 346 nm using an UVM 340 microplate reader (Biochrom, AYSY, Cambridge, UK), to generate a standard curve. Then, the same method was used to measure the absorbance of PIP- or PL-NP solution (5mg/mL in DMSO). To correct for the absorbance of the NP polymer, the absorbance of empty NPs was subtracted from that of PIP- or PL-NPs. Finally, the equation of the standard curve was used to determine the amount of PIP or PL in 5 mg NP sample and ultimately in the entire NP sample. The encapsulation efficiency was measured by comparing the amount of PIP or PL measured in NPs with their initial amount used for NP preparation, according to Equation 2.1. The encapsulation efficiency of every batch of PIP- or PL-NPs prepared in this study was determined according to the method described above.

Equation 2.1 Estimating the encapsulation efficiency of NPs

$$\text{Encapsulation efficiency} = \frac{Actual\ amount\ of\ drug}{Theoretheical\ amount\ of\ drug} x\ 100$$

2.6 Cell Viability Assay

2.6.1 MTT Assay

Cellular growth and viability was measured by assessing the mitochondrial succinate dehydrogenase activity using a modified MTT assay. Actively respiring cells convert water-soluble MTT substrate into lipid-soluble formazan crystals, which are then dissolved in DMSO and measured by spectrophotometric technique as a suitable indicator of cellular metabolic activity or the number of living cells (263). In brief, cells were seeded in quadruplicate wells of a 96-well plate at a concentration of 5 x 10^3 cells/ well in 100 μL cDMEM and incubated overnight. Following cell attachment, cells were treated with free PL (dissolved in DMSO) and PL-NP (2.5-10 μM), free PIP (dissolved in DMSO) and PIP-NP (50-150 μM), medium, vehicle (DMSO), or empty NP controls and cultured for 48 hours. Following culture, 20 μL MTT solution (5 mg/mL of yellow tetrazolium salt in PBS) was added to each well. Plates were then incubated for additional

2 hours. Next, the plate was centrifuged at 1,400 rcf for 5 minutes, the medium was removed, and formazan crystals were solubilized in 100 µL DMSO, generating a purple color. The plate was shaken for 3 minutes at 600 rpm on a microplate Genie (Montreal Biotech Inc., Montreal, QC). Finally, the optical density of each well was measured at 570 nm using an Expert 96 microplate reader (Biochrom ASYS, Cambridge, UK). Absorbance values from each biological replicate were averaged and normalized relative to medium control.

2.6.2 Apoptosis Assay

To determine the cytotoxic potential of PIP and PL on breast cancer cells we used flow cytometric analysis of Annexin-V-FLUOS/PI stained cells. The assay is based on the premise that Annexin-V is a Ca^{2+}-dependent protein with high affinity for phosphatidylserine, which is exclusively found in the inner leaflet of plasma membrane (35). However, during apoptosis, phosphatidylserine is transferred to the other leaflet in almost all cells regardless of the trigger of apoptosis (35). This allows detection of apoptotic cells using Annexin-V conjugated with a fluorophore like fluorescein isothiocyanate (FITC). PI is a red fluorescent DNA intercalating agent that is excluded by live cells and apoptotic cells due to their intact membrane, however PI can stain necrotic cells (35). Therefore, the combination of Annexin-V-FLUOS/PI can be used with flow cytometry to distinguish between apoptotic and necrotic cells.

MDA-MB-468 breast cancer cells and HDF cells were seeded in 6-well plates at density of 5 x 10^4 cells/well and allowed to adhere overnight. The following day, cells were treated with 150 µM of free PIP or PIP-NP or 10 µM of free PL or PL-NP along with DMSO and empty NP controls. Following 48 hours of treatment, cells were harvested using TrypLE Express™, combined with non-adherent cells, centrifuged at 500 rcf for 5 minutes, and washed in 1 mL of 1X PBS. The supernatant was discarded and the cells were resuspended in 50 µL of Annexin-V-FLUOS/PI buffer (5 mM $CaCl_2$, 10mM HEPES, 40 mM NaCl, 2% Annexin-V-FLUOS, and 1µg/mL PI). Samples were incubated at room temperature for 15 minutes, then combined with 450 µM of Annexin-V-FLUOS/PI buffer (without the Annexin-V-FLUOS/PI) and analyzed with BD FACSCalibur™ flow cytometer (BD Biosciences, Mississauga, ON).

To compensate for overlapping of the emission spectra of Annexin-V-FLUOS and PI, unstained cells, Annexin-V-FLUOS single-stained cells, and PI single stained cells were used as proper controls. The flow cytometry data was acquired as total of 1 x 10^4 counts per sample with a BD CellQuest™ software (version 3.3, BD Biosciences, Mississauga, ON) and analyzed using FCS Express software (version 3.0, De Novo software, Thornhill, ON).

2.7 Spheroid Culture and Acid Phosphatase Assay

To investigate the effects of free PL and PL-NP on the growth of mammary epithelial cancer cells in suspension culture, which is a better representation of the clinical cancer outgrowth in situ, we used the mammosphere assay. In brief, MCF-7 human breast carcinoma cells were seeded at a density of 3 x 10^4 cells/well in ultra-low attachment 6-well Costar® plates (Corning Inc, Tewksbury, MA), and cultured in mammosphere medium (F-12 medium supplemented with 20 ng/mL bFGF, 20 ng/mL EGF, 100 U/mL penicillin, 100 µg/mL streptomycin and 1X B27 serum free supplement) at 37 ℃ in a humidified 10% CO_2 atmosphere. The spheroids were allowed to develop for 7 days prior to use and were fed with mammosphere medium every 72 hours. Following the mammosphere development period, the medium was removed and the spheroids were resuspended in mammosphere medium containing 10 µM free PL or PL-NP, as well as proper medium and vehicle (DMSO and empty NP) controls, and cultured for 72 hours. Following 72 hours of incubation, spheroids were photographed at 20X magnification using a Nikon® Digital Sight camera (Nikon Canada Inc., Mississauga, ON), and the cell viability was measured using a modified acid phosphatase assay.

Quantification of cytoplasmic acid phosphatase activity was employed to assess cellular viability of free PL or PL-NP treated mammospheres. The assay is based on the premise that p-nitrophenyl phosphate is hydrolyzed by cytosolic acid phosphatases of viable cells into p-nitrophenol, whose absorbance at 405 nm is directly proportional to its concentration, and therefore the cell number (264). Following the 72 hours of treatment period, spheroids were transferred into 5 mL Falcon™ round-bottom polystyrene tubes (Corning Inc, Tewksbury, MA), centrifuged at 500 rcf for 5 minutes, and the supernatant was discarded. The samples were washed with 1 mL of 1X PBS, then resuspended in 500

μL of 1X PBS and 500 μL assay buffer (0.1 M sodium acetate pH 5.5, 1 μL/mL Triton X-100, and 4 mg/mL phosphatase substrate). Samples were incubated for 90 minutes at 37 ℃ with humidified 10% CO_2 atmosphere. Finally, 50 μL of 1N NaOH was added to each sample, the mixture was transferred to quadruplicate wells of a 96-well clear flat-bottom tissue culture plate, and the optical density was measured at 405 nm using an Expert 96 microplate reader (Biochrom ASYS, Cambridge, UK). Absorbance values from each biological replicate were averaged and normalized relative to medium control.

2.8 Trans-well Invasion Assay

MDA-MB-231 cells were initially cultured in T-75 mm^2 flasks at density of 5 x 10^5 cells/flask, for overnight to allow cells to adhere to the plate. The following day, cells were treated with 2.5 μM of free PL and PL-NP, along with the DMSO and empty NP controls, using cDMEM for the first 36 hours, and sfDMEM during the last 12 hours of the treatment period. For experiments with ARP 100 (selective MMP-2 inhibitor), cells were treated with DMSO control or 12 nM – 20 μM of ARP 100 for 36 hours in cDMEM and 12 hours in sfDMEM. Cultures were incubated at 37 ℃ in humidified 10% CO_2 atmosphere for the duration of the treatment. Following the treatment period, cells were harvested using TrypLE Express™, washed and resuspended in 1 mL of appropriate treatment in sfDMEM prior to counting.

The bottom chamber of a 48-well Micro Chemotaxis apparatus (Neuro Probe Inc., Gaithersburg, MD) was filled with 26 μL/well of cDMEM or sfDMEM. Next, a polycarbonate membrane with 8 μm pore size (Neuro Probe Inc., Gaithersburg, MD) either uncoated or coated with fibronectin (0.05% w/v) or gelatin (0.01% w/v) on one side for at least 12 hours, was placed on the bottom chamber covering both cDMEM and sfDMEM wells. The top chamber of the apparatus was then placed on the membrane, and 50 μL of 1x 10^6 cells/mL in treatment sfDMEM was loaded on each well of the top chamber that is positioned exactly above the corresponding well on the bottom chamber. Therefore, cells in each treatment were seeded above both cDMEM and sfDMEM. Ultimately, during chemotaxis, cells above the cDMEM side must cross the coated or uncoated membrane to reach cDMEM, and the migration of cells above the sfDMEM side would be used as background migration value that is subtracted from the migration

value on the cDMEM side. The chemotaxis chamber was incubated at 37 ℃ humidified 10% CO_2 atmosphere for 22 hours. The chambers were then disassembled and the cells on the upper surface of the membrane were removed with a plastic swab, while the cells that passed through the membrane were stained with Diff-Quick™ staining kit (Siemens Inc., Newark, DE) according to manufacturer's protocol. These migrated cells were then photographed with a Nikon® Digital Sight camera (Nikon Canada Inc., Mississauga, ON) counted using ImageJ software (version 1.47, National Institute of Health, Bethesda, MD). Percentages of migrating cells from each biological replicate were averaged and normalized relative to DMSO control.

2.9 Gap-closure Assay

MDA-MB-231 cells were seeded at 10,000 cells/100 μL cDMEM in each well of the Ibidi® 2-well culture inserts (Ibidi, Fitchburg, WI) in a 6-well plate. After 24 hours of culture, medium was removed and the cells were treated with 100 μL of 10 μg/mL mitomycin C in cDMEM for 2 hours to terminate cell proliferation. Following mitomycin C treatments, cells were allowed to recover in cDMEM for 12 hours, and then treated with 50 μM of free PIP or PIP-NP, or 2.5 μM of free PL or PL-NP, along with medium and vehicle (DMSO and empty NP) controls in cDMEM, for 24 hours. At the end of the treatment period, culture inserts were removed, cells were washed with PBS, and cDMEM containing treatments were added to the cells. Cells were left in the 10% CO_2 incubator with 37 ℃ humidified atmosphere. Images of the cell migration were captured at 0 and 18 hours following insert removal, using a Nikon® Digital Sight camera (Nikon Canada Inc., Mississauga, ON).

2.10 Protein Isolation

Breast cancer cell lines, MDA-MB-231 and BT-549, as well as human breast epithelial cells, MCF-10A were seeded in T-75 mm^2 flask (5 x 10^5 cells/10 mL of cDMEM or cDMEM/F-12) and incubated overnight. Cells were then treated with 2.5 - 5 μM of free PL or PL-NP with appropriate controls (DMSO and empty NP) in 10 mL of cDMEM, for 48 - 72 hours. For experiments involving TGF-β, MCF-10A cells were treated with 2.5

μM of PL or DMSO for 24 hours, then treated with 5 ng/mL of TGF-β in the presence or absence of PL, as well as DMSO and free PL controls, for additional 48 hours.

Following treatment period, breast cancer cells were harvested using TrypLE Express™, centrifuged at 500 rcf for 5 minutes at 4 ℃, and washed with cold 1X PBS. The total protein was extracted with 50 μL of cold lysis buffer (0.1% v/v NP-40, 0.25% w/v sodium deoxycholate, 50 mM Tris-HCl (pH 7.5), 150 mM NaCl, 5 mM EDTA, 5 mM EGTA pH 7.5 with a mixture of phosphatase and protease inhibitors like 1 mM PMSF, 5 μg/mL leupeptin, 5 μg/mL pepstatin, 10 μg/mL apotinin, 100 μM Na_3VO_4, 1 mM DTT, 10 mM NaF, and 10 μM PAO), for 15 minutes on ice. Debris was removed by centrifugation (14,000 rcf, 10 minutes, 4 °C). The supernatant containing cellular proteins was collected and stored at -80 ℃ for a maximum of 4 days prior to protein quantification.

2.11 Protein Quantification

A colorimetric Bradford assay was used to quantify and equalize the total protein concentration in each sample using the Bio-Rad protein assay dye reagent concentrate. In brief, 5 μL of each sample was dissolved in 1 mL of diluted Bio-Rad protein assay dye (1:5 with dH_2O). BSA was treated the same way to generate a protein standard curve with concentrations ranging from 0.5 μg/mL – 16 μg/mL. The diluted standards and samples were plated in quadruplicate wells onto a 96-well flat bottom plate, and the absorbance of plate was measured at 570 nm using an Expert 96 microplate reader (Biochrom ASYS, Cambridge, UK). Using the standard curve, the concentration of proteins in each sample was calculated, and the lysis buffer was used to dilute all samples to a same concentration and volume. Finally, samples were further diluted with SDS-PAGE buffer (40 μL sample with 20 μL of 3X SDS-PAGE buffer; 6% w/v SDS, 30% v/v glycerol, 15% v/v β-mercaptoethanol, 0.01% v/v bromophenol blue, and 200 mM Tris-HCl [pH 6.8]), then heated to 95 °C for 5 minutes to denature the proteins. Samples were stored at -80 °C, prior to use.

2.12 Western Blotting

Protein samples (30 μg) were run on a 10% SDS-Polyacrylamide gel electrophoresis (10% acrylamide, 0.1% w/v SDS, 375 mM Tris-HCl [pH 8.8], 0.15% v/v TEMED, and 0.1% w/v APS) with a 4% stacking gel (4% acrylamide, 0.1% w/v SDS, 125 mM Tris-HCl [pH 6.8], 0.15% v/v TEMED, and 0.1 % APS) at 200 volts for 1 hour. Electrophoresis was performed in the presence of SDS running buffer (0.1% w/v SDS, 200 mM glycine, and 200 mM Tris-HCl [pH 8.3]). Following electrophoresis, proteins were transferred to a nitrocellulose membrane using an iBlot™ dry transfer system (Invitrogen, Burlington, ON) for 6.5 minutes according to manufacturer's protocol. Membranes were blocked with 5% fat-free milk in Tween-20 Tris-buffered saline (TTBS) (20 mM Tris-HCl [pH 6.8], 200 mM NaCl, and 0.05% v/v Tween-20) for 1 hour at room temperature. Primary Abs were used to probe for specific proteins overnight at 4 °C. The following day, membranes were washed for 30 minutes with TTBS (changing wash every 5 minutes), and then incubated with HRP-conjugated secondary Ab for 2 hours at room temperature, followed by 30 minutes of washing with TTBS. After the final wash, Luminata™ Forte Western HRP substrate was added to the membrane and incubated at room temperature for 1 minute. The blots were then exposed to X-ray film (Sci-Med Inc., Truro, NS.) in a dark room, and developed using Kodak X-OMAT 1000A automated X-ray developer. To account for variations in protein loading, membranes were later probed for β-actin.

The intensities of protein bands were quantified by densitometry using ImageJ software (version 1.47, National Institute of Health, Bethesda, MD). The intensities of proteins band were divided by the intensity of β-actin band for the corresponding treatment. The actin normalized intensities were further normalized to the medium control for each replicate. Protein blots for BT-549 and MCF-10A cell lines were developed using ChemiDoc Imaging System (Bio-Rad, Hercules, CA), and the intensities of protein bands were quantified using Image Lab software (version 5.2, Bio-Rad, Hercules, CA).

2.13 RNA Isolation and Quality Control

MDA-MB-231 and BT-549 breast cancer cell lines, as well as MCF-10A human breast epithelial cells, were seeded in T-75 mm^2 flask (5 x 10^5 cells/10 mL of cDMEM or cDMEM/F-12) and incubated overnight. The following day, cells were treated with the indicated concentrations of free PL or PL-NPs, as well as the vehicle controls (DMSO and empty NP). The treatment period was set for 48 or 72 hours and the treatment was changed every 24 hours. Experiments with MCF-10A epithelial cells and TGF-β were performed as described in section 2.10. Following the treatment period, cells were harvested using TrypLE Express™, centrifuged at 500 rcf for 5 minutes, and the supernatant was discarded. Cellular mRNA was isolated using RNeasy Mini kit (Qiagen, Valenica, CA) according to manufacturer's instructions. To measure the quantity and quality of our RNA, 5 µL of each sample was applied to the Nanovue Plus Spectrometer (GE Healthcare Life Sciences, Piscataway Township, NJ). RNA concentration was used for measurements in cDNA preparation as described in section 2.14. An optical density 268/280 ratio within the range of 1.8-2.0 was considered good quality RNA that is devoid of protein and phenol contamination.

2.14 cDNA Synthesis

Approximately 500 ng of RNA, in a final volume of 10 µL, was reverse transcribed to cDNA using iScript™ cDNA synthesis kit (Bio-Rad, Hercules, CA), according to manufacturer's protocol. The reaction was incubated in a Bio-Rad T100™ Thermocycler with the following steps: 5 minutes at 25 ℃, 30 minutes at 42 ℃, and 5 minutes at 85 ℃. Following synthesis, cDNA samples were kept at -20 ℃, prior to use.

2.15 Primer Optimization and Efficiency

Primer sets were designed and tested for optimal activity and efficiency, according to MIQE guidelines (265). Primers suggested by other publications were compared to the online database Primer-Blast (https://www.ncbi.nlm.nih.gov/tools/primer-blast/) to ensure that they are unique and specific for the gene of interest. A list of primers used in this study is shown in Table 2.1.

Primer optimization was set to determine the temperature at which primers produces the amplicon of interest while avoiding any primer secondary structure or formation of unintended amplicons. In brief, cDNA, 10 µM primer mix (forward and reverse), nuclease-free water, and SsoFast EvaGreen™ Supermix®, were mixed thoroughly with the ratio of 1:1:3:5, respectively. For qRT-PCR reaction involving the MMP genes, SYBR® Green PCR master mix (Qiagen, Valenica, CA) was used instead of SsoFast EvaGreen™. Next, 10 µL of the mixture was placed in 250 µL PCR tubes labeled for eight different temperatures and incubated in Bio-Rad T100™ Thermocycler with the following steps: 10 minutes at 95℃, 40 x (10 seconds at 95℃, 30 seconds at 54-64℃ temperature gradient, and 30 seconds at 72℃). Following the incubation period, samples in each tube were mixed with 10% w/v BlueJuice™ gel loading buffer (Fisher Scientific, Waltham, NA), and loaded on a 1% w/v agarose gel (1.0 g agarose, 2 mL of 50X TAE buffer [0.242% w/v Tris-base, 0.06% v/v glacial acetic acid, 50 µM EDTA, pH 8.0], and 98 mL of dH_2O). Electrophoresis was carried out at 100 V for 45 minutes. The gel was then imaged using ChemiDoc Imaging System (Bio-Rad, Hercules, CA). The temperature at which no bands other than the expected amplicon were observed was used for the annealing phase of the qRT-PCR reaction. The specificity of primers was confirmed using the melt curve analysis performed during qRT-PCR, as described in section 2.16.

Primer efficiency was used to determine at which cDNA dilutions the qRT-PCR reaction occurs optimally and the PCR product of interest is doubling with each cycle. Primer efficiency was conducted in a similar manner as described in section 2.16, except a serial dilution of pooled cDNA from all samples (1:1, 1:2, 1:4, …1:32) was used by the qRT-PCR system. The amplification curves were analyzed using CFX Manager software (version 3.1, Bio-Rad, Hercules, CA), and the plot of cDNA dilution vs C_q values was used to choose the optimal cDNA dilution. Percent efficiency of qRT-PCR reaction was determined using slope of standard curve, according to the following equation:

Equation 2.2 Determination of qRT-PCR reaction efficiency

$$\% \text{ efficiency} = \left(10^{\left(\frac{-1}{slope}\right)} - 1\right) x100$$

2.16 Quantitative Reverse Transcription Polymerase Chain Reaction

Quantitative reverse transcription polymerase chain reaction (qRT-PCR) was used to amplify cDNA samples using primer sets that target gene of interest. To correct for the difference in quantities of cDNA used from each sample, β-actin was also amplified at the same time and used as a reference gene. Appropriate dilution of cDNA sample along with primer mix (10 μM forward and reverse primer), nuclease-free water, and SsoFast EvaGreen™ Supermix® (Bio-Rad, Hercules, CA) or SYBR® Green PCR master mix (Qiagen, Valenica, CA), were mixed in 1:1:3:5 ratio, respectively, and mixed thoroughly. Next, 10 μL of each sample was transferred in triplicate wells of a Multiplate™ 96-well unskirted polypropylene PCR plate (Bio-Rad, Hercules, CA). The no-template control did not contain any cDNA, allowing us to test for possible DNA contamination and primer dimers. A Microseal 'B' Adhesive sealing film (Bio-Rad, Hercules, CA) was used to cover the plate during qRT-PCR reaction. The plate was then centrifuged at 14,000 rcf for 10 seconds, and placed in the CFX Connect™ Real-Time PCR detection system (Bio-Rad, Hercules, CA). The reaction steps were designed as follows: 10 minutes of activation at 95 ℃, 40 cycles of 10 seconds denaturation at 95 ℃, 20 seconds at the primer-specific annealing temperature (Table 2.2), and 30 seconds at 72 ℃, followed by a melt curve analysis, 10 seconds at 95 ℃, 0.5 seconds at 65 ℃, and 5 seconds at 95 ℃. Data obtained from the qRT-PCR reaction were analyzed using CFX Manager software (version 3.1, Bio-Rad, Hercules, CA). Cycle (C_q) value for each treatment, the cycle at which the fluorescence achieves a defined threshold, were first normalized relative to the reference gene (ΔC_q= C_q gene of interest – C_q reference gene), then normalized relative to the untreated medium control ($\Delta\Delta C_q$= ΔC_q treated sample - ΔC_q medium control), and eventually converted to fold change in gene expression (fold change = $2^{-\Delta\Delta Cq}$).

2.17 Transfection

2.17.1 Plasmids

Plasmids used in this study were pcDNA3 containing cDNA sequences of Flag-tagged human HDAC-1 (a gift from Eric Verdin; Addgene plasmid # 13820) (266), and myc-tagged human DNMT-1 (a gift from Arthur Riggs; Addgene plasmid # 36939) (267).

Plasmids were obtained from Addgene repository in the form of bacterial stab culture. Bacteria were recovered from the stab and cultured on LB agar plate containing 100 µg/mL carbenicillin at 37 ℃ overnight. The following day, single colonies were transferred to 100 mL of carbenicillin-supplemented (100 µg/mL) broth and grown for 24 hours at 37 ℃ in a shaking incubator. Following 24 hours, the turbid bacterial cultures pelleted by centrifugation at 8,000 rcf for 15 minutes before plasmids were recovered from the pellet using QIAfilter™ Plasmid midi kit (Qiagen, Valenica, CA) according to manufacturer's instructions. The authenticity of plasmids was verified by Sanger sequencing (performed by Genewiz, Boston, MA). In all transfection experiments, a pcDNA empty vector (EV), lacking a human cDNA expression cassette was used as negative control.

2.17.2 Transfection of MDA-MB-231 Cells

For efficient recombinant transgene expression, MBA-MB-231 cells were transiently transfected using the Lipofectamine® 2000 reagent, according to manufacturer's instructions, with some modifications. In brief, MDA-MB-231 were seeded at the density of 5 x 10^5 in a 100 mm tissue culture plates, and cultured at 37 ℃ with 10% CO_2 humidified incubator. The following day, cells were treated with 2 mL of Opti-MEM™ medium containing 10 µL of lipofectamine reagent and 9 µg of plasmid followed by addition of 8 mL of Ab-free cDMEM and incubation at 37 ℃ in a humidified 10% CO_2 incubator for 24 hours. The following day, 2.5 µM of PL or DMSO control was added to the cells, and 24 hours later, cells were treated with the same concentration of PL or DMSO in fresh Ab-free cDMEM for additional 24 hours. Following the treatment period, cells were harvested using TrypLE Express™ and divided into two equal groups. The RNA was isolated from one group, as described in section 2.13, for qRT-PCR, and the proteins were isolated from the other group, as described in section 2.10, for western blotting.

2.18 Statistical Analysis

The significance of the difference between the mean values was determined by one-way analysis of variance (ANOVA) with the Tukey-Kramer or Bonferroni multiple

comparisons post-tests, where appropriate, using GraphPad Prism analysis software (version 5.0, GraphPad Software Inc., La Jolla, CA). The Tukey-Kramer post-test was used for experiments in which multiple treatments were compared to each other, while the Bonferroni post-test was used to compare a single treatment (free drug or encapsulated drug) to its appropriate vehicle control (DMSO or empty NP). Data were tested at different significant levels as denoted by asterisks (*) for 95%, (**) for 99%, and (***) for 99.9% confidence levels. Results were considered significant at $p < 0.05$. When p value was greater than 0.05, data was considered not significant (n.s.). At least three independent biological repeats of each experiment were conducted, unless otherwise indicated. The analysis of the data, including the average of the raw data, and the standard error of the mean (SEM) were generated using GraphPad Prism.

Table 2.1 List of human primer sequences used for qRT-PCR experiments

Pair	Primer	Sequence (5' to 3')	Annealing temperature (℃)
1	β-actin F	AAGATCAAGATCATTGCTCCTC	N.A.
	β-actin R	CAACTAAGTCATAGTCCGCC	
2	c-Myc F	GCTCCTGGCAAAAGGTCAGA	54
	c-Myc R	CAGTGGGCTGTGAGGAGGTT	
3	E-cadherin F	CAGCCACAGACGCGGACGAT	64
	E-cadherin R	CTCTCGGTCCAGCCCAGTGGT	
4	MMP2 F	TGGCAAGTACGGCTTCTGTC	63
	MMP2 R	TTCTTGTCGCGGTCGTAGTC	
5	MMP3 F	GCATAGAGACAACATAGAGCT	64
	MMP3 R	TTCTAGATATTTCTGAACAAGG	
6	MMP9 F	GGAGGTTCGACGTGAAGG	64
	MMP9 R	TCCTGGCAGAAATAGGCTTTC	
7	MMP13 F	GACTTCCCAGGAATTGGTGA	54
	MMP 13 R	TGACGCGAACAATACGGTTA	
8	NDRG1 F	ACTCCTCTGGAAAGACTTGTG	60
	NDRG1 R	AGTTGGGAGGAGGAAGTAGTCC	
9	N-cadherin F	TCGCCATCCAGACCGACCCA	64
	N-cadherin R	GCAGTTGACTGAGGCGGGTGC	
10	Slug F	TGGTTGCTTCAAGGACACAT	62
	Slug R	GTTGCAGTGAGGGCAAGAA	

CHAPTER 3

RESULTS

3.1 Preparation and Characterization of NPs

Effective drug delivery systems, like NPs, which improve the potency of existing anti-cancer compounds and overcome the limitations of conventional treatments, are of utmost importance for cancer therapy. Several phytochemicals like PIP and PL show great anti-cancer potential (201, 218, 268); however, their dose-limiting toxicity and hydrophobic nature has delayed the potential use of these phytochemicals in a clinical setting. In this project, mPEG-PLGA synthetic polymers were made into NPs containing PIP and PL, using both the single emulsion solvent extraction and the thin-film hydration methods. To confirm the formation of NPs and compare the two methods, particles were negatively stained and visualized using the TEM at high magnification (Figure 3.1A and 3.1B). The thin-film hydration method resulted in the formation of NPs that were more spherical in shape and uniform in size distribution, while the NPs formed by the emulsion solvent extraction method varied greatly in size and shape (Figure 3.1C). As summarized in Table 3.1, the average size of NPs was 165.2±5.48 nm and 52.77±1.21 nm in diameter, for the emulsion solvent extraction and the thin-film hydration methods, respectively.

3.2 Encapsulation Efficiencies of PIP- and PL-NPs

Encapsulation efficiency of NPs is a parameter that is frequently measured using high performance liquid chromatography (HPLC); however, to measure the encapsulation efficiencies of PIP and PL in our NPs, we used a simple spectrophotometric method. At a certain concentration range, both PIP and PL obey the Beer-Lambert law, meaning that their absorbance is proportional to their concentration. Therefore, a standard curve was generated using a concentration range of these phytochemicals against their absorbance at 346 nm wavelength (Figure 3.2). The equation of the line of best fit for each primer allowed us to determine the unknown amount of PIP or PL in the NP samples. Using the thin-film hydration method, the encapsulation efficiencies of PIP- and PL-NPs were approximately 18% and 20%, respectively (Table 3.1). Ultimately, the stock solution of

NPs was made at the desired concentrations based on the encapsulation efficiency data. The amount of PIP and PL in NPs prepared by the emulsion solvent extraction method was very low that could not be detected using the method described above, suggesting a very low encapsulation efficiency (Table 3.1). However, stock solutions were prepared with the assumption that only 1% of PIP or PL were encapsulated into NPs. The 1% encapsulation efficiency for PIP and PL was used to determine if these NPs show any growth inhibitory effects on cancer cells or if the NPs lack PIP or PL.

3.3 PIP- and PL-NPs Prepared by the Thin-Film Hydration Method Reduce the Growth of TNBC Cells and are Comparable to Free PIP and PL

The effects of PIP- and PL-NPs, prepared by the methods described above, were compared to free PIP or PL, using the MTT assay. During this assay, mitochondrial function is used as an assessment of cellular growth and viability. The higher the number of cells present, the more MTT substrate will be metabolized by mitochondrial succinate dehydrogenase into lipid soluble formazan crystal, whose absorbance can be measured once dissolved in DMSO and interpreted as relative viable cell number. PIP- and PL-NPs formulated by the emulsion solvent extraction method did not cause the same reduction in cell growth as free PIP and PL did, after 48 hours of treatment of MDA-MB-468 cells (Figure 3.3A). While PIP-NPs showed no significant decrease in cell metabolic activity, PL-NPs exhibited a lesser effect compare to free PL (Figure 3.3A), suggesting a very low encapsulation efficiency of PL into NPs made by emulsion solvent extraction method. However, PIP- and PL-NPs prepared by the thin-film hydration method showed a similar effect on the metabolic activity of MDA-MB-468 cells as free PIP and PL did, respectively (Figure 3.3B). Based on this data, only NPs prepared by the thin-film hydration method were used for the remaining experiments.

The effectiveness of PIP- and PL-NPs prepared by the thin-film hydration method was tested in three different TNBC cell lines, which were cultured in the presence of different concentrations of free PIP or PIP-NP (50 – 150 μM) and free PL or PL-NP (2.5 – 10 μM) for 48 hours. Following treatment, the MTT assay showed a dose-dependent reduction in the number of TNBC cells (MDA-MB-468 and BT-549) by PIP and PIP-NP (Figure 3.4A and E). In MDA-MB-468 and BT-549 cells, 150 μM of PIP or PIP-NP

caused a significant reduction in metabolic activity, while MDA-MB-231 cells remained largely resistant to the growth inhibitory effects of PIP (Figure 3.4C). Similarly, BT-549 cells appeared resistant to the growth inhibition by lower concentrations of PIP, and a significant reduction in the number of viable cells is only seen at 100 - 150 μM of PIP (Figure 3.4E). As expected, cells treated with various doses PIP-NP also exhibited a very similar reduction in growth compare to free PIP. However, it is worth mentioning that high doses of empty NP significantly reduced the growth MDA-MB-468 cells (Figure 3.4A). The amounts of empty NPs used as control for each experiment were set to match the amounts of NPs in the highest concentrations of PIP-NPs and PL-NPs. Consequently, more empty NPs were used as control for 150 μM of PIP-NPs than 10 μM of PL-NPs. Ultimately, lower dose of empty NPs, used as control for 10 μM of PL-NPs, did not cause a significant reduction in growth of MDA-MB-468 cells (Figure 3.4B). Furthermore, MDA-MB-231 and BT-549 cells appeared to be more resistance to the growth inhibitory effects of high dose empty NPs (Figure 3.4C and E).

Meanwhile, PL was a more potent growth inhibitory compound against TNBC cell lines compared to PIP. As shown in Figure 3.4B, as little as 2.5 μM of PL or PL-NP resulted in a significant reduction in the metabolic activity/growth of MDA-MB-468 cells. PL and PL-NP also caused a dose-dependent reduction in the growth of MDA-MB-231 and BT-549 cells (Figure 3.4D and F). Given that 2.5 μM of PL or PL-NP did not cause a significant decrease in the growth of BT-549 cells and only a modest reduction in the growth of MDA-MB-231, this concentration of PL was considered to be minimally cytotoxic in these TNBC cell lines. Similarly, 50 μM or PIP or PIP-NP was also largely ineffective at reducing the growth of TNBC cells; hence, it was considered non-cytotoxic.

3.4 PIP- and PL-NPs Induce Apoptosis in MDA-MB-468 Breast Cancer Cells, while having Minimal Effects on the Viability of HDF Compared to Free PIP and PL

The selective growth inhibitory effects of PIP and PL against cancer cells is often associated with the induction of apoptosis (197, 218). Therefore, we aimed to examine the cytotoxic potential of PIP- and PL-NPs against MDA-MB-468 breast mammary carcinoma cells, and normal HDFs. Cells were cultured in the presence of 150 μM of PIP or PIP-NP and 10 μM of PL or PL-NP, as well as medium and vehicle controls for 48

hours, then stained with Annexin-V-FLUOS and PI. Flow cytometric analysis of MDA-MB-468 cells showed that both PIP and PL resulted in a significant increase in the percent of early apoptotic cells, as indicated by the number of Annexin-V-FLUOS positive/PI negative cells found in the bottom right quadrant (Figure 3.5A). PIP and PL also increased the percentage of Annexin-V-FLUOS/PI positive cells found in the upper right quadrant, indicating late apoptotic/necrotic cells (Figure 3.5A). While the total number of cell death was consistent between free and encapsulated PIP (approximately 40%) or PL (approximately 50%), PIP-NP and PL-NP treatment resulted in a noticeable higher percentage of early apoptotic cells and lower percentage of late apoptotic cells compared to free PIP and PL (Figure 3.5B and C).

Normal HDF cells were relatively resistant to the cytotoxic effects of 150 μM PIP, as expected, but PL resulted in a significant increase in percent cell death compared to the control cells (Figure 3.5D). Interestingly, both PIP-NP and PL-NP had less cytotoxic effect on HDF cells compared to free PIP and PL, respectively (Figure 3.5E and F). In fact, 10 μM of PL resulted in a significant increase in the number of apoptotic cells compare to the DMSO control, while 10 μM of PL-NP only caused a minor increase in the number of cell death that was not statistically significant compared to the empty NP control (Figure 3.5F). These results confirm the cytotoxic potential of PIP- and PL-NPs on MDA-MB-468 cells, while showing a less cytotoxic effect on normal HDFs compared to free PIP and PL.

3.5 Free PL and PL-NPs Inhibit the Growth of MCF-7 Mammospheres

To further examine the cytotoxic potential of PL, we used MCF-7 mammosphere, which have cancer stem-cell features, e.g., propagation in suspension cultures, and are more representative of the tumor microenvironment (269, 270). MCF-7 mammospheres, grown in appropriate culture medium for 7 days, were exposed to 10 μM of PL or PL-NP for 72 hours. Following the treatment period, cell viability was measured using the acid phosphatase assay, which measures the activity of cytosolic acid phosphatase as an indicator of the viable cell number. As shown in Figure 3.6A, PL- and PL-NP-treated spheroids were smaller compared to control spheroids and were surrounded by floating

dead cells. PL and PL-NP significantly impaired the growth these spheroids in a similar manner, compared to their respective vehicle controls (Figure 3.6B).

3.6 Non-cytotoxic Doses of PL and PL-NPs Interfere with the Migration and Invasive Potential of MDA-MB-231 Cells

Migration and invasion of tumor cells are essential components of the invasion-metastasis cascade during cancer progression (55). To investigate the anti-metastatic potential of PIP and PL, we performed gap closure and trans-well invasion assays with MDA-MB-231 cells using non-cytotoxic doses of PIP and PL. While vehicle-treated MDA-MB-231 cells filled the gap by 18 hours following insert removal, 50 μM of PIP or PIP-NPs and 2.5 μM of PL or PL-NPs drastically impaired the migration of MDA-MB-231 into the gap (Figure 3.7). In addition, PL and PL-NPs significantly reduced the chemoattractant-induced migration of MDA-MB-231 cells through an uncoated membrane in a trans-well invasion assay (Figure 3.8A and B).

Next, we sought to determine the effects of PL on the invasiveness of MDA-MB-231 through components of the ECM, using the trans-well invasion assay and membranes coated with fibronectin or gelatin. As expected, 2.5 μM of PL or PL-NPs significantly decreased the invasion of MDA-MB-231 through both fibronectin- and gelatin coated membranes (Figure 3.8C and E). Compared to the vehicle controls, both PL and PL-NPs caused a 50 – 60 % reduction in the percentage of cells migrating through ECM-coated membranes (Figure 3.8D and F).

Interestingly, treatment of MDA-MB-231 cells with 5 – 20 μM of the MMP inhibitor ARP-100 also reduced the invasion of these cells through a gelatin-coated membrane (Figure 3.9). Therefore, the effects of PL and PL-NPs on the expression matrix-degrading proteases involved in breast cancer metastasis, e.g., MMP-2, MMP-3, MMP-9 and MMP-13, was examined using qRT-PCR. Non-cytotoxic doses of PL and PL-NPs significantly reduced the mRNA expression of MMP-2 (Figure 3.10A). However, PL or PL-NPs failed to decrease the mRNA expression of MMP-9 and MMP-13 (Figure 3.10C and D), while mRNA expression of MMP-3 was slightly increased by 2.5 μM PL-NPs (Figure 3.10B). These results indicate that non-cytotoxic doses of PIP- and PL-NPs decreased migration and invasion of MDA-MB-231 cells, and PL's

inhibitory effect on MDA-MB-231 cell invasion could be mediated through suppression of MMP-2 expression.

3.7 Expression of EMT-TFs and Mesenchymal Markers in TNBC Cells is Decreased by PL and PL-NPs

The process of EMT is central to tumor invasion and metastasis (95). The role of EMT-TFs like ZEB1 and Slug in loss of epithelial marker E-cadherin and gain of mesenchymal phenotype is outlined in Chapter 1.4. Since PL was a more potent phytochemical compared to PIP, we decided to determine if PL had any inhibitory effects on the already mesenchymal phenotypes observed in MDA-MB-231 and BT-549 breast mammary carcinoma cells. Low doses of PL and PL-NPs (2.5 μM) significantly reduced the protein levels of ZEB1, β-catenin, and Slug in MDA-MB-231 (Figure 3.11A-D) and BT-549 (Figure 3.11E-H) cells. Although, PL had no significant effect on the β-catenin protein levels in BT-549 cells (Figure 3.11G), ZEB1 and Slug protein levels in these cells were decreased to a greater extent compared to MDA-MB-231 cells when treated with PL or PL-NP.

To confirm that these changes in EMT-TFs following PL treatment also affected the mesenchymal markers of cancer cells, the protein levels of N-cadherin was analyzed in PL-treated MDA-MB-231 cells using western blotting. As shown in Figure 3.12A-B, low doses of PL and PL-NPs (5.0 μM) decreased the protein levels of N-cadherin. To our surprise, qRT-PCR analysis showed that mRNA expression of N-cadherin was increased in MDA-MB-231 cells following treatment with low dose of PL and PL-NPs (5.0 μM) (Figure 3.13). These findings demonstrate that PL and PL-NPs inhibit EMT in TNBC cells.

The use of multiple doses of 5.0 μM PL on MDA-MB-231 cells instead of the 2.5 μM dose was to establish the effectiveness of PL at a higher dose, since some of the expected PL targets were not affected much by the 2.5 μM of PL. Although the cytotoxicity of 5.0 μM of PL on MDA-MB-231 cells was not directly tested, cells appeared healthy with some growth reduction effects seen following three treatments of PL at 5.0 μM.

3.8 Effects of PL and PL-NPs on the TGF-β and the Wnt Signaling Pathways

The TGF-β/Smad and the Wnt/β-catenin signaling pathways are among the main mediators of the EMT (95), particularly in breast cancer (271). NDRG1 is a well-known metastasis suppressor that has been implicated in inhibition of the TGF-β and Wnt pathways during EMT (149, 150). To determine if PL had any effects on NDRG1 expression, MDA-MB-231 cells were treated with low dose of PL or PL-NPs (5.0 μM) for 72 hours. As determined by western blotting, PL and PL-NPs increased the expression of NDRG1 at the protein level (Figure 3.14A and B). PL and PL-NPs also increased the mRNA level of NDRG1 by 5-8-fold compared to the vehicle control (Figure 3.14C). Similarly, the protein levels of Smad3, which is an essential component of the canonical TGF-β/Smad pathway, was decreased in MDA-MB-231 cells following treatment with PL or PL-NPs (Figure 3.12C and D). These results suggest that PL and PL-NPs may inhibit TGF-β/Smad and the Wnt/β-catenin signaling pathways through regulation of NDRG1 and Smad3 protein levels.

3.9 E-cadherin Expression is Restored in MDA-MB-231 Cells, but not in BT-549 Cells, Following Treatment with PL

Loss of E-cadherin expression is the hallmark of EMT. Associated with poor clinical outcome, E-cadherin suppression is sufficient to a induce metastatic phenotype in otherwise non-metastatic cancer cells (67). Since PL decreased the migration and invasiveness of MDA-MB-231cells, as well as the cellular protein levels of several key EMT-TFs, including ZEB1 and Slug, we sought to determine the effects of PL on E-cadherin expression in TNBC cells. As shown in Figure 3.15A, 2.5 μM of PL resulted in up to a 4-fold increase in E-cadherin mRNA expression. A similar dose of PL-NPs also caused a significant upregulation in E-cadherin mRNA expression, compared to empty NP control (Figure 3.16). However, PL was unable to increase E-cadherin expression in BT-549 cells (Figure 3.15D). PL also failed to change Slug and cMyc mRNA expression in MDA-MB-231 cells (Figure 3.15B and C). PL- and PL-NPs-mediated upregulation of E-cadherin mRNA expression in MDA-MB-231 cells is consistent with their EMT-inhibitory effects in these cells.

3.10 TGF-β-induced Mesenchymal Change in MCF-10A Cells is not Inhibited by PL

To determine if the EMT inhibitory effects of PL also impact non-cancerous cells, we used the immortalized MCF-10A mammary epithelial cells as our model. MCF-10A cells undergo EMT when cultured in the presence of TGF-β (272). To confirm this effect, we treated MCF-10A cells with 5.0 ng/mL of human TGF-β, and examined their cellular morphology after 48 hours. As shown in Figure 3.17A, MCF-10A epithelial cells appeared more mesenchymal in the presence of TGF-β, as the cells had lost their cell-cell contact and appeared more spindle-shaped. Western blot analysis of these cells revealed that mesenchymal markers such as N-cadherin and vimentin were upregulated by 2-4-fold in these cells following TGF-β treatment (Figure 3.17B, C and E); however, the protein levels of β-catenin and Slug were not changed relative to the vehicle control in these cells (Figure 3.17B, D and F).

Interestingly, pre-treatment of MCF-10A cells with 2.5 μM of PL did not interfere with TGF-β signaling as N-cadherin and vimentin protein levels remained elevated following treatment with both PL and TGF-β (Figure 3.17C and E). In fact, PL alone had no effect on the N-cadherin, β-catenin, vimentin, and Slug protein levels in MCF-10A cells. Similarly, TGF-β induced N-cadherin mRNA upregulation by about 3-fold relative to the control, and pre-treatment with PL had no effect on TGF-β-induced N-cadherin expression (Figure 3.18A). Contrary to the effects that I saw with N-cadherin expression, E-cadherin expression did not change in the presence of TGF-β and/or PL in MCF-10A cells (Figure 3.18B).

Next, we sought to determine if the effect of PL on MMP expression in MDA-MB-231 cells is also seen in MCF-10A cells. As expected, expression of MMP-2, MMP-9, and MMP-13 were significantly upregulated, compare to vehicle control, in TGF-β-treated MCF-10A cells (Figure 3.19A, C and D). MMP-3 expression was also upregulated by about 2-fold; however, this effect was not statistically significant (Figure 3.19B). Consistent with the effects of PL on MMP expression in MDA-MB-231 cells, PL significantly inhibited TGF-β-induced MMP-2 expression, while the mRNA expressions of MMP-3, MMP-9, and MMP-13 did not change significantly in TGF-β/PL treated cells,

when compared to the TGF-β treated MCF-10A cells. These results suggest that PL-mediated inhibition of EMT is cancer-cell specific.

3.11 PL and PL-NP Modulate the Expression of HDAC and DNMT-1 Proteins in TNBC and MCF-10A Cells

As mentioned earlier, epigenetic modification plays a key role during EMT and tumor progression (273). Give the reversible nature of epigenetic changes and the possible role of dietary phytochemicals in modulating the cancer cell epigenome (193), we decided to investigate the effects of PL and PL-NPs on the expression of HDAC and DNMT proteins in TNBC cells and MCF-10A cells. Interestingly, non-cytotoxic dose of PL significantly decreased HDAC-1, HDAC-4, and HDAC-6 protein levels in MDA-MB-231 cells, while levels of HDAC-2 and HDAC-3 proteins were not affected (Figure 3.20A-F). Although not significant, multiple repeats showed a trend towards decreased protein levels of HDAC-1 and HDAC-4 in MDA-MB-231 cells following treatment with 2.5 μM PL-NPs (Figure 3.20B and E). At non-cytotoxic doses, PL and PL-NPs did not affect the levels of HDAC-1 protein in BT-549 cells, as shown in Figure 3.20G and H. However, HDAC-4 and HDAC-6 protein levels were still significantly downregulated by PL in BT-549 cells (Figure 3.20K and L). Non-cytotoxic doses of PL-NPs also significantly decreased the protein levels of HDAC-4, while only a trend towards decrease in HDAC-6 protein levels was observed in BT-549 cells.

The effect of PL and PL-NPs on the epigenetic machinery was not cancer-cell specific. As shown in Figure 3.21, non-cytotoxic doses of PL and PL-NPs caused a decrease in the protein levels of HDAC-4 and HDAC-6 in MCF-10A cells. PL also appeared to significantly decrease the levels of HDAC-2 protein in MCF-10A cells, while HDAC-1 and HDAC-3 levels remained unchanged (Figure 3.21).

Furthermore, we examined the protein levels of DNMT-1 in PL-treated TNBC and MCF-10A cells. Figure 3.22 shows that low doses of PL and PL-NPs decreased the levels of DNMT-1 protein in MDA-MB-231 and MCF-10A cells; however, DNMT-1 protein expression in BT-549 cells was not significantly changed following treatment with 2.5 μM of PL and PL-NPs (Figure 3.22C and D).

3.12 PL-induced Expression of E-cadherin in MDA-MB-231 Cells may be Independent of HDAC-1 and DNMT-1 Protein Levels

Since PL decreased HDAC-1 and DNMT-1 protein expression while increasing the expression of E-cadherin in MDA-MB-231 cells, I decided to further study the possible mechanism of PL-induced E-cadherin expression in MDA-MB-231 cells. We hypothesized that if the PL-mediated increase in E-cadherin expression is mediated through suppression of HDAC-1 or DNMT-1, overexpression of these proteins should reduce the enhancing effect of PL on E-cadherin expression in MDA-MB-231 cells. Therefore, I transfected MDA-MB-231 cells with plasmids containing genomic sequences of human HDAC-1 (flag-tagged) or DNMT-1 (myc-tagged) for 48 hours. These cells were then cultured with 2.5 μM of PL at 24 hours post-transfection, and continued for 48 hours. Following the treatment period, cellular proteins and mRNA were isolated from cells and analyzed by western blotting and qRT-PCR.

Figure 3.23A and B shows that MDA-MB-231 cells were successfully transfected, as higher protein levels of HDAC-1 and DNMT-1 was observed in cells transfected with the respective plasmids, compared to the cells transfected with empty vector. Although, the enhancing effect of PL on E-cadherin mRNA expression was not statistically significant with the empty vector-transfected cells, multiple repeats of the experiment showed a trend that PL had a similar effect on E-cadherin expression in HDAC-1 or DNMT-1 transfected cells (Figure 3.23C-D). These results suggest that overexpression of HDAC-1 or DNMT-1 may not affect PL-induced E-cadherin expression in MDA-MB-231 cells, and the induction of E-cadherin in PL-treated MDA-MB-231 cells may be independent of the PL-mediated suppression of HDAC-1 and DNMT-1.

Figure 3.1 Particle size distribution for the NPs prepared by emulsion solvent extraction and thin-film hydration methods.

Following preparation and lyophilization, NPs were re-dissolved in water, subjected to negative staining, and viewed under TEM. (A) NPs prepared by emulsion solvent extraction and (B) NPs prepared by the thin-film hydration method are shown with 80,000X magnification. (C) Particle size was measured using the AMT Image Capture Engine (version 7.0, AMT Crop. USA), and 90 random particles were selected from each group for measuring the average particle size ($p<0.0001$, two-tailed student *t*-test).

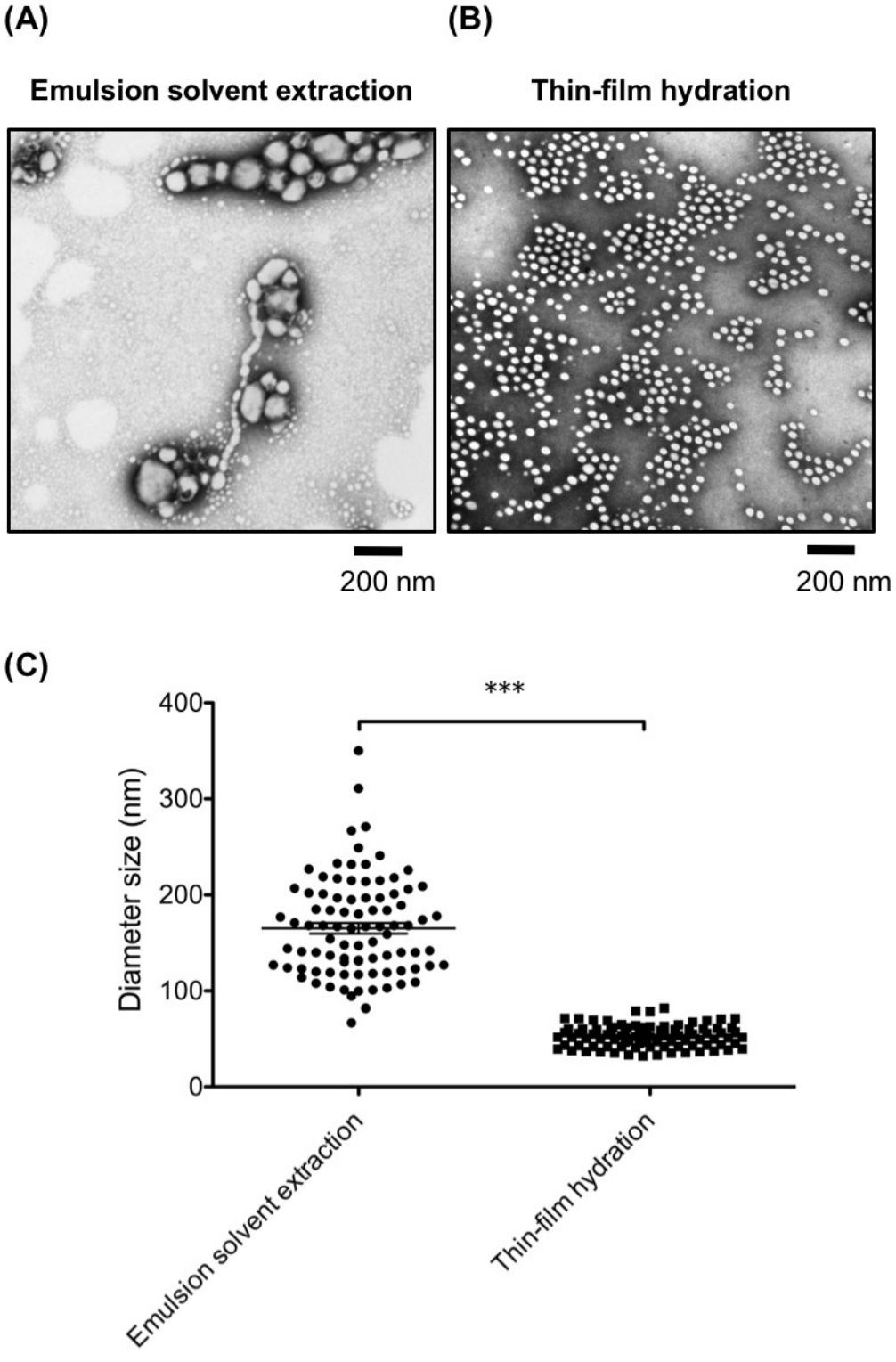
(A)
(B)
Emulsion solvent extraction
Thin-film hydration
200 nm
200 nm
(C)
***
Diameter size (nm)
400
300
200
100
0
Emulsion solvent extraction
Thin-film hydration

Figure 3.1

Figure 3.2 Standard curves for determining the relationship between PIP or PL concentrations and their optical density.

The absorbance for various concentrations of PIP or PL dissolved in DMSO, were measured and a standard curve was generated using the average of four independent trials (n=4). Using the linear regression, the relationship between intensity and concentration is shown as a line of best-fit. The equation of the line and R^2 value for each phytochemical was prepared using GraphPad Prism analysis software (version 5.0, GraphPad Software Inc., La Jolla, CA). The equation of the line was used to determine the concentration of PIP or PL in NP samples and ultimately determine the encapsulation efficiency.

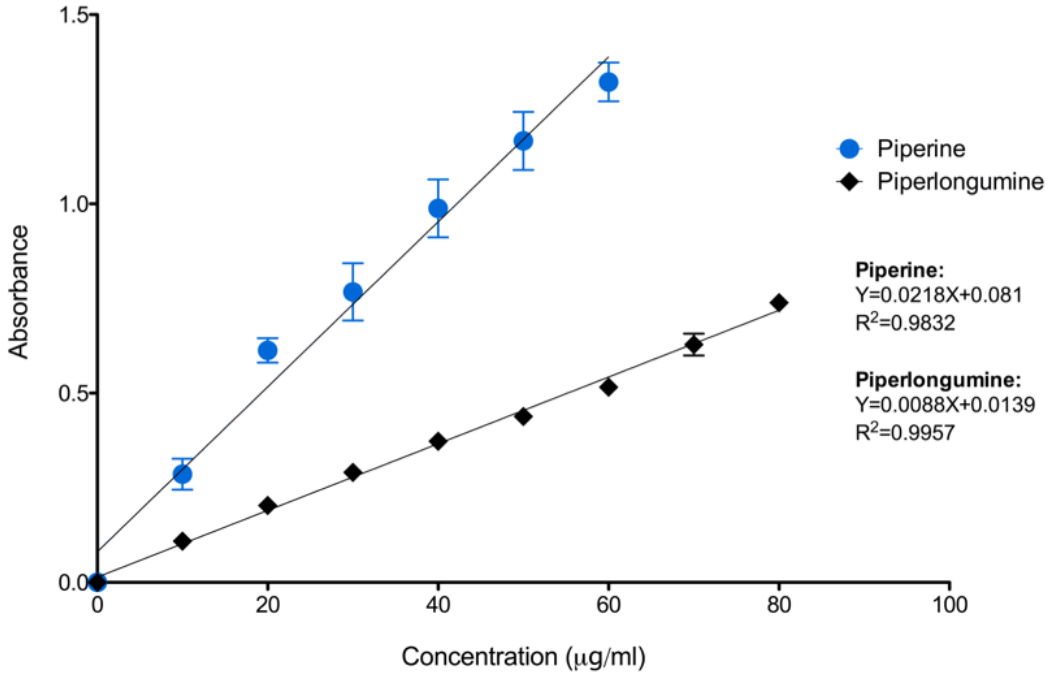
1.5
1.0
0.5
0.0
Absorbance
0
20
40
60
80
100
Concentration (µg/ml)
Piperine
Piperlongumine
Piperine:
Y=0.0218X+0.081
R2=0.9832
Piperlongumine:
Y=0.0088X+0.0139
R2=0.9957

Figure 3.2

Table 3.1 NP size distribution and the drug encapsulation efficiencies of the PIP- and PL-NPs prepared by emulsion solvent extraction and thin-film hydration methods.

Preparation method	Size range (nm)	Average NP size (nm) ±SEM	Encapsulation efficiency
Emulsion solvent extraction	66.9 – 350.0	165.2 ± 5.48	Not detectable
Thin-film hydration	32.2 – 82.0	52.77 ± 1.21	18 ± 2 % (PIP) 20 ± 1 % (PL)

Figure 3.3 PIP- or PL-NPs prepared by the thin-film hydration method are more effective at reducing the metabolic activity of MDA-MB-468 cells than those prepared by the emulsion solvent extraction method.

PIP or PL induced reduction in the metabolic activity of MDA-MB-468 was measured using the MTT assay. (A) For NP samples prepared by the emulsion solvent extraction method, the encapsulation efficiency was assumed at 1%, and the cells were treated with 150 μM of PIP or PIP-NP, 10 μM of PL or PL-NP, along with empty NP, DMSO, and medium controls. (B) For NP samples prepared by the thin-film hydration method, encapsulation efficiencies were first measured using spectrophotometric techniques, samples were then diluted to desired concentrations, and cells were treated with 75 μM of PIP or PIP-NP, 10 μM of PL or PL-NP, along with empty NP, DMSO, and medium controls. Following the treatment period of 48 hours, MTT reagent was added to the cells for additional two hours, and the formazan crystals were dissolved in DMSO. The absorbance values were normalized relative to the medium control. Data represents mean values ± SEM of three independent trials. Asterisks indicate significant reduction in cells' metabolic activity as determined by ANOVA with the Tukey multiple comparisons post-test (PIP- or PL- treated cells were compared to DMSO control, while PIP-NP- or PL-NP-treated cells were compared to empty NP control).

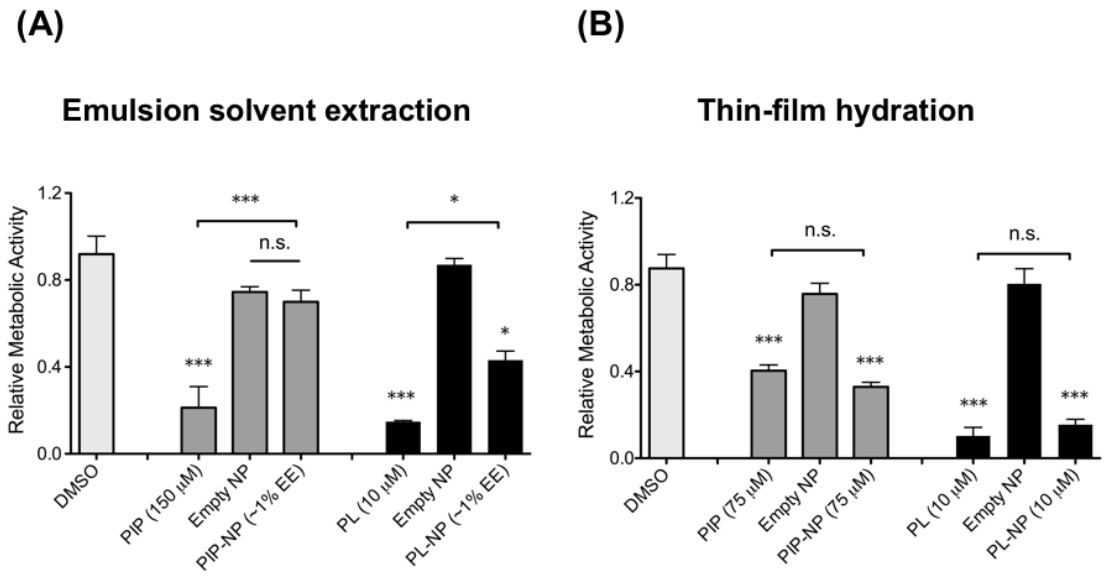
(A)
Emulsion solvent extraction
Relative Metabolic Activity
1.2
0.8
0.4
0.0
***
n.s.
*
***
***
*
DMSO
PIP (150 μM)
Empty NP
PIP-NP (~1% EE)
PL (10 μM)
Empty NP
PL-NP (~1% EE)
(B)
Thin-film hydration
Relative Metabolic Activity
1.2
0.8
0.4
0.0
n.s.
n.s.
***
***
***
***
DMSO
PIP (75 μM)
Empty NP
PIP-NP (75 μM)
PL (10 μM)
Empty NP
PL-NP (10 μM)

Figure 3.3

Figure 3.4 PIP- and PL-NPs prepared by the thin-film hydration method are as effective as free PIP and PL in reducing the metabolic activity and growth of TNBC cells.

The growth inhibitory and effectiveness of PIP- and PL-NPs were tested against a panel of TNBC cell lines including (A-B) MDA-MB-468, (C-D) MDA-MB-231, and (E-F) BT-549, using the MTT assay. Cells were seeded at 5 x 10^3 cells/well density in a flat-bottom 96-well plate and incubated overnight. The following day, cells were treated with various concentrations of free PIP or PIP-NP (50 μM – 150 μM) and free PL or PL-NP (2.5 μM – 10 μM) for 48 hours. At the end of the treatment period, MTT reagent was added to the cells for additional two hours, and the formazan crystals were dissolved in DMSO. The absorbance values were normalized relative to the medium control. Data represents mean values ± SEM of three independent trials. Asterisks indicate significant reduction in cells' metabolic activity as determined by ANOVA with the Tukey multiple comparisons post-test (PIP- or PL- treated cells were compared to DMSO control, while PIP-NP- or PL-NP-treated cells were compared to empty NP control).

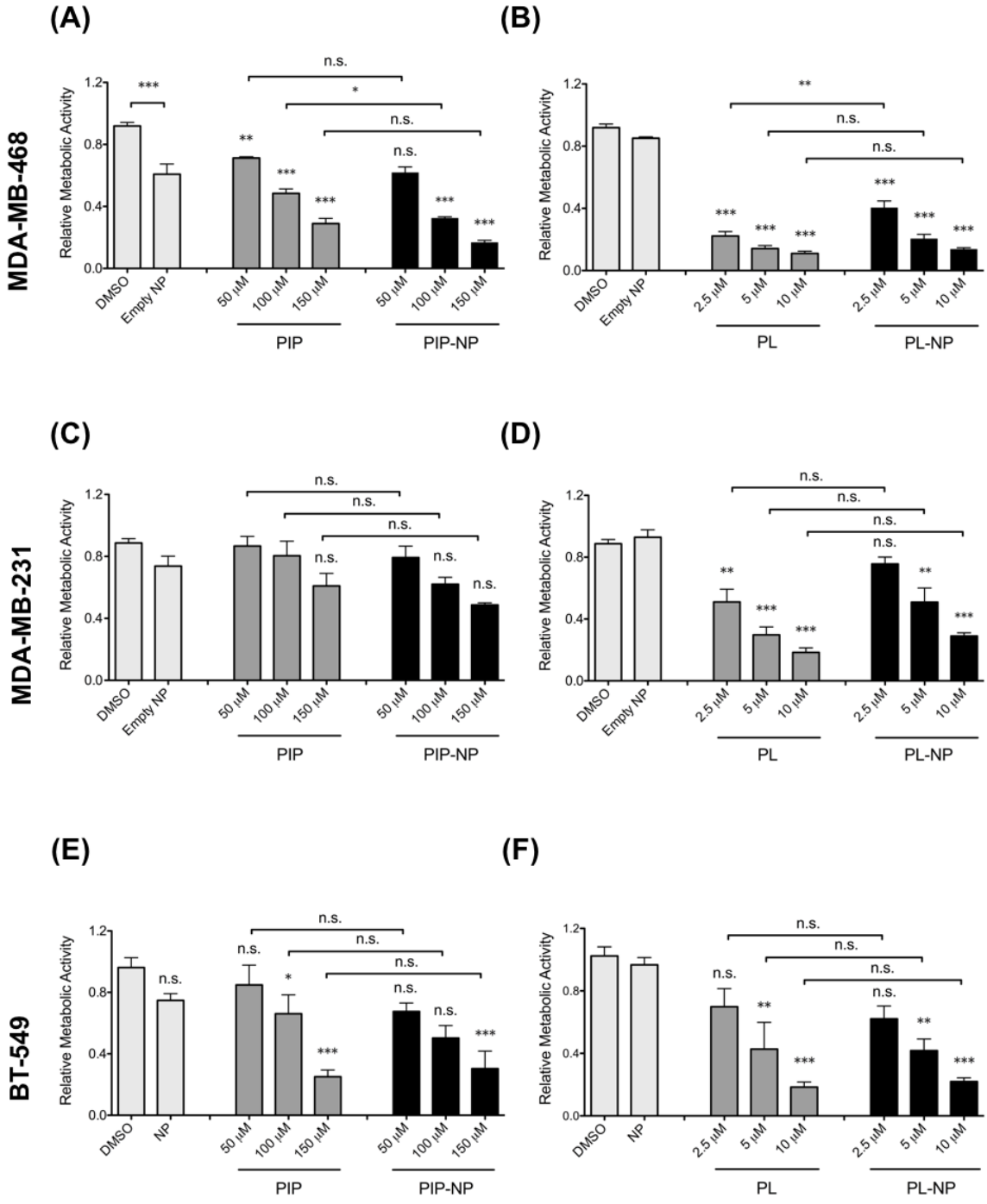
(A)
(B)
(C)
(D)
(E)
(F)
MDA-MB-468
MDA-MB-231
BT-549
Relative Metabolic Activity
DMSO
Empty NP
NP
50 μM
100 μM
150 μM
2.5 μM
5 μM
10 μM
PIP
PIP-NP
PL
PL-NP
n.s.

Figure 3.4

Figure 3.5 PIP- and PL-NPs reduce the viability of MDA-MB-468 cells while having minimal effects on HDF cells, compared to free PIP or PL.

The cytotoxicity of PIP- and PL-NP was tested in (A-C) MDA-MB-468 and (D-F) HDF cell lines, using the Annexin-V-FLUOS/PI apoptosis assay. Cells were seeded at 5 x 10^4 cells/well density in a 6-well plate and incubated overnight for adhesion. The following day, cells were treated with 150 μM of free PIP or PIP-NP or 10 μM of free PL or PL-NP for 48 hours. Then, cells were harvested and stained with Annexin-V/PI, and their fluorescence was measured using flow cytometry. Unstained cells, Annexin-V-FLUOS single-stained cells, and PI single stained cells were used as proper controls to compensate for the overlapping spectra of Annexin-V and PI. Cells that were stained with Annexin-V were counted as early apoptotic cells, and cells positive for both Annexin-V and PI were considered late apoptotic/necrotic cells. (A) and (D) show flow cytometry dot plots of a representative experiment while (B-C) and (E-F) are the mean percent of cell death ± SEM of three independent trials. Asterisks indicate significant increase in cell death as determined by ANOVA with the Tukey multiple comparisons post-test (PIP- or PL- treated cells were compared to DMSO control, while PIP-NP- or PL-NP-treated cells were compared to empty NP control).

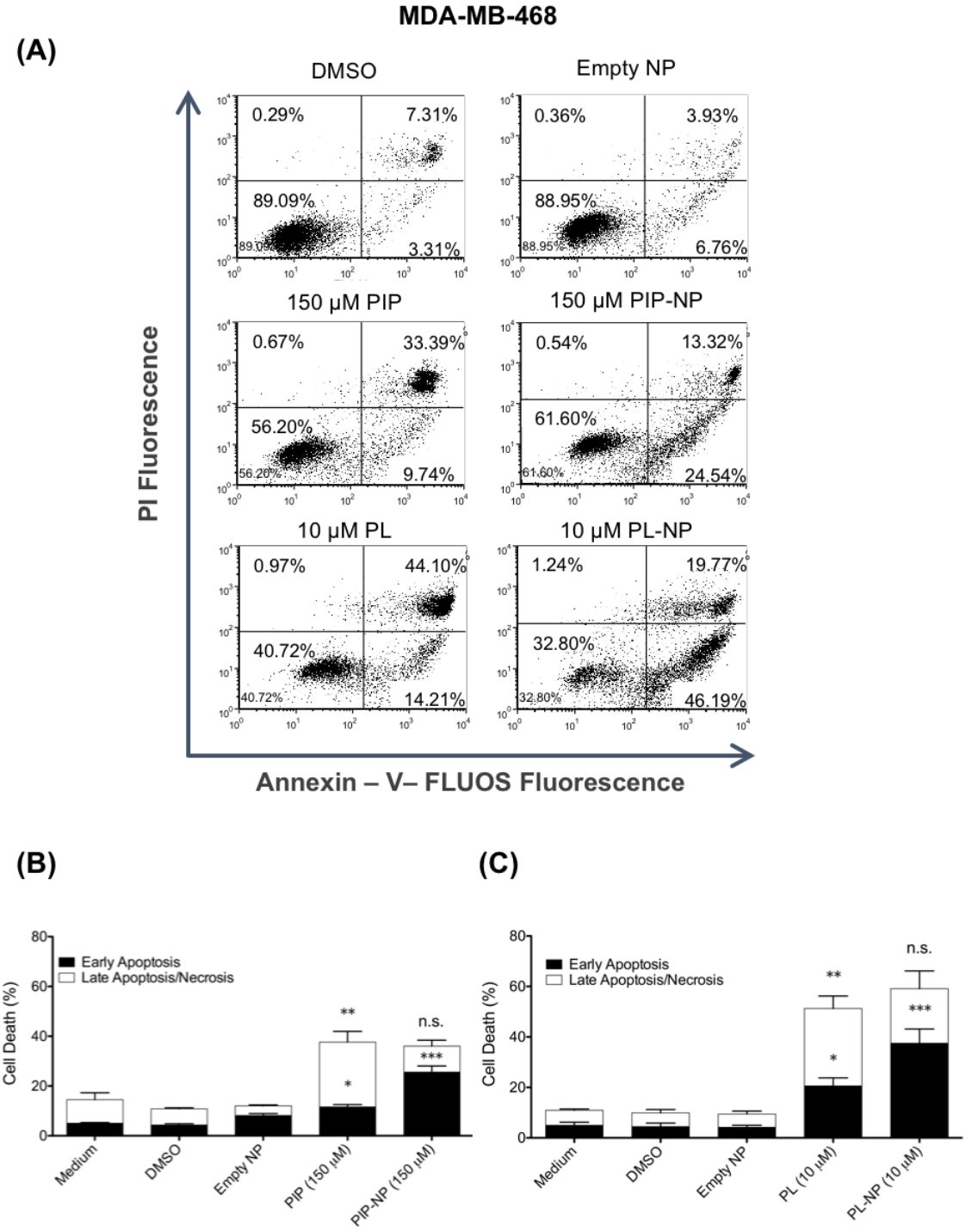
MDA-MB-468
(A)
DMSO
Empty NP
0.29%
7.31%
89.09%
3.31%
0.36%
3.93%
88.95%
6.76%
150 μM PIP
150 μM PIP-NP
0.67%
33.39%
56.20%
9.74%
0.54%
13.32%
61.60%
24.54%
10 μM PL
10 μM PL-NP
0.97%
44.10%
40.72%
14.21%
1.24%
19.77%
32.80%
46.19%
PI Fluorescence
Annexin – V– FLUOS Fluorescence
(B)
(C)
Early Apoptosis
Late Apoptosis/Necrosis
Cell Death (%)
Medium
DMSO
Empty NP
PIP (150 μM)
PIP-NP (150 μM)
PL (10 μM)
PL-NP (10 μM)
n.s.

Figure 3.5

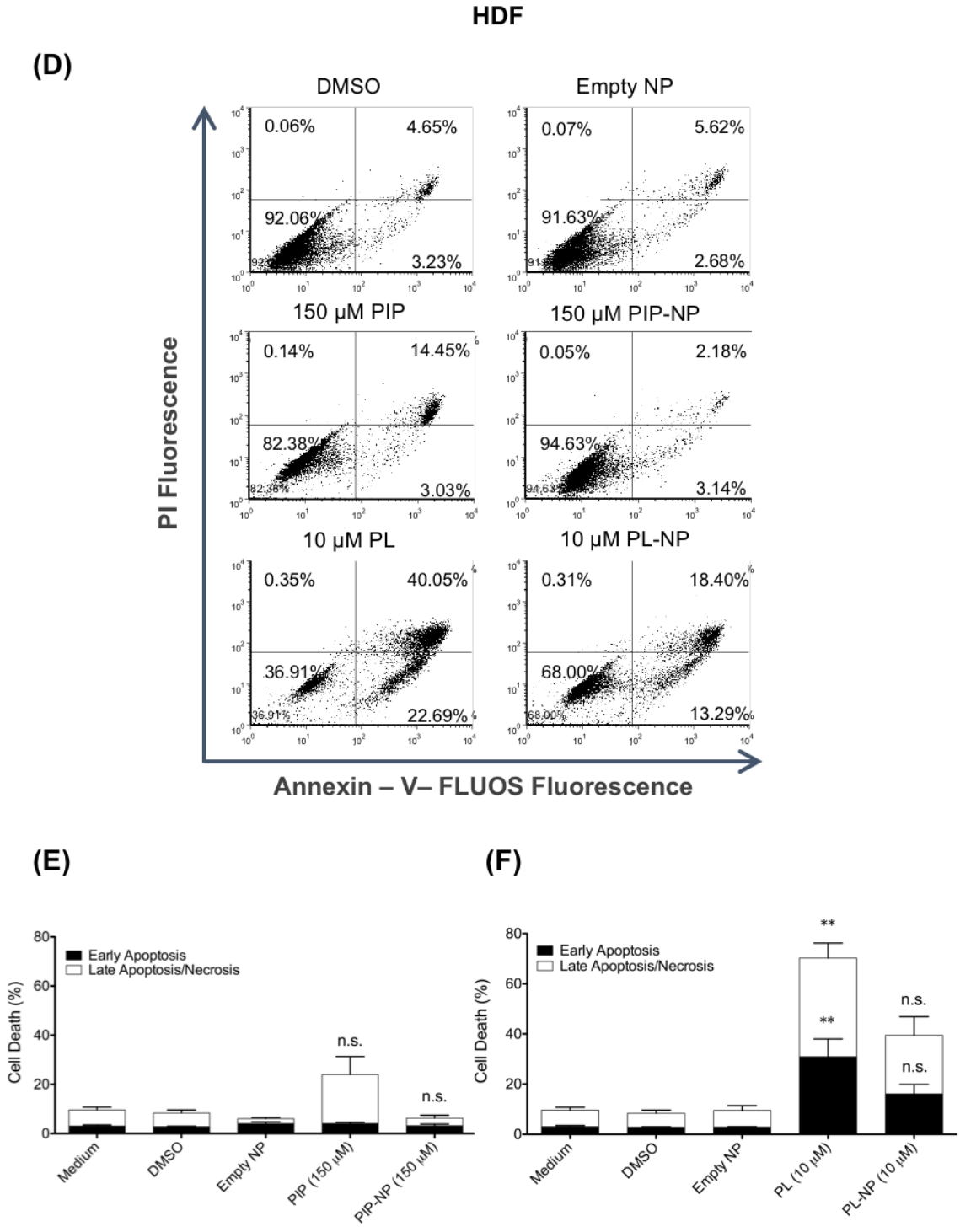

Figure 3.5 continued

Figure 3.6 PL-NPs inhibit the growth of MCF-7 mammospheres.

The cytotoxic potential of free PL and PL-NP was further examined on MCF-7 mammosphere cultures using the acid phosphatase assay. MCF-7 cells were seeded at the density of 3 x 10^4 cells/well in ultra-low attachment 6-well plates, to allow mammospheres to develop for 7 days. Spheroids were then treated with 10 μM of free PL or PL-NP for 72 hours. (A) Following the treatment period, the mammospheres were photographed with 20X magnification. (B) Then, the cell viability was determined using a modified acid phosphatase colorimetric assay. Following treatment, cells were lysed and incubated with acid phosphatase substrate for 90 minutes. Later, the optical density of samples was measured as percentage of phosphatase activity or the number of viable cells. Data shown is the mean values of treatments (normalized relative to medium control) ± SEM of 4 independent trials. Asterisks indicate a significant reduction in viable cell number as determined by ANOVA with the Bonferroni multiple comparisons post-test.

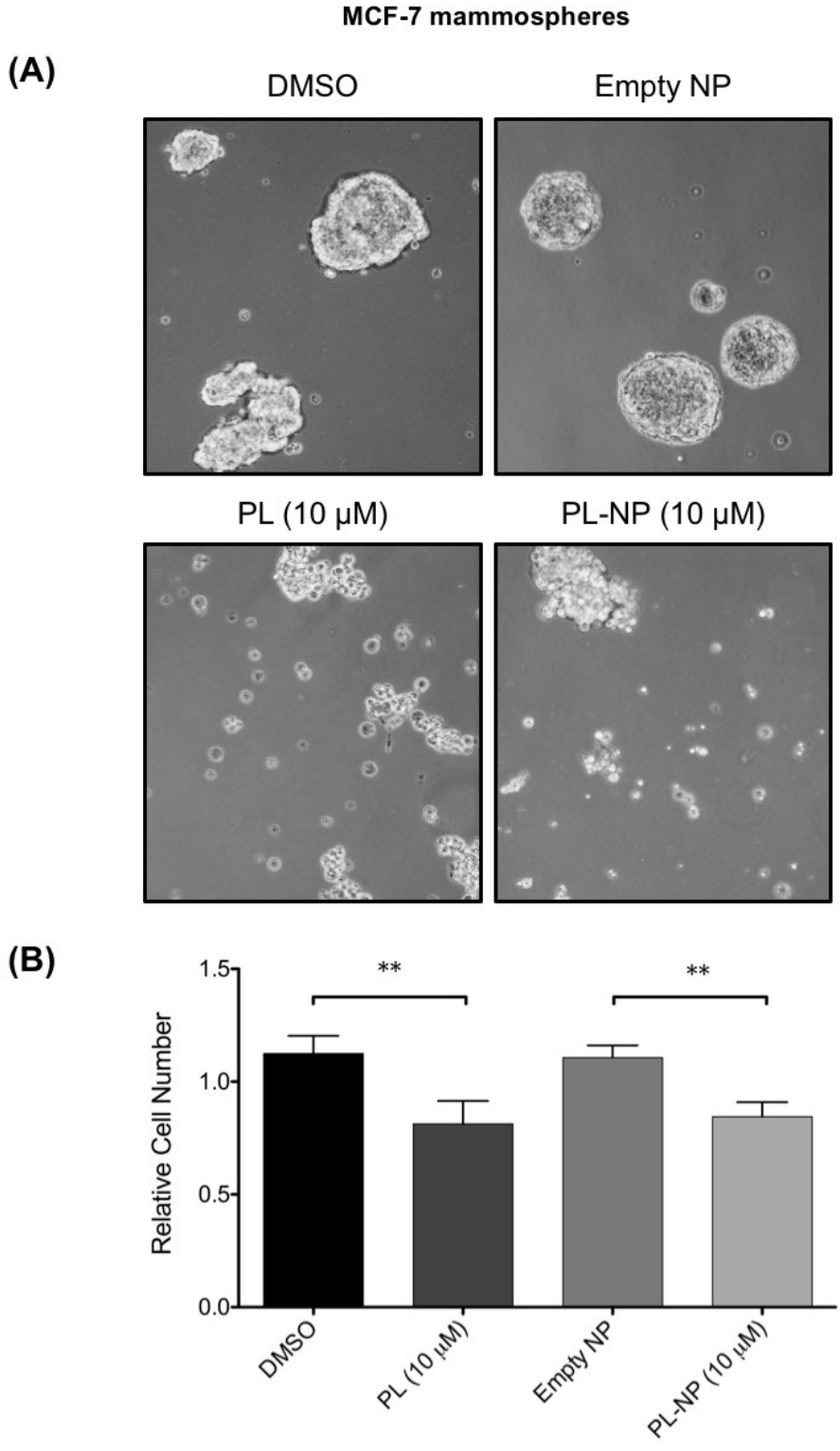
MCF-7 mammospheres
(A)
DMSO
Empty NP
PL (10 μM)
PL-NP (10 μM)
(B)
Relative Cell Number
1.5
1.0
0.5
0.0
**
**
DMSO
PL (10 μM)
Empty NP
PL-NP (10 μM)

Figure 3.6

Figure 3.7 Low doses of PIP- and PL-NPs inhibit the migration of MDA-MB-231 breast mammary carcinoma cells.

The effects of PIP and PL on MDA-MB-231 cells was tested at non-cytotoxic doses, using the gap closure assay. MDA-MB-231 cells were seeded in 2-well culture inserts at the density of 1 x 10^4 cells/well. The following day, cells were treated with 10 μg/mL of mitomycin C for 2 hours to stop cellular proliferation. Following mitomycin C treatment and 12 hours of recovery in cDMEM, cells were treated with indicated concentrations of free PIP or PIP-NP and free PL or PL-NP for 24 hours. Then, the culture inserts were removed and cells were left in treatment cDMEM. (A) Cells were photographed immediately following insert removal, (B) and at 18 hours post-insert removal, with a 20X magnification objective. Experiment was repeated 3 times, and images from a representative trial is shown in this figure.

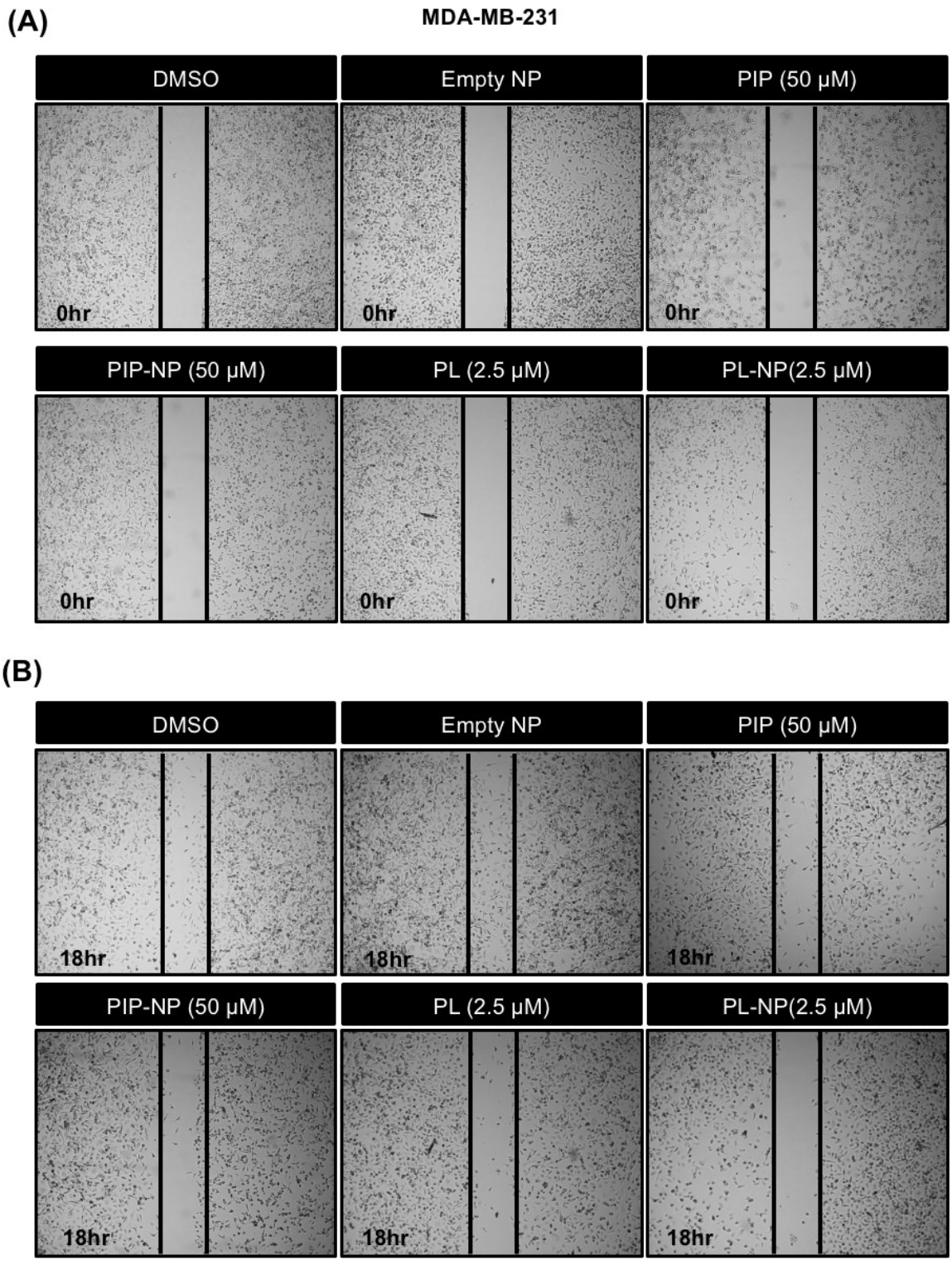
(A)
MDA-MB-231
DMSO
Empty NP
PIP (50 μM)
0hr
0hr
0hr
PIP-NP (50 μM)
PL (2.5 μM)
PL-NP(2.5 μM)
0hr
0hr
0hr
(B)
DMSO
Empty NP
PIP (50 μM)
18hr
18hr
18hr
PIP-NP (50 μM)
PL (2.5 μM)
PL-NP(2.5 μM)
18hr
18hr
18hr

Figure 3.7

Figure 3.8 The migratory and invasiveness of MDA-MB-231 cells are significantly decreased by non-cytotoxic doses of free PL or PL-NP.

A chemotaxis assay was used to investigate the effects of PL on breast cancer cell migratory and invasiveness. MDA-MB-231 mammary epithelial cells were treated with 2.5 μM of free PL or PL-NP for 36 hours in cDMEM and 12 hours in sfDMEM. Following treatment, cells were loaded at the density of 1 x 10^6 cells/ml on to the 48-well Micro Chemotaxis apparatus. The membrane separating cells from the cDMEM was (A-B) uncoated, (C-D) coated with Fibronectin, or (E-F) coated with gelatin. Following 22 hours of incubation, membranes were scraped off of the non-migrating cells and the migrating cells were stained, photographed with a 20X magnification objective, and counted. The number of migrating cells were normalized relative to the DMSO control. Panels (A), (C), and (E) are photos from one representative experiment, while panels (B), (D), and (F) are the mean number of migrating cells ± SEM of 3 (uncoated), 5 (fibronectin-coated) and 4 (gelatin-coated) independent experiments. Asterisks indicate significant reduction in the number of invasive or migratory cells as determined by ANOVA with the Bonferroni multiple comparisons post-test, prior to normalization.

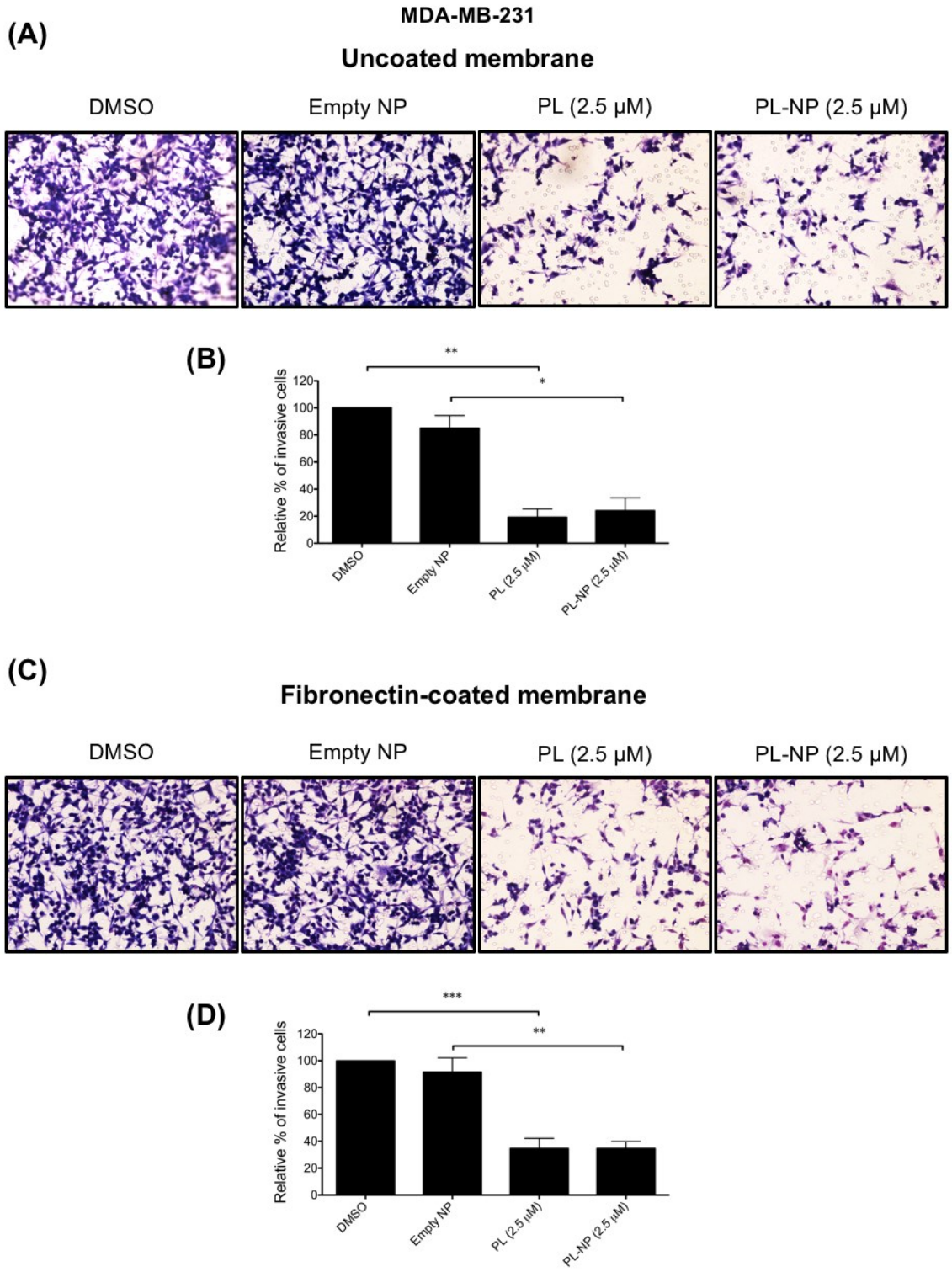
(A)
MDA-MB-231
Uncoated membrane
DMSO
Empty NP
PL (2.5 μM)
PL-NP (2.5 μM)
(B)
Relative % of invasive cells
120
100
80
60
40
20
0
**
*
DMSO
Empty NP
PL (2.5 μM)
PL-NP (2.5 μM)
(C)
Fibronectin-coated membrane
DMSO
Empty NP
PL (2.5 μM)
PL-NP (2.5 μM)
(D)
Relative % of invasive cells
120
100
80
60
40
20
0
***
**
DMSO
Empty NP
PL (2.5 μM)
PL-NP (2.5 μM)

Figure 3.8

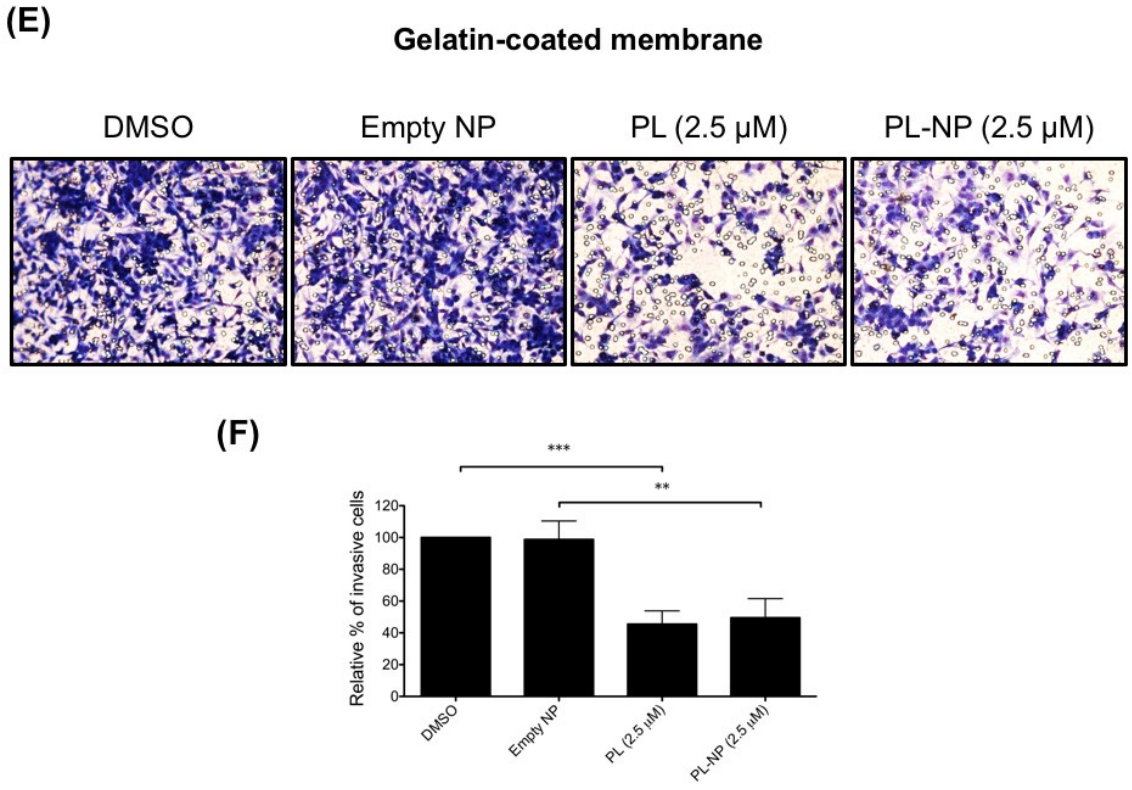

Figure 3.8 continued

Figure 3.9 ARP-100, selective MMP-2 inhibitor, also impairs the invasiveness of MDA-MB-231 breast cancer cells.

MDA-MB-231 mammary epithelial cells were treated with 5 - 20 μM of ARP-100, DMSO control for 36 hours in cDMEM and 12 hours in sfDMEM. Following treatment, cells were loaded at the density of 1 x 10^6 cells/ml on to the 48-well Micro Chemotaxis apparatus. The membrane separating cells from the cDMEM was coated with 0.05% w/v gelatin. Following 22 hours of incubation, membranes were scraped off the non-migrating cells and the migrating cells were stained, viewed under 20X magnification objective and photographed.

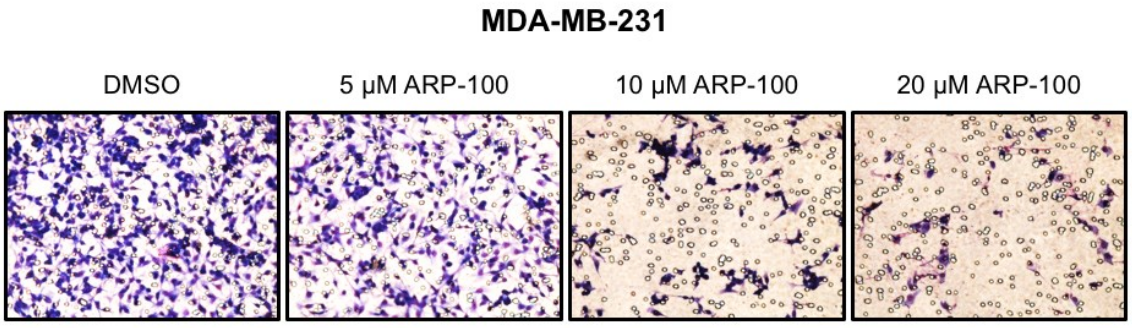

Figure 3.9

Figure 3.10 Free PL and PL-NPs modulate the mRNA expressions of MMP-2 and MMP-3 while leaving MMP-9 and MMP-13 unaffected.

MDA-MB-231 breast cancer cells were treated with 2.5 μM of free PL or PL-NPs for 48 hours, with the treatment changed every 24 hours. Following the treatment period, RNA was isolated from cells and converted to cDNA. The expression levels of (A) MMP-2, (B) MMP-3, (C) MMP-9, and (D) MMP-13 were determined using qRT-PCR. β-actin was used as the reference gene. Data shown are the mean values of mRNA expression level (normalized relative to the medium control) ± SEM of 3 independent trials. Asterisks indicate significant difference in the level of gene expression compared to the control, as determined by ANOVA with the Bonferroni multiple comparisons post-test.

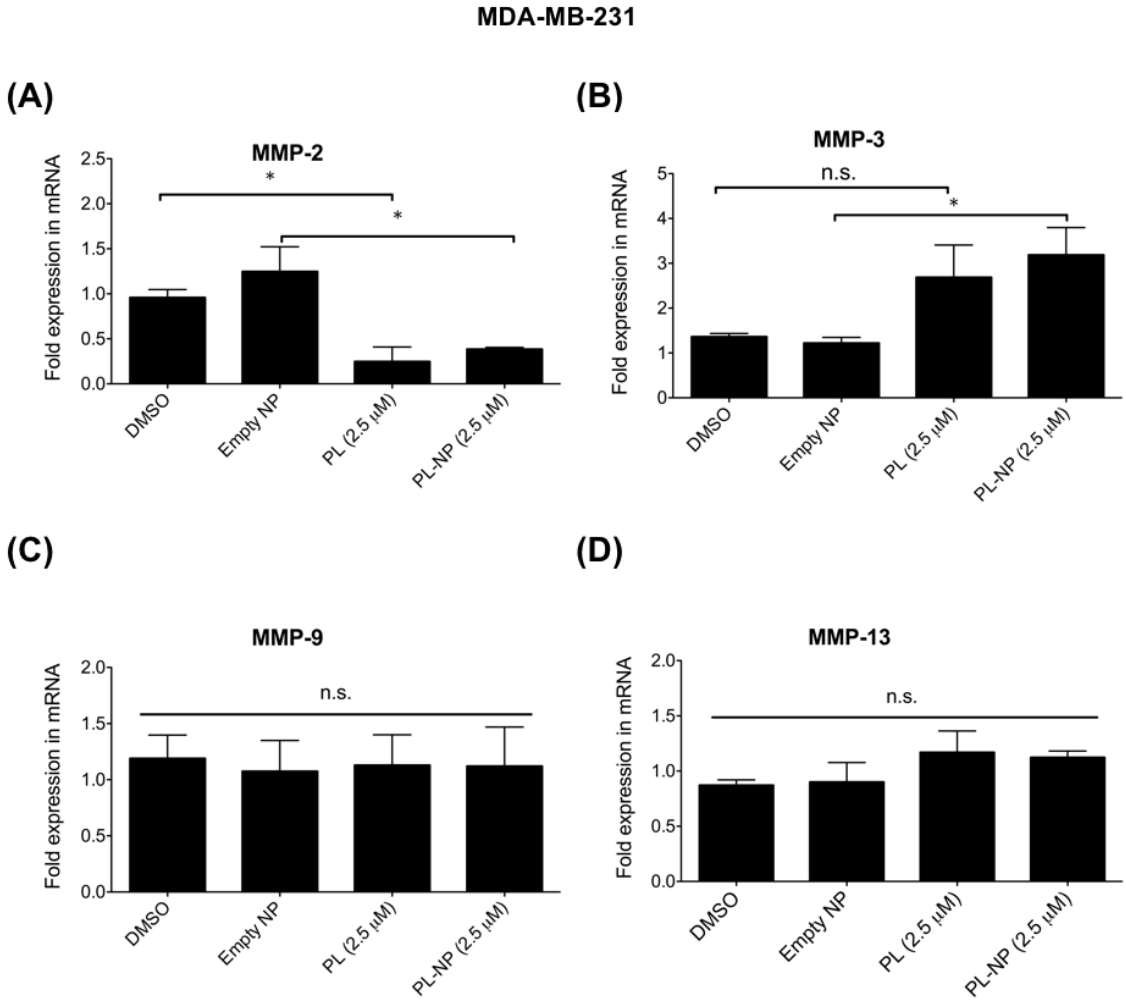
MDA-MB-231
(A)
MMP-2
Fold expression in mRNA
2.5
2.0
1.5
1.0
0.5
0.0
*
*
DMSO
Empty NP
PL (2.5 μM)
PL-NP (2.5 μM)
(B)
MMP-3
Fold expression in mRNA
5
4
3
2
1
0
n.s.
*
DMSO
Empty NP
PL (2.5 μM)
PL-NP (2.5 μM)
(C)
MMP-9
Fold expression in mRNA
2.0
1.5
1.0
0.5
0.0
n.s.
DMSO
Empty NP
PL (2.5 μM)
PL-NP (2.5 μM)
(D)
MMP-13
Fold expression in mRNA
2.0
1.5
1.0
0.5
0.0
n.s.
DMSO
Empty NP
PL (2.5 μM)
PL-NP (2.5 μM)

Figure 3.10

Figure 3.11 Protein levels of EMT-associated transcription factors are decreased by free PL and PL-NPs in MDA-MB-231 and BT-549 breast mammary carcinoma cells.

(A-D) MDA-MB-231, and (E-H) BT-549 cells were treated with 2.5 μM of free PL or PL-NPs for 48 hours. Following treatment, cells were lysed, proteins were isolated and separated by western blotting. Nitrocellulose membranes were probed with the indicated primary Abs and appropriate secondary Abs. Panels (A) and (E) are images of blots from one representative experiment, while panels (B-D) and (F-H) are mean densities of protein expression ± SEM of 3 (MDA-MB-231), and 4 (BT-549) independent experiments. Densities of the bands were normalized relative to the medium control. Asterisks indicate significant reduction in the protein levels as determined by ANOVA with the Bonferroni multiple comparisons post-test.

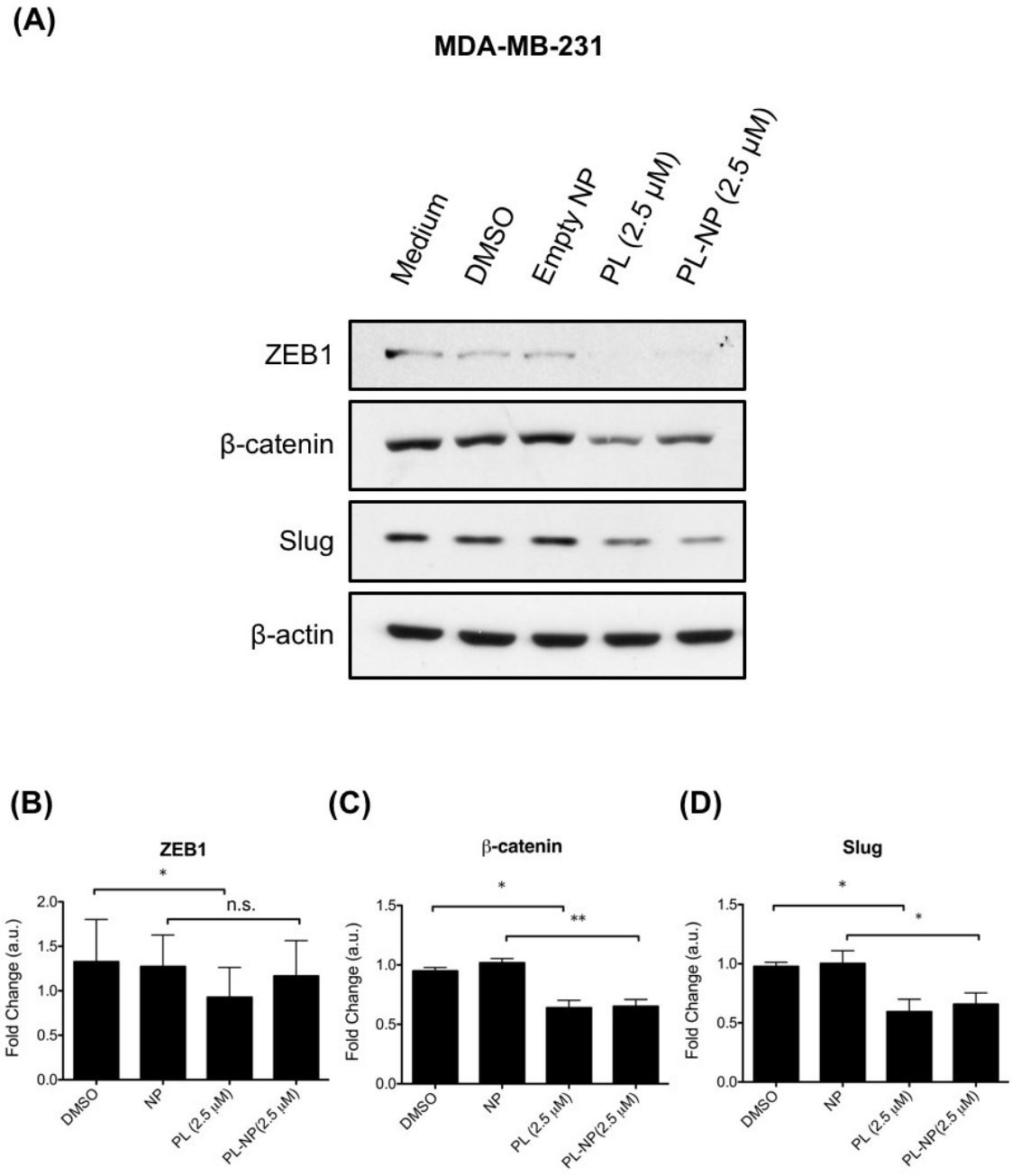
(A)
MDA-MB-231
Medium
DMSO
Empty NP
PL (2.5 μM)
PL-NP (2.5 μM)
ZEB1
β-catenin
Slug
β-actin
(B)
ZEB1
Fold Change (a.u.)
n.s.
DMSO
NP
PL (2.5 μM)
PL-NP(2.5 μM)
(C)
β-catenin
Fold Change (a.u.)
(D)
Slug
Fold Change (a.u.)

Figure 3.11

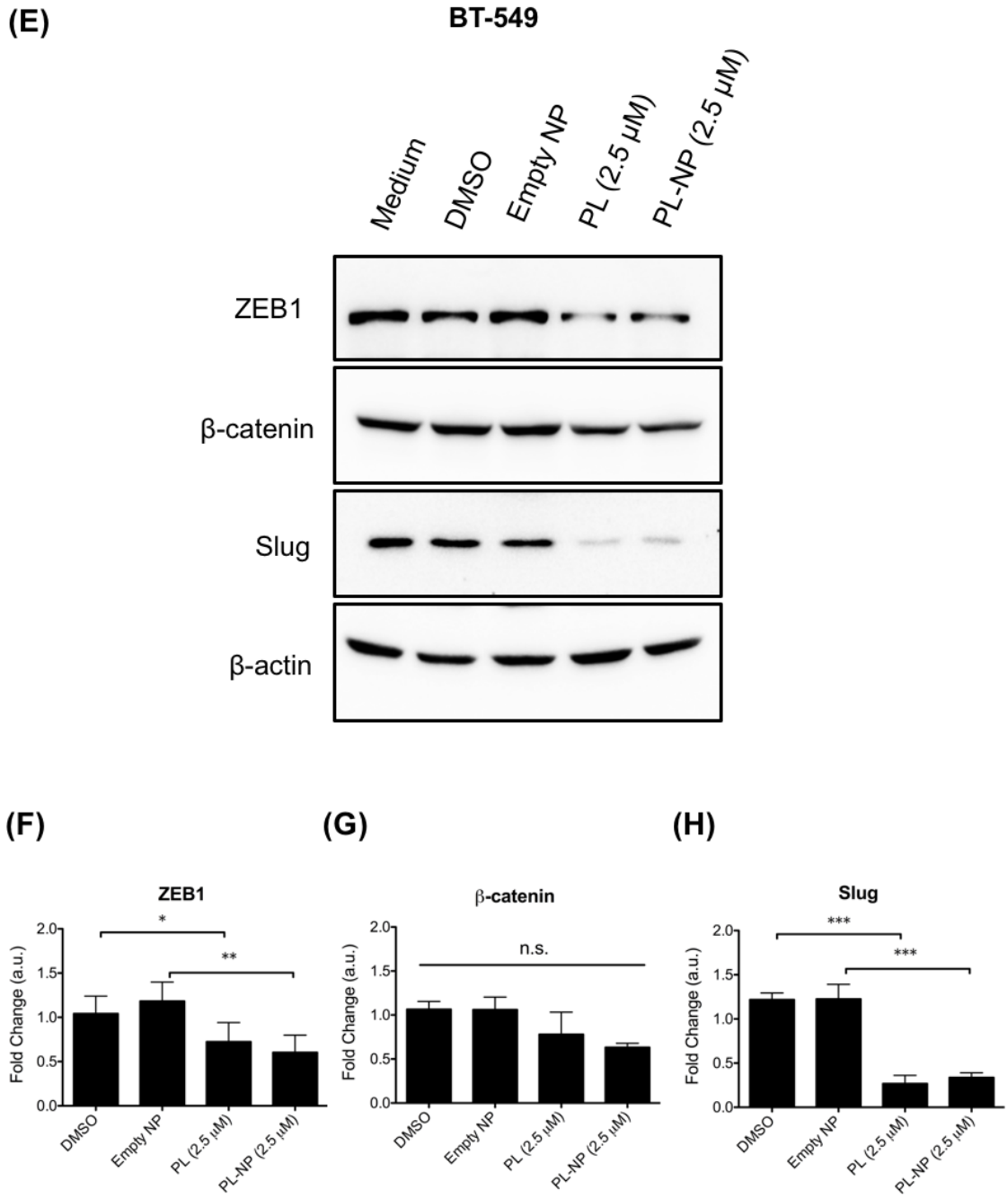

Figure 3.11 continued

Figure 3.12 Protein levels of mesenchymal marker, N-cadherin, and Smad3 are decreased by free PL and PL-NPs in MDA-MB-231 breast mammary carcinoma cells.

MDA-MB-231 were treated with 5.0 μM of free PL or PL-NPs for 72 hours with treatment changed every 24 hours. Following treatment, cells were lysed, proteins were isolated and separated by western blotting. Nitrocellulose membranes were probed with primary Abs targeting N-cadherin and Smad3, as well as appropriate secondary Abs. β-actin was used as the reference protein. Panels (A) and (C) are images of blots from one representative experiment, while panels (B) and (D) are mean densities of protein expression ± SEM of 3 independent experiments. Densities of the bands were normalized relative to the medium control. Asterisks indicate significant reduction in the protein levels as determined by ANOVA with the Bonferroni multiple comparisons post-test.

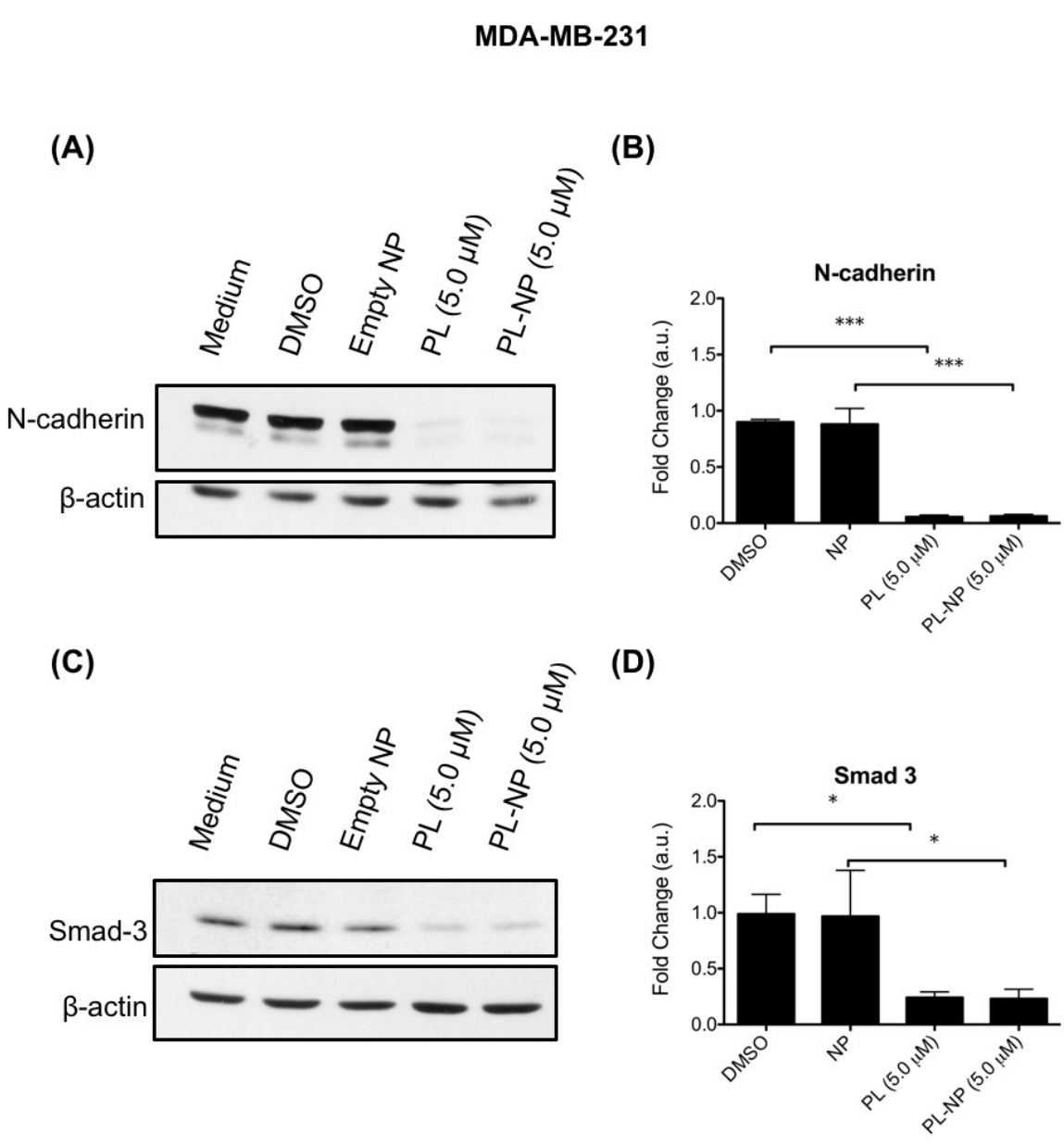
MDA-MB-231
(A)
Medium
DMSO
Empty NP
PL (5.0 μM)
PL-NP (5.0 μM)
N-cadherin
β-actin
(B)
N-cadherin
Fold Change (a.u.)
2.0
1.5
1.0
0.5
0.0
***
***
DMSO
NP
PL (5.0 μM)
PL-NP (5.0 μM)
(C)
Medium
DMSO
Empty NP
PL (5.0 μM)
PL-NP (5.0 μM)
Smad-3
β-actin
(D)
Smad 3
Fold Change (a.u.)
2.0
1.5
1.0
0.5
0.0
*
*
DMSO
NP
PL (5.0 μM)
PL-NP (5.0 μM)

Figure 3.12

Figure 3.13 Free PL and PL-NPs increase the mRNA levels of N-cadherin in MDA-MB-231 cells.

MDA-MB-231 breast cancer cells were treated with 5.0 μM of free PL or PL-NP for 72 hours, with the treatment changed every 24 hours. Following the treatment period, RNA was isolated from cells and converted to cDNA. The expression level of N-cadherin was determined using qRT-PCR. β-actin was used as the reference gene. Data shown are the mean values of mRNA expression level (normalized relative to the medium control) ± SEM of 4 independent trials. Asterisks indicate significant difference in the level of gene expression compared to the control, as determined by ANOVA with the Bonferroni multiple comparisons post-test.

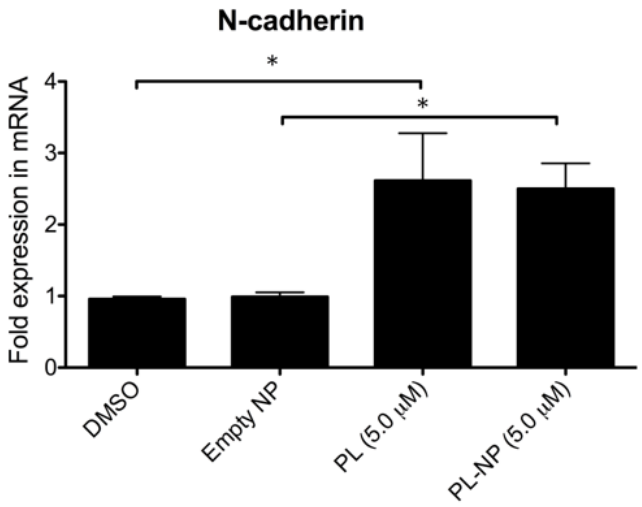
MDA-MB-231
N-cadherin
Fold expression in mRNA
0
1
2
3
4
*
*
DMSO
Empty NP
PL (5.0 μM)
PL-NP (5.0 μM)

Figure 3.13

Figure 3.14 Free PL and PL-NPs increase the expression of anti-metastatic NDRG1 in MDA-MB-231 cells.

(A) MDA-MB-231 cells were treated with 5.0 μM of free PL or PL-NPs for 72 hours, with treatment changed every 24 hours. Following treatment, cells were lysed, proteins were isolated and separated by western blotting. Nitrocellulose membranes were probed with anti-NDRG1 primary Ab, as well as an appropriate secondary Ab. β-actin was used as the reference protein. (A) Representative images of blots of NDRG1 protein levels in MDA-MB-231 cells are shown. (B) Mean densities of protein expression ± SEM of 3 independent experiments. Densities of the bands were normalized relative to the medium control. (C) Similar experiment was performed, where RNA was isolated from treated cells for qRT-PCR analysis. Data shown are the mean values of mRNA expression level (normalized relative to the medium control) ± SEM of 4 independent trials. β-actin was used as the reference gene. Asterisks indicate significant change in protein or mRNA levels, compared to vehicle control, as determined by ANOVA with the Bonferroni multiple comparisons post-test.

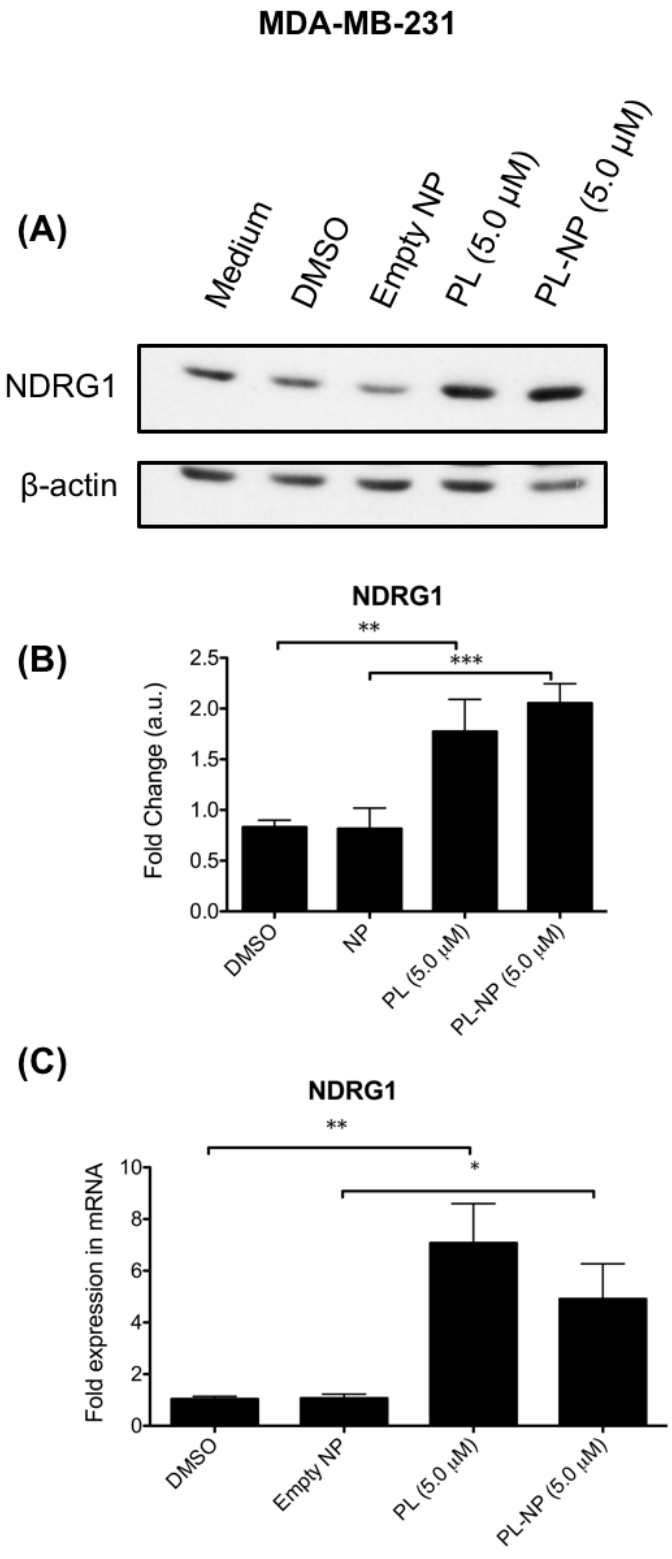
MDA-MB-231
(A)
Medium
DMSO
Empty NP
PL (5.0 μM)
PL-NP (5.0 μM)
NDRG1
β-actin
(B)
NDRG1
**
***
Fold Change (a.u.)
2.5
2.0
1.5
1.0
0.5
0.0
DMSO
NP
PL (5.0 μM)
PL-NP (5.0 μM)
(C)
NDRG1
**
*
Fold expression in mRNA
10
8
6
4
2
0
DMSO
Empty NP
PL (5.0 μM)
PL-NP (5.0 μM)

Figure 3.14

Figure 3.15 PL increases the expression of E-cadherin mRNA in MDA-MB-231 cells, but not in BT-549 cells.

(A-C) MDA-MB-231, and (D) BT-549 breast cancer cells were treated with 0.5 - 2.5 μM of free PL for 72 hours, with the treatment changed every 24 hours. Following the treatment period, RNA was isolated from cells and converted to cDNA. The expression levels of E-cadherin in both cell lines, as well as Slug and cMyc in MDA-MB-231 cells were determined using qRT-PCR. β-actin was used as the reference gene. Data shown are the mean values of mRNA expression level (normalized relative to the medium control) ± SEM of 5 (A and D) and 3 (B and C) independent trials. Asterisks indicate significant difference in the level of gene expression compared to the control, as determined by ANOVA with the Tukey multiple comparisons post-test.

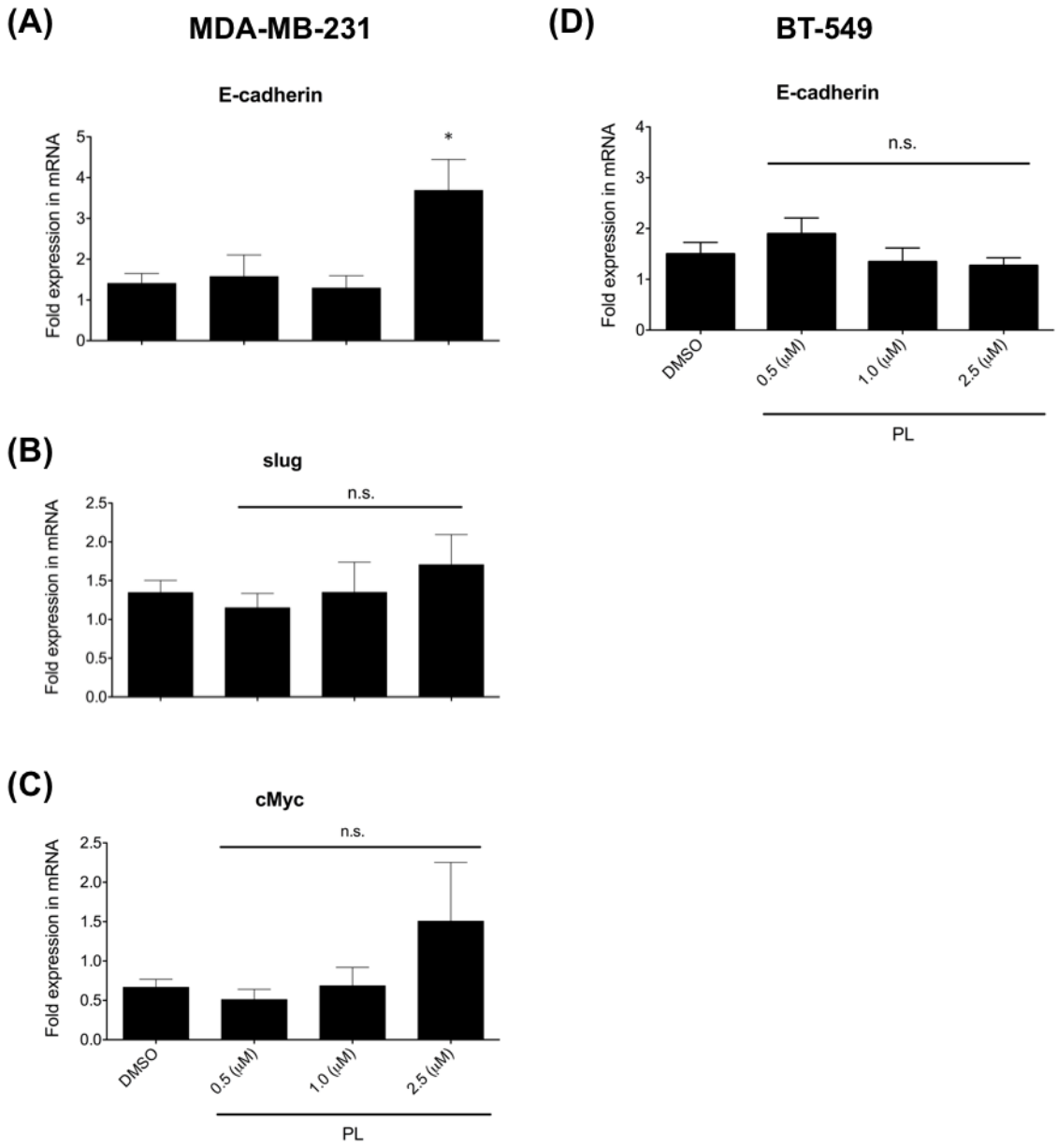
(A)
MDA-MB-231
E-cadherin
Fold expression in mRNA
*
(B)
slug
n.s.
Fold expression in mRNA
(C)
cMyc
n.s.
Fold expression in mRNA
DMSO
0.5 (μM)
1.0 (μM)
2.5 (μM)
PL
(D)
BT-549
E-cadherin
n.s.
Fold expression in mRNA
DMSO
0.5 (μM)
1.0 (μM)
2.5 (μM)
PL

Figure 3.15

Figure 3.16 PL-NPs increase the expression of E-cadherin mRNA in MDA-MB-231 cells to the same extent as free PL.

MDA-MB-231 breast cancer cells were treated with 2.5 μM of free PL or PL-NPs for 48 hours, with the treatment changed every 24 hours. Following the treatment period, RNA was isolated from cells and converted to cDNA. The expression level of E-cadherin was determined using qRT-PCR. β-actin was used as the reference gene. Data shown are the mean values of mRNA expression level (normalized relative to the medium control) ± SEM of 3 independent trials. Asterisks indicate significant difference in the level of gene expression compared to the control, as determined by ANOVA with the Bonferroni multiple comparisons post-test.

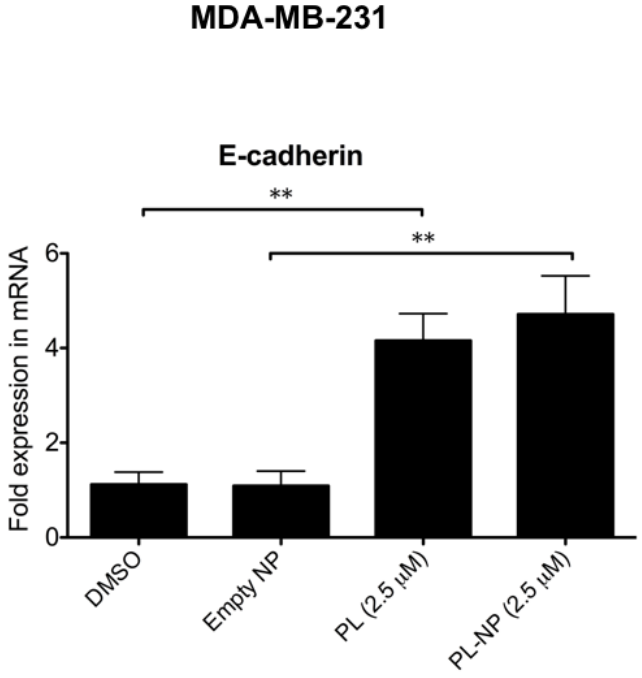
MDA-MB-231
E-cadherin
**
**
Fold expression in mRNA
6
4
2
0
DMSO
Empty NP
PL (2.5 μM)
PL-NP (2.5 μM)

Figure 3.16

Figure 3.17 TGF-β – induced mesenchymal changes in MCF-10A, breast epithelial cells, are not inhibited by PL.

(A) MCF-10A normal breast epithelial cells were treated with 5.0 ng/mL of human TGF-β for 48 hours. Following treatment, cell morphology was visualized and photographed using the 20X magnification objective. (B-F) MCF-10A cells were incubated with 2.5 μM of PL for 24 hours, then treated with 5.0 ng/mL of TGF-β alone or in combination with 2.5 μM of PL for another 48 hours. Following treatment, cells were lysed, proteins were isolated and separated by western blotting. Nitrocellulose membranes were probed with the indicated primary Abs and appropriate secondary Abs. (B) Representative images of blots of MCF-10A cells are shown. (C-F) Mean densities of protein expression ± SEM of 4 independent experiments. Densities of the bands were normalized relative to the medium control. Asterisks indicate significant change in the protein levels as determined by ANOVA with the Tukey multiple comparisons post-test.

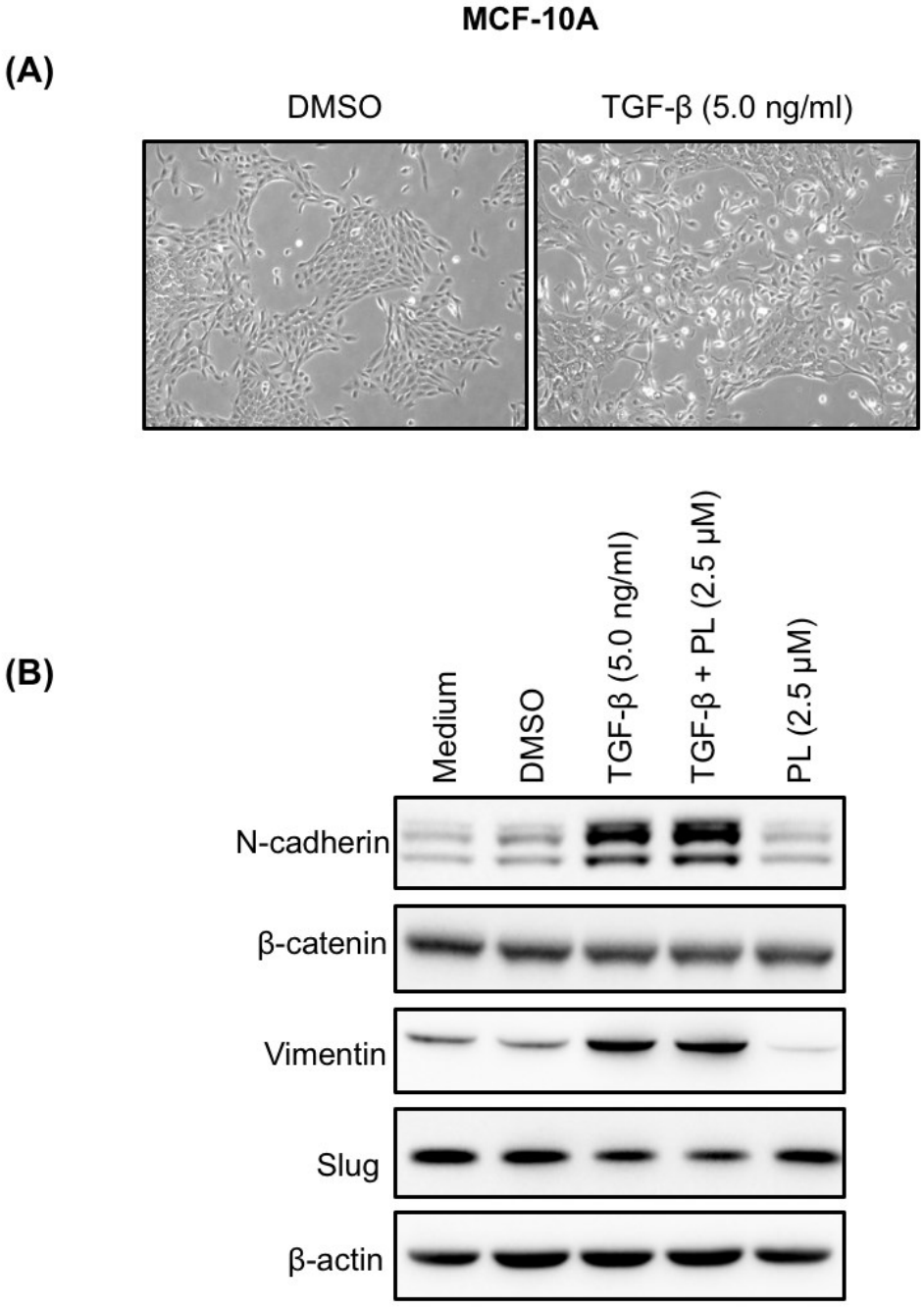
MCF-10A
(A)
DMSO
TGF-β (5.0 ng/ml)
(B)
Medium
DMSO
TGF-β (5.0 ng/ml)
TGF-β + PL (2.5 μM)
PL (2.5 μM)
N-cadherin
β-catenin
Vimentin
Slug
β-actin

Figure 3.17

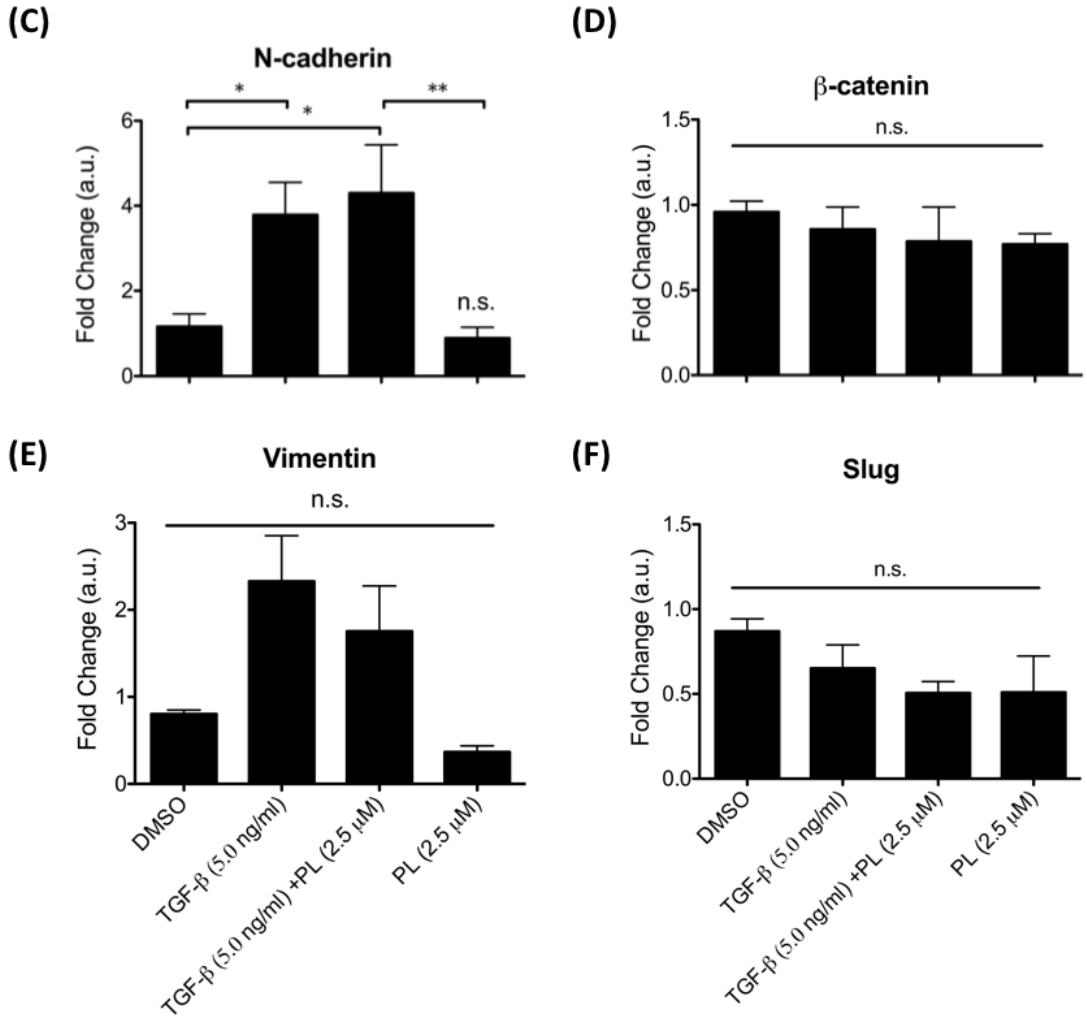

Figure 3.17 continued

Figure 3.18 PL does not affect TGF-β-induced expression of N-cadherin mRNA in MCF-10A epithelial cells.

MCF-10A normal breast epithelial cells were incubated with 2.5 μM of PL for 24 hours, then treated with 5.0 ng/mL of TGF-β alone or in combination with 2.5 μM of PL for another 48 hours. Following the treatment period, RNA was isolated from cells and converted to cDNA. The expression levels of N-cadherin and E-cadherin were determined using qRT-PCR. β-actin was used as the reference gene. Data shown are the mean values of mRNA expression level (normalized relative to the medium control) ± SEM of 4 independent trials. Asterisks indicate significant difference in the level of gene expression compared to the control, as determined by ANOVA with the Tukey multiple comparisons post-test.

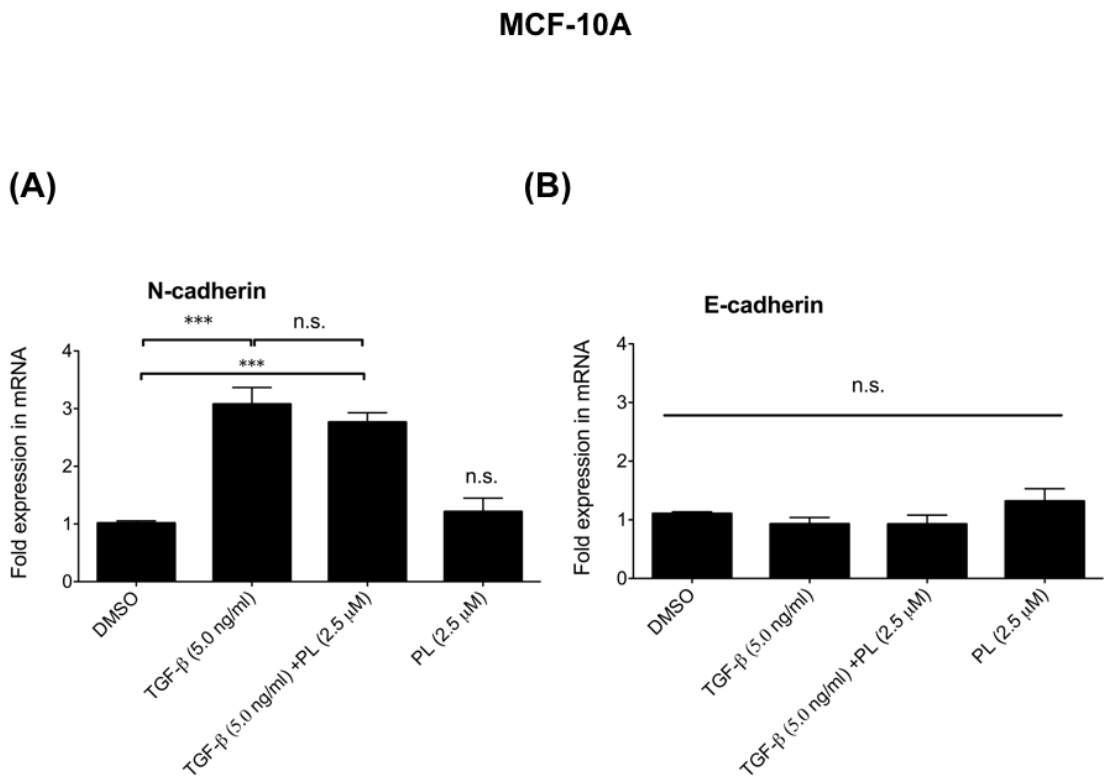
MCF-10A
(A)
(B)
N-cadherin
***
n.s.
***
n.s.
Fold expression in mRNA
0
1
2
3
4
DMSO
TGF-β (5.0 ng/ml)
TGF-β (5.0 ng/ml) +PL (2.5 μM)
PL (2.5 μM)
E-cadherin
n.s.
Fold expression in mRNA
0
1
2
3
4
DMSO
TGF-β (5.0 ng/ml)
TGF-β (5.0 ng/ml) +PL (2.5 μM)
PL (2.5 μM)

Figure 3.18

Figure 3.19 PL inhibits the increased mRNA expression of MMP-2 following TGF-β treatment in MCF-10A epithelial cells, but does not affect the expression of other MMPs.

MCF-10A normal breast epithelium were incubated with 2.5 μM of PL for 24 hours, then treated with 5.0 ng/mL of TGF-β alone or in combination with 2.5 μM of PL for another 48 hours. Following the treatment period, RNA was isolated from cells and converted to cDNA. The expression levels of (A) MMP-2, (B) MMP-3, (C) MMP-9, and (D) MMP-13 were determined using qRT-PCR. β-actin was used as the reference gene. Data shown are the mean values of mRNA expression level (normalized relative to the medium control) ± SEM of 4 independent trials. Asterisks indicate significant difference in the level of gene expression compared to the control, as determined by ANOVA with the Tukey multiple comparisons post-test.

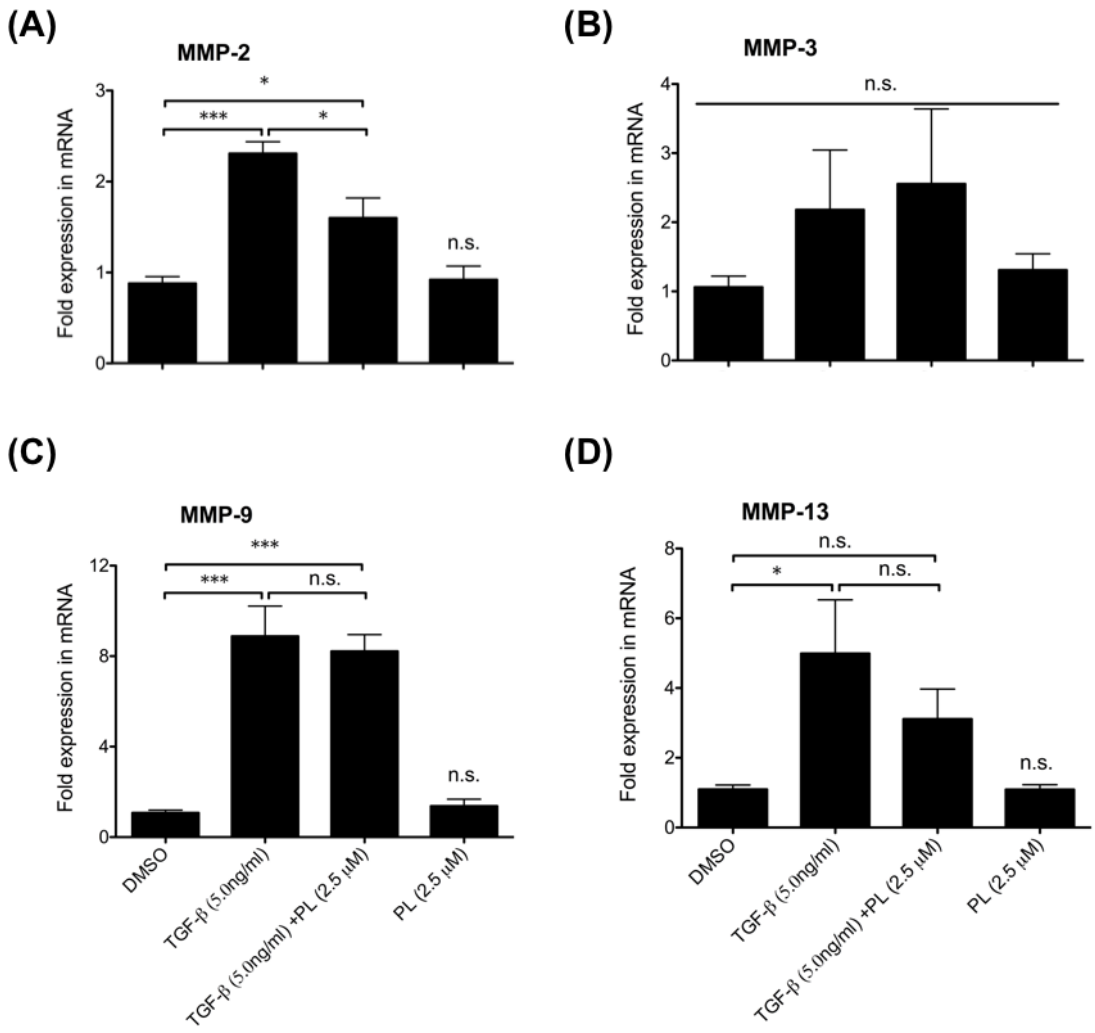
MCF-10A
(A)
MMP-2
Fold expression in mRNA
*
***
*
n.s.
(B)
MMP-3
Fold expression in mRNA
n.s.
(C)
MMP-9
Fold expression in mRNA
***
***
n.s.
n.s.
(D)
MMP-13
Fold expression in mRNA
n.s.
*
n.s.
n.s.
DMSO
TGF-β (5.0ng/ml)
TGF-β (5.0ng/ml) +PL (2.5 μM)
PL (2.5 μM)

Figure 3.19

Figure 3.20 PL downregulates HDAC-4 and HDAC-6 protein levels in both MDA-MB-231 and BT-549 cells; however, HDAC-1 is only decreased in MDA-MB-231 cells.

(A-F) MDA-MB-231, and (G-L) BT-549 cells were treated with 2.5 μM of free PL or PL-NPs for 48 hours. Following treatment, cells were lysed, proteins were isolated and separated by western blotting. Nitrocellulose membranes were probed with the indicated primary Abs and appropriate secondary Abs. Panels (A) for MDA-MB-231 and (G) for BT-549 cells are images of blots from one representative experiment, while panels (B-F) and (H-L) are mean densities of protein expression ± SEM of 4 independent experiments. Densities of the bands were normalized relative to the medium control. Asterisks indicate significant reduction in the protein levels as determined by ANOVA with the Bonferroni multiple comparisons post-test.

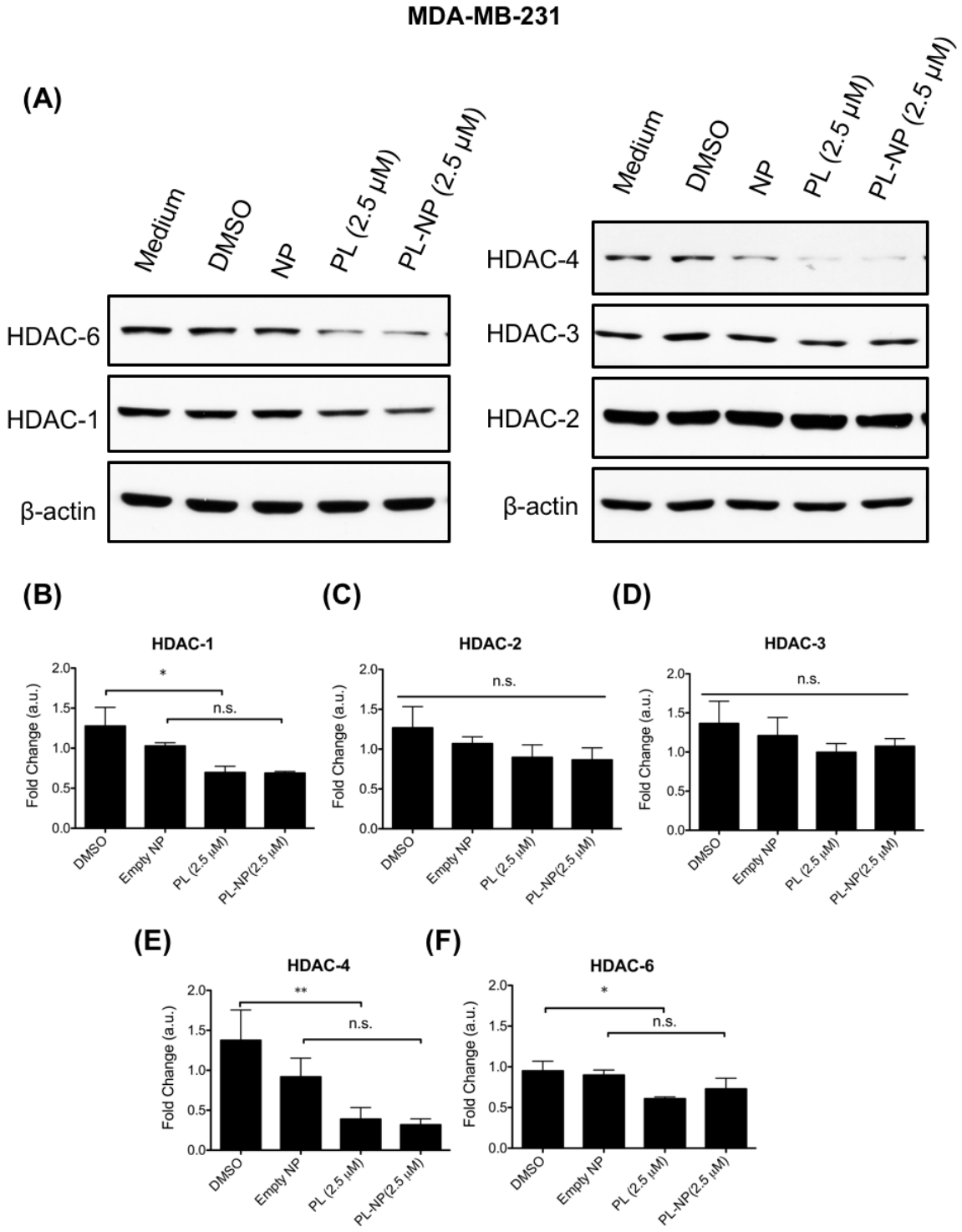
MDA-MB-231
(A)
Medium
DMSO
NP
PL (2.5 μM)
PL-NP (2.5 μM)
HDAC-6
HDAC-1
β-actin
HDAC-4
HDAC-3
HDAC-2
β-actin
(B)
HDAC-1
(C)
HDAC-2
(D)
HDAC-3
Fold Change (a.u.)
DMSO
Empty NP
PL (2.5 μM)
PL-NP(2.5 μM)
*
n.s.
(E)
HDAC-4
(F)
HDAC-6
**

Figure 3.20

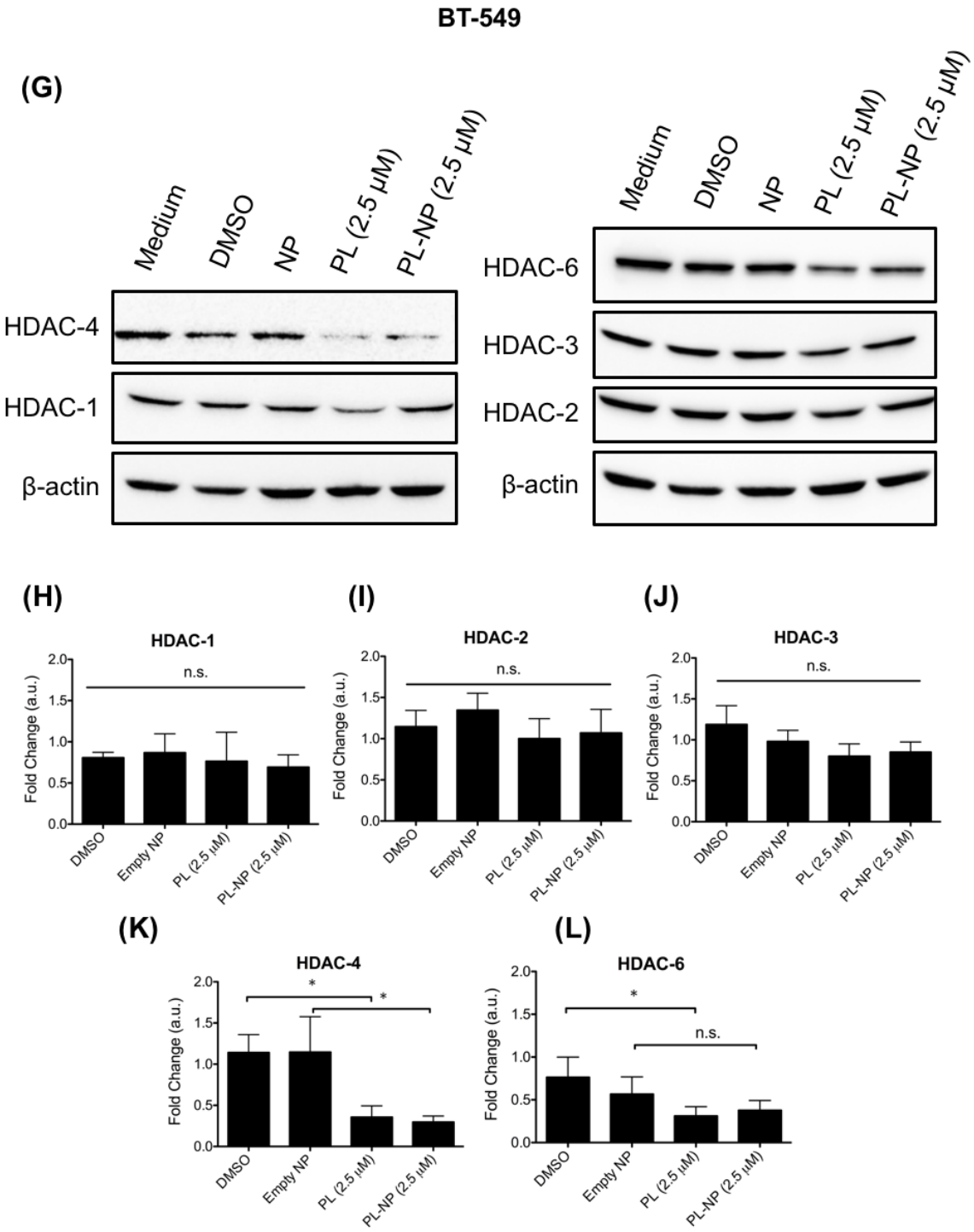

Figure 3.20 continued

Figure 3.21 HDAC-4 and HDAC-6 protein levels are reduced in MCF-10A cells following treatment with free PL or PL-NPs.

MCF-10A cells were treated with 2.5 μM of free PL or PL-NPs for 48 hours. Following treatment, cells were lysed, proteins were isolated and separated by western blotting. Nitrocellulose membranes were probed with the indicated primary Abs and appropriate secondary Abs. (A) Representative images of blots from one experiment are shown. (B-F) Mean densities of protein expression ± SEM of 4 independent experiments. Densities of the bands were normalized relative to the medium control. Asterisks indicate significant reduction in the protein levels as determined by ANOVA with the Bonferroni multiple comparisons post-test.

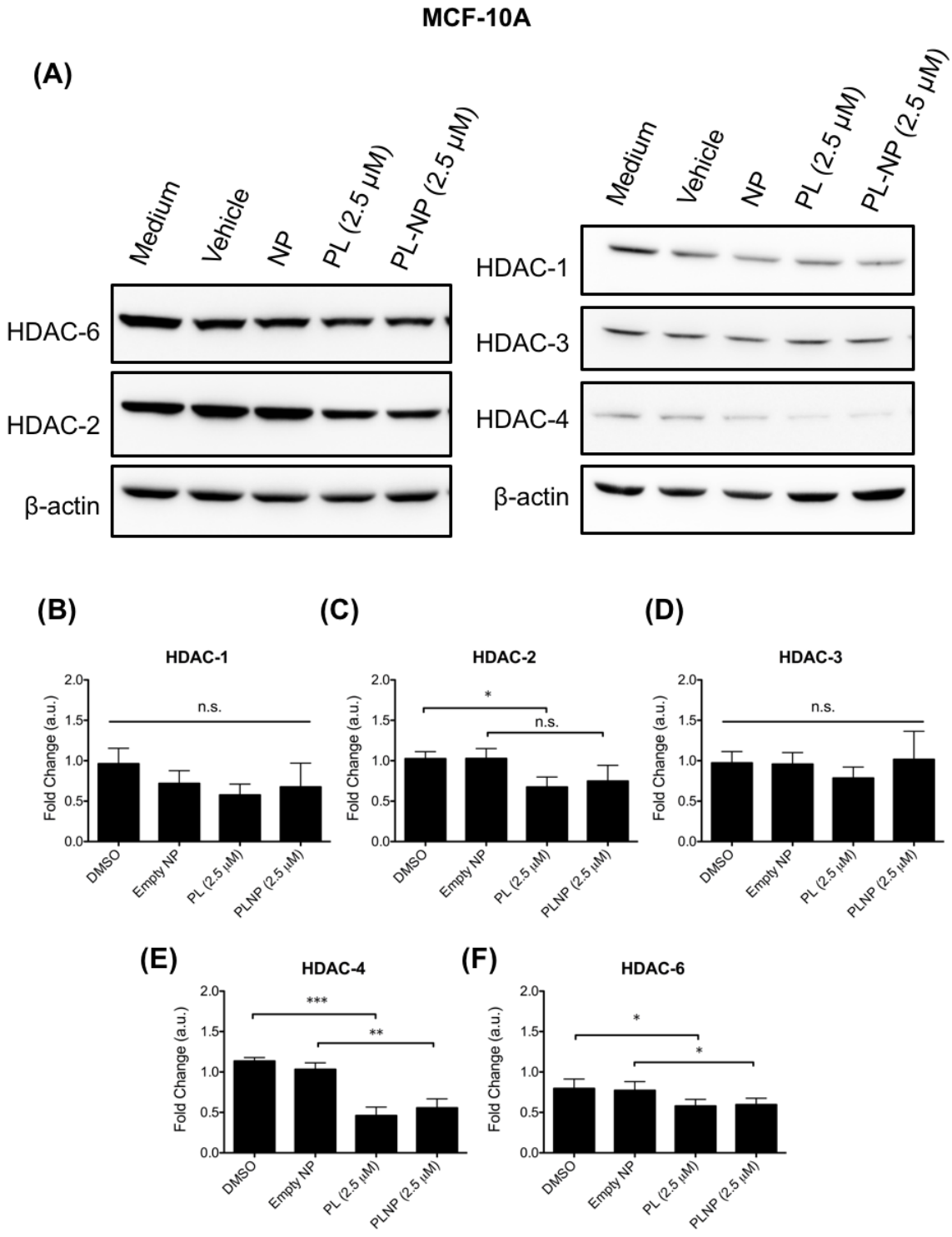
MCF-10A
(A)
Medium
Vehicle
NP
PL (2.5 μM)
PL-NP (2.5 μM)
HDAC-6
HDAC-2
β-actin
HDAC-1
HDAC-3
HDAC-4
β-actin
(B)
HDAC-1
(C)
HDAC-2
(D)
HDAC-3
Fold Change (a.u.)
n.s.
*
DMSO
Empty NP
PL (2.5 μM)
PLNP (2.5 μM)
(E)
HDAC-4
(F)
HDAC-6
***
**

Figure 3.21

Figure 3.22 PL and PL-NPs reduce DNMT-1 protein levels in MDA-MB-231 breast cancer cells, and MCF-10A normal breast epithelial cells, but not in BT-549 breast cancer cells.

(A-B) MDA-MB-231, (C-D) BT-549, and (E-F) MCF-10A cells were treated with 2.5 μM of free PL or PL-NPs for 48 hours. Following treatment, cells were lysed, proteins were isolated and separated by western blotting. Nitrocellulose membranes were probed with the antiDNMT-1 primary Ab and an appropriate secondary Ab. Panels (A) for MDA-MB-231, (C) for BT-549, and (E) for MCF-10A cells are images of blots from one representative experiment, while panels (B), (D), (F) are mean densities of protein expression ± SEM of 4 independent experiments, respectively. Densities of the bands were normalized relative to the medium control. Asterisks indicate significant reduction in the protein levels as determined by ANOVA with the Bonferroni multiple comparisons post-test.

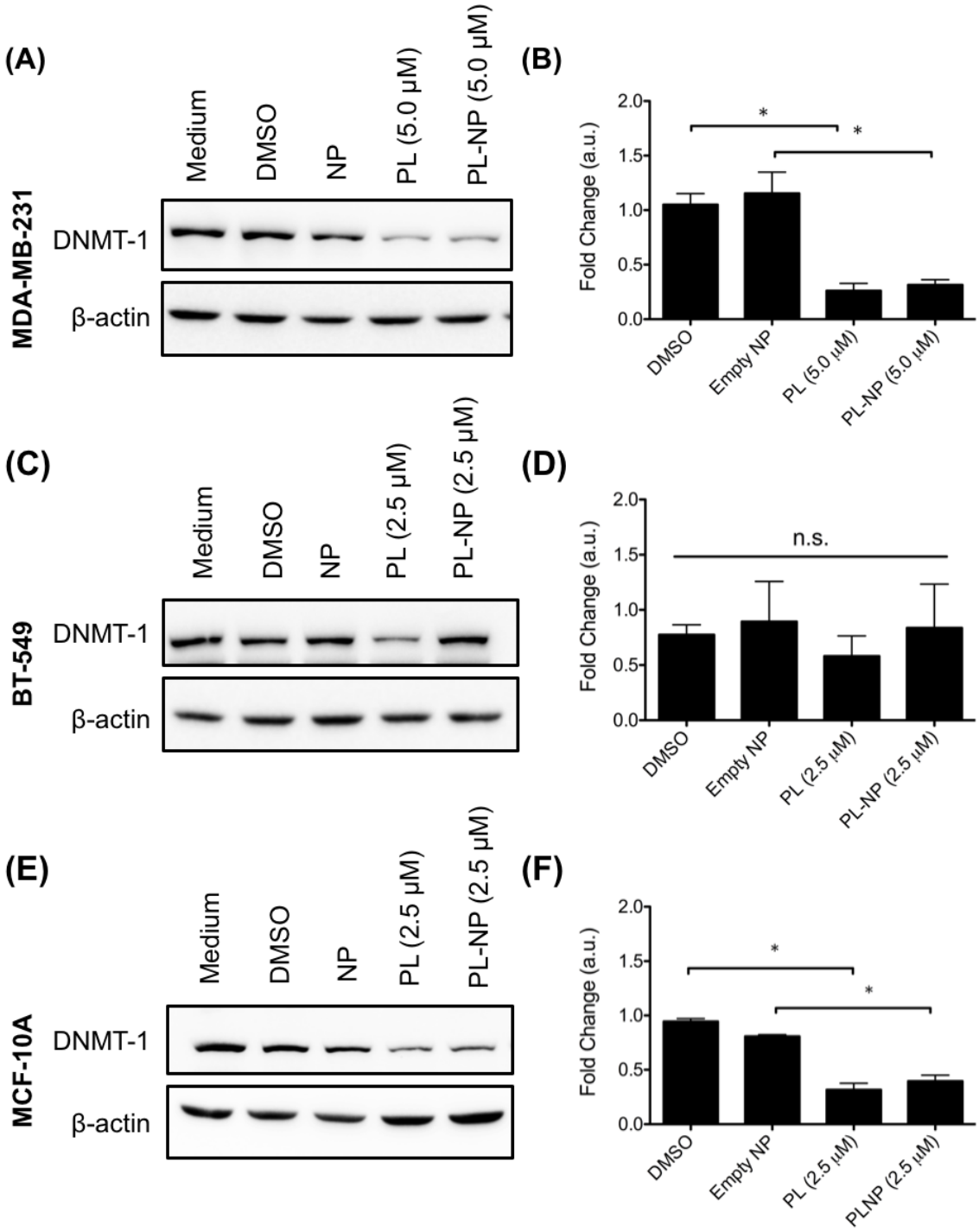
(A)
Medium
DMSO
NP
PL (5.0 μM)
PL-NP (5.0 μM)
MDA-MB-231
DNMT-1
β-actin
(B)
Fold Change (a.u.)
2.0
1.5
1.0
0.5
0.0
*
*
DMSO
Empty NP
PL (5.0 μM)
PL-NP (5.0 μM)
(C)
Medium
DMSO
NP
PL (2.5 μM)
PL-NP (2.5 μM)
BT-549
DNMT-1
β-actin
(D)
Fold Change (a.u.)
n.s.
DMSO
Empty NP
PL (2.5 μM)
PL-NP (2.5 μM)
(E)
Medium
DMSO
NP
PL (2.5 μM)
PL-NP (2.5 μM)
MCF-10A
DNMT-1
β-actin
(F)
Fold Change (a.u.)
*
*
DMSO
Empty NP
PL (2.5 μM)
PLNP (2.5 μM)

Figure 3.22

Figure 3.23 Overexpression of HDAC-1 or DNMT-1 does not affect PL-induced E-cadherin expression in MDA-MB-231 cells.

MDA-MB-231 were seeded at 5 x 10^5 in 100 mm tissue culture plates, and incubated over-night. Once 50% confluency was reached, cells were transfected with plasmids containing genomic sequences of HDAC-1 or DNMT-1, as well as the empty vector control, using the lipofectamine reagent for 48 hours. PL treatment started at 24 hours post transfection and continued for 48 hours. Following treatment, cells were lysed, proteins were isolated and separated by western blotting. Nitrocellulose membranes were probed with the (A) anti-HDAC-1 and anti-FLAG tag, (B) anti-DNMT-1 and anti-Myc tag primary Abs, as well as appropriate secondary Abs. β-actin was used as the reference protein. Images shown are blots of MDA-MB-231 cells from one experiment. (C and D) Similar experiment was performed, where RNA was isolated from treated cells for qRT-PCR analysis. Expression levels of E-cadherin were measured in PL-treated MDA-MB-231 cells transfected with HDAC-1 or DNMT-1 plasmid. Data shown are the mean values of mRNA expression level (normalized relative to the medium control) ± SEM of 4 independent trials. β-actin was used as the reference gene. Asterisks indicate significant change in the E-cadherin mRNA levels, compared to vehicle control, as determined by ANOVA with the Tukey multiple comparisons post-test.

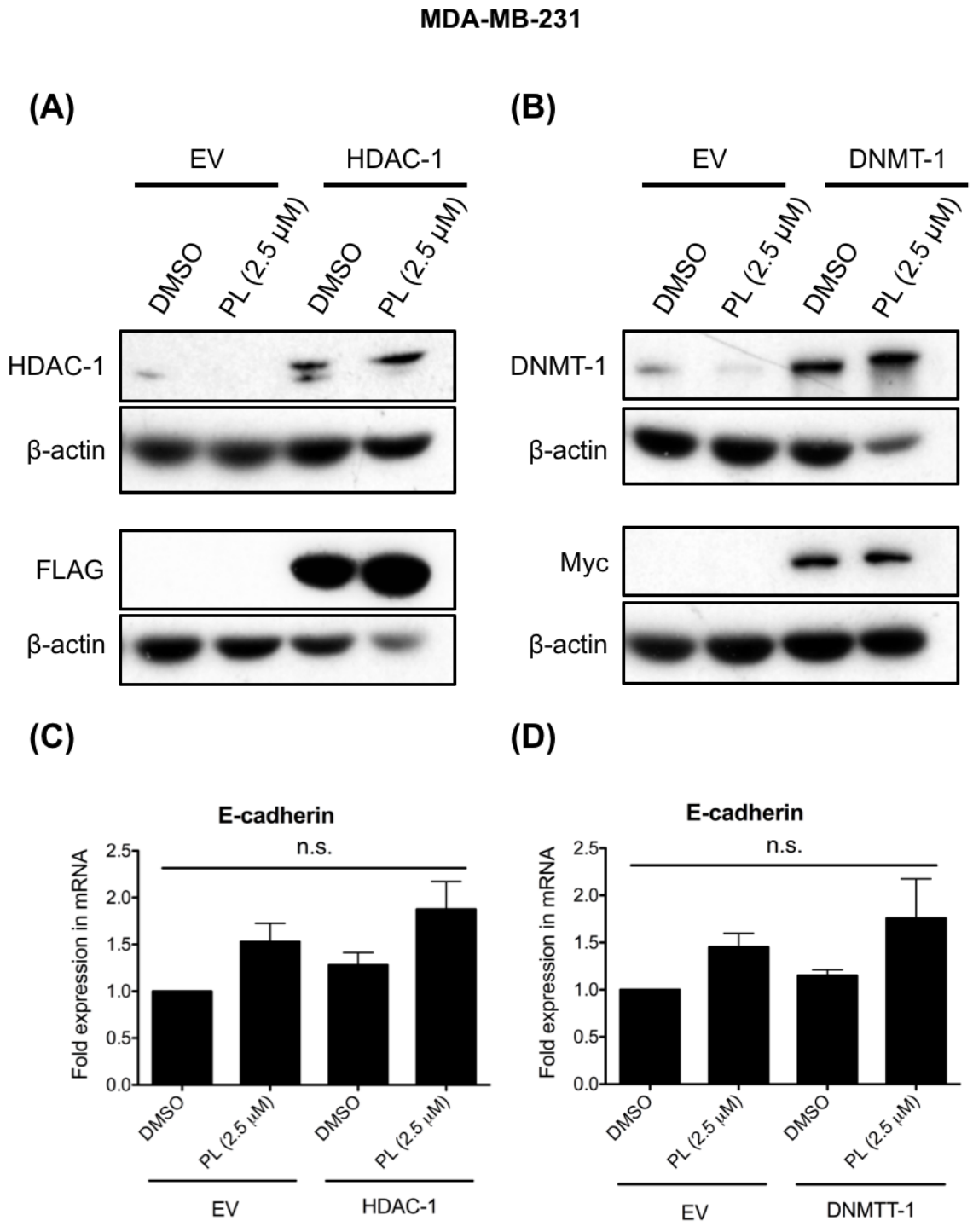
MDA-MB-231
(A)
EV
HDAC-1
DMSO
PL (2.5 μM)
DMSO
PL (2.5 μM)
HDAC-1
β-actin
FLAG
β-actin
(B)
EV
DNMT-1
DMSO
PL (2.5 μM)
DMSO
PL (2.5 μM)
DNMT-1
β-actin
Myc
β-actin
(C)
E-cadherin
n.s.
Fold expression in mRNA
2.5
2.0
1.5
1.0
0.5
0.0
DMSO
PL (2.5 μM)
DMSO
PL (2.5 μM)
EV
HDAC-1
(D)
E-cadherin
n.s.
Fold expression in mRNA
2.5
2.0
1.5
1.0
0.5
0.0
DMSO
PL (2.5 μM)
DMSO
PL (2.5 μM)
EV
DNMTT-1

Figure 3.23

CHAPTER 4

DISCUSSION

Despite decades of advancements in early detection and treatment strategies, cancer remains as one of the major causes of death in the world. Current conventional treatments fail to prevent the relapse of disease through metastasis, which is a critical determinant of cancer prognosis. The success of chemotherapy remains under a shadow of severe toxicities. Nausea, bone-marrow toxicity, immune toxicity, cardiotoxicity, secondary tumors, and increased susceptibility to hair loss are among the many side effects associated with chemotherapy (274). These side effects have been, in part, due to the inefficient pharmacokinetics of cancer therapeutic. Therefore, NP-based delivery of therapeutic agents has been at the forefront of medical research for several decades. Furthermore, pepper-derived phytochemicals, PL and PIP, show great anti-tumor potential, while their anti-metastatic effects have not been fully elucidated. The goal of this study was to examine the anti-metastatic potential of PL and PIP on breast cancer cells using NPs as an alternative drug delivery approach.

4.1 Encapsulation of PIP and PL into NPs

The use of NP for the delivery of anti-cancer drugs has been shown to improve the water solubility of hydrophobic drugs, their plasma circulation time, and the overall therapeutic efficacy of delivered drugs while reducing undesirable side effects (239). Successful examples of NPs-based drug delivery in cancer includes liposomal doxorubicin, Doxil® and Caelyx® (239, 249), paclitaxel polymeric NPs Abraxane® (239, 252), and NP delivery of curcumin (243, 255), a potent anti-cancer phytochemical. In this study, two different NP formulations were employed to optimize a method for encapsulation of PIP and PL into mPEG-PLGA NPs. The emulsion solvent extraction and the thin-film hydration methods have been described numerous times in the literature (243, 258–260). As seen under the TEM, NPs generated by the thin-film hydration were more spherical and homogenous in size and shape, compared to the NPs prepared by the emulsion/extraction method (Figure 3.1A and B). Sonication of NP samples during the thin-film hydration method reduced the particle size to the optimal length for passive

targeting, generated a uniform NP size distribution, and improved the encapsulation efficiency of PIP and PL into NPs. These effects of sonication during NP preparation are consistent with previous reports (242, 275). The use of acoustic energy allows for the breaking up and re-formation of NPs in the aqueous solution, which reduces particle size and increases the rate of drug entrapment within the NPs (276).

As seen in Table 3.1, the encapsulation efficiency of PIP and PL into NPs using emulsion/extraction method was below the level of detection, but with the thin-film hydration, it was ~18%. The presence of larger NPs (>200nm) generated by the emulsion/extraction method and the absence of sonication means that these larger NPs, which contain large amounts of PIP and PL, are likely removed during filter sterilization. This factor could account for the discrepancies in the encapsulation efficiencies seen between these two methods (Table 3.1). However, the emulsion/extraction method is, by no means, an inefficient method of encapsulation. Although drug structure could affect encapsulation efficiency, optimization of several parameters like sonication, the volumes of the organic and aqueous phase, drug-to-polymer ratio and type of polymer could enhance the encapsulation efficiency of PIP and PL into NPs using the emulsion/extraction method. Khalil and colleagues used a modified version of the emulsion/extraction method with 10 mL of aqueous phase and the use of sonication to encapsulate curcumin into PEG-PLGA NPs and achieve a 73.22% encapsulation efficiency (243). In fact, recent report indicates the use of a similar method to encapsulate PIP into PEG-PLGA NPs with a 37.82 % encapsulation efficiency (277).

The type of drug, method of encapsulation, and type of polymer affect the efficiency of encapsulation. A recent study showed that the molar ratios of mPEG:PCL or mPEG:PLGA affects the encapsulation efficiency (278). Generally, the use of mPEG-PCL or the use of tri-block polymers such as PCL-PEG-PCL, has been associated with higher encapsulation and improved in solubility (258, 259, 279). A difference in the drug-to-polymer ratio during preparation also affects the encapsulation efficiency (279). Ultimately, modification of these parameters could improve the encapsulation efficiency of PIP and PL, lower the time required for preparation of NPs, and improve the in vivo use of PIP-NPs and PL-NPs.

In this study, both PIP and PL were successfully encapsulated into mPEG-PLGA NPs using the thin-film hydration method, with 18-20% encapsulation efficiency (Table 3.1). The particle size ranged from ~32-82 nm in diameter, which is an ideal size for passively targeting the tumor while avoiding NP retention in kidney, liver, and spleen (246). PIP-NPs prepared by Pachauri and colleagues (2015) are larger in size at approximately 134 nm (277), which is more prone to opsonization and hepatic retention, regardless of the PEGylation status (246, 248, 280). Indeed, an analysis of in vivo pharmacokinetics shows only a modest improvement in the plasma concentration of PIP-NPs compared to free PIP (277). PL encapsulation into mPEG-PCL NPs has also been reported using the thin-film hydration method with an impressive 99.9% encapsulation efficiency (260). However, the authors did not use centrifugation or dialysis of their NPs to remove any unencapsulated PL, which suggests that their measured encapsulation efficiency of ~100% is incorrect. Collectively, the results of this study show the efficient encapsulation of PIP and PL into mPEG-PLGA NPs using the thin-film hydration method, and highlight the importance of taking into account several parameters during preparation in order to achieve an ideal size and encapsulation efficiency.

4.2 PIP- and PL-NPs Show Growth Inhibition and Cytotoxicity for TNBC Cells

Both PIP and PL have been reported to show cytotoxicity and growth inhibitory effects on several human tumor cell lines (201, 203, 204, 218, 227, 230, 233). TNBC is an invasive form of breast cancer that is hormone-independent; hence, patients with TNBC do not benefit from hormone-targeted therapy (11, 17). Therefore, the efficacy of PIP-NPs and PL-NPs, prepared by the thin-film hydration method, was tested against a panel of TNBC cell lines consisting of MDA-MB-468, MDA-MB-231, and BT-549 cells, using the MTT assay. As shown in Figure 3.4, PIP-NPs and PL-NPs were as effective as free PIP and PL dissolved in DMSO in inhibiting the metabolic activity, and therefore growth, of TNBC cells. These results were consistent with the findings of Greenshields *et al.* (2015), and Raj *et al.* (2011) (201, 218). Although the encapsulation of PIP and PL into NPs improved the solubility of these alkaloids, the in vitro growth inhibitory effects of PIP-NPs and PL-NPs were comparable to free PIP and PL. Given that in vitro experiments do not fully confirm the improved efficacy of encapsulated PIP and PL,

similar effects were observed following cell culture studies of fisetin-NPs (258), oridonin-NPs (259), curcumin-NPs (255), luteolin-NPs (256), and paclitaxel-NPs (281).

It was evident from these results that PL is more potent at inhibiting the growth of TNBC than PIP. As little as 2.5 μM of PL resulted in a significant growth inhibition of MDA-MB-231 cells, while 150 μM of PIP or PIP-NP did not have as great an effect (Figure 3.4C and D). These results are also consistent with the findings of Bezerra *et al.* (2006), in which 100 mg/kg b.w. of PL resulted in a significant reduction in Sarcoma 180 cell proliferation in mice, while 100 mg/kg b.w. of PIP did not (282). The growth suppression effects of PIP and PL are due to inhibition of cell proliferation, as determined by cell cycle analysis and expression levels of cell cycle progression mediators like cyclin D, cyclin B1, and p21 (202, 203, 218, 226, 228). Given the potency of PL on cancer cells, PL-NPs were also tested on the growth of MCF-7 mammospheres in vitro and a significant decrease in the number of viable cells was observed (Figure 3.6). The effects of PIP on MCF-7 mammospheres have been reported (218); however, this study is the first to show the effectiveness of PL-NPs on the in vitro growth of tumor cells in three dimensions, which more closely resembles tumor growth in situ.

The cytotoxic effects of PIP-NPs and PL-NPs were investigated on MDA-MB-468 TNBC cells using Annexin-V-FLUOS/PI. As expected, high doses of PIP and PL significantly increased MDA-MB-468 cell death. The cytotoxic effects of PIP are mediated through inhibition of PI3K/Akt signaling, decreased levels of Bcl-2, increased levels of pro-apoptotic Bax, and activation of caspase-dependent apoptosis (218, 227). Similarly, PL-induced ROS inhibits cell survival signaling pathways such as NF-κB and PI3K/Akt, while inhibiting Bcl-2 and inducing Bax to cause apoptosis (201, 203–206). In this study, although the total cell death is comparable between encapsulated and DMSO-dissolved PIP or PL, both PIP-NPs and PL-NPs had a higher percentage of early apoptotic cell death (Annexin-V-FLUOS positive/PI negative) compared to their free counterparts (Figure 3.5B and C). These results show a delayed cytotoxic effect of PIP-NPs and PL-NPs compare to free PIP and PL, and suggest the controlled release profile of PIP and PL from NPs. These findings are consistent with the potential applicability of synthetic polymeric NPs for prolonged circulation time and a more sustained release of drugs (239, 240, 251). I did not see these effects with the MTT assay (Figure 3.4),

because cytotoxicity requires a higher dose of these phytochemicals compared to growth inhibition.

The cytotoxic effects of PIP and PL were also tested on normal HDFs. While high-dose PIP did not induce significant cell death in HDFs, 10 μM of PL had a significant cytotoxic effect on these cells (Figure 3.5D). This result contradicts the findings of Raj *et al.* (2011) that show PL, even at 15 μM, does not significantly reduce the viability of HDFs and other normal cells (201). However, in their study, Raj and colleagues (2011) treated cells with PL for only 24 hours, whereas in my study a 48-hour time point was chosen. Furthermore, the Raj lab used trypan blue dye exclusion staining to measure cell viability, which fails to recognize early apoptotic cells as dead cells given that the membrane integrity of early apoptotic bodies is relatively intact and would not be permeable to trypan blue (35).

Interestingly, both PIP-NPs and PL-NPs were less cytotoxic for HDFs compared to PIP and PL dissolved in DMSO (Figure 3.5E and F). In fact, while 10 μM of PL significantly induced HDF cell death compare to vehicle control, 10 μM of PL-NP did not have a significant cytotoxic effect on HDFs, compared to the empty NP control (Figure 3.5F). These results could be due to a lower uptake of NPs by normal cells like HDFs compared to cancer cells. Selective uptake of NPs by cancer cells rather than normal cells has been reported in previous studies (283, 284). Although normal cells exhibit a well-regulated endocytosis pathway, cancer cells on the other hand, adapt their endocytic systems to meet the nutritional needs of their high proliferation rate (285). Understanding of the mechanism of NP uptake is required to optimize the therapeutic efficacy of NP drug delivery. Nevertheless, these results suggest that mPEG-PLGA NPs may preferentially target cancer cells in a tumor microenvironment, and reflect on the potentially improved therapeutic outcome of treatment with PIP-NPs and PL-NPs.

4.3 PIP-NPs and PL-NPs Inhibit the Migration and Invasion of MDA-MB-231 Cells

Migration and invasion are essential components of invasion/metastatic cascade, which remains as the major cause of breast cancer mortality (53, 54). Inhibition of cancer cell migration and invasiveness through basement membrane and ECM are therefore critical

for successful anti-metastatic therapy. High doses of PIP-NPs and PL-NPs reduced the growth and viability of TNBC cells; however, I also determined the effects of non-cytotoxic doses of these encapsulated phytochemicals on MDA-MB-231 migration and invasion. MDA-MB-231 cells appear more spindle-shaped with mesenchymal-like morphology that has a higher metastatic potential, and drug-resistance characteristics, compared to epithelial-like MDA-MB-468 cells. Hence, MDA-MB-231 cells were more resistant to PIP than were MDA-MB-468 cells (Figure 3.4A and C). Using a gap closure assay, I determined that low doses of PIP-NPs and PL-NPs prevented the migration of MDA-MB-231 cells into the gap, and these effects were comparable to free PIP and PL (Figure 3.7). Free PL and PL-NP also inhibited the migration of MDA-MB-231 through the chemotaxis chamber with uncoated membrane (Figure 3.8A and B). The inhibitory effect of PIP on cell migration has already been reported for MDA-MB-231TNBC cells (218), SKBR3 HER2-enriched breast cancer cells (230), endothelial cells (234), 4T1 mouse mammary carcinoma cells (233), and HT-1080 fibrosarcoma cells (231). However, the inhibitory effect of PL on cancer cell migration has not been thoroughly investigated.

Cancer cell migration involves membrane ruffling and protrusions, which are driven by actin polymerization and depolymerization along with adhesion of the cell to ECM via integrins and immunoglobulin superfamily receptors (286). In fact, integrin-mediated signal transduction results in the activation of cytoplasmic focal adhesion kinase (FAK), which can couple with PI3K to mediate the migration of cells (287), through a downstream target, Rac, followed by regulation of actin and lamellipodia in cell (287, 288). Therefore, PIP and PL inhibition of PI3K/Akt signaling (203, 218, 234), is also predicted to interfere with the migration of cancer cells. The other possible mechanism for inhibition of cell migration by PIP and PL is loss of MMP expression. PIP decreases the expression MMP-2 and MMP-9 in MDA-MB-231 cells (218). In this study, I showed that PL and PL-NPs also decreased the mRNA expression of MMP-2 in MDA-MB-231 cells (Figure 3.10A). These effects are also likely the result of PIP- and PL-mediated inhibition of PI3K/Akt signaling, which regulates the expression of MMP-2 and MMP-9 (88, 89). In addition to their role as ECM proteases, MMPs are also involved in the regulation of cell adhesion molecules. MMP-2 targets P-cadherin and interacts with

integrins in cell adhesion (286, 289), while MMP-3 is a known protease for E-cadherin (81), leading to enhanced invasion and migration of cancer cells. These results further support the reduced migratory properties of MDA-MB-231 in the presence of low doses of PIP-NPs and PL-NPs.

MMPs have also been identified as key enzymes in the degradation of ECM components during cancer cell invasion of surrounding tissue. The attachment of integrins to a ECM component recruits membrane proteases such as MMPs to degrade ECM components (286). MMP-2 and MMP-9 are involved in breast cancer invasion and metastasis (79). Consistent with my finding of reduced MMP-2 mRNA expression following treatment with 2.5 μM of PL or PL-NP, I also saw a decrease in the invasiveness of PL-treated MDA-MB-231 cells through a fibronectin- or a gelatin-coated membrane (Figure 3.8C-F). Interestingly, Figure 3.8 shows a higher percentage of cells migrated through a ECM-coated membrane compared to the uncoated membrane (Figure 3.8A and B), which could be due to the exposure of these cells to ECM materials, fibronectin or gelatin, that enhanced their invasiveness. A previous study has shown an increase in the invasive properties of cancer cells, in vitro, in response to matrigel (93). Further investigation is needed to determine if MMP-2 plays a role in migration of MDA-MB-231 cells.

The loss of MDA-MB-231 cell invasion following PL treatment is similar to the decreased invasiveness of these cells following treatment with a MMP inhibitor, ARP-100 (Figure 3.9), which suggests that loss of MMP may be responsible for PL-mediated suppression of MDA-MB-231 invasion. However, I did not see a PL-mediated downregulation of MMP-3, MMP-9, and MMP-13 mRNA expression, which are also implicated in breast cancer metastasis (Figure 3.10B-D) (80). In fact, MMP-3 appeared to be upregulated by two-fold by PL (Figure 3.10B). Interestingly, the NF-κB pathway can repress or stimulate the expression MMP-3, depending on various stimuli and cytokines (290, 291). NF-κB can bind to repressive elements on the MMP-3 promoter and prevent MMP-3 transcription (290). Therefore, the inhibitory effects of PL on the NF-κB pathway could explain the increase in MMP-3 levels. It is possible that PL did not suppress the expression of MMP-9 and MMP-13. As seen in Figure 3.8, there appears to be more invasion of cells through a gelatin-coated membrane, compare to the fibronectin-

coated membrane. Both fibronectin and gelatin are target proteins for MMP-2, and only gelatin is a target of MMP-9 (83). These results suggest that PL specifically targeted MMP-2 expression and PL-treated MDA-MB-231 cells retained some level of MMP-9 activity to digest gelatin and migrate through the membrane. Despite their similarities, differences between MMP-2 and MMP-9 in terms of their function and mechanism of regulation have been reported before (292). Overall, these findings indicate that PL and PL-NPs inhibit breast cancer cell migration, invasion and the expression of MMP-2, which may account for the ability of PL to interfere with metastatic activities of breast cancer cells. Further analysis of the protein levels of MMPs, as well as the activity of MMPs, following exposure of breast cancer cells to PL is required to completely understand the mechanism by which PL and PL-NPs decreased the invasiveness of MDA-MB-231 cells. More importantly, the effects of PL on the expression of MMPs by tumor stroma should also be investigated.

4.4 PL-NPs Modulate EMT in TNBC Cells but not in MCF-10A Breast Epithelium

Control of metastasis by today's conventional therapeutics is somewhat limited. The signaling pathways and processes that lead to tumor progression serve as a suitable target for therapeutic intervention of a metastatic disease. Central to metastasis is the process of EMT (95). Given the high potency of PL on invasive TNBC cells, the effects of PL and PL-NP, at non-cytotoxic doses, was also investigated on EMT mediators in breast cancer cells. Using western blotting, this study revealed that exposure to 2.5 μM of PL or PL-NPs resulted in a significant decrease in the protein levels of ZEB1 and Slug in MDA-MB-231 and BT-549 cells, as well as β-catenin in MDA-MB-231 cells (Figure 3.11). Consequently, expression of epithelial and mesenchymal markers was also affected in MDA-MB-231 cells in response to PL or PL-NP treatment. While, expression of E-cadherin was upregulated by PL and PL-NPs (Figure 3.16), the protein levels of N-cadherin were significantly decreased in MDA-MB-231 cells (Figure 3.12). Interestingly, MDA-MB-231 and BT-549 cells express high levels of EMT-TFs such as Snail, Slug, ZEB1, and Twist, as well as β-catenin (121, 195, 293, 294). Indeed, the presence of β-catenin is essential for TNBC migration, stemness, and chemoresistance (293). Wnt/β-

catenin signaling is involved in the expression of EMT-TFs like Snail and Slug, which contribute to the downregulation of E-cadherin in cancer cells (129, 130, 294, 295). Several of these EMT-TFs such as Snail, Slug, and ZEB1 have also been implicated in cadherin switch from E-cadherin to N-cadherin during EMT (76, 97–99). High levels of N-cadherin in breast cancer cells is associated with an invasive phenotype (68, 69). In fact, ectopic expression of E-cadherin by MDA-MB-231 cells results in the reversion of their mesenchymal phenotype into epithelial morphology (296).

The effects of PL on E-cadherin re-expression and N-cadherin suppression in MDA-MB-231 cells could be explained by the inhibitory effects of PL on ZEB1 and Slug. Similarly, cytoplasmic stability and nuclear localization of β-catenin in cancer cells is linked to loss of E-cadherin (295). Furthermore, previous studies have confirmed that PL inhibits the PI3K/Akt pathway (203), and Akt enhances the nuclear localization of β-catenin through inhibition of GSK-3β (Figure 1.1) (132). Therefore, it can be postulated that PL inhibited PI3K/Akt in MDA-MB-231 cells, thereby relieving the Akt-mediated inhibition of GSK-3β, which can now prevent nuclear localization of β-catenin by targeting it for phosphorylation and proteosomal degradation. The inability of β-catenin to translocate to the nuclease would affect the expression of EMT-TFs and E-cadherin. Further proof of PL-mediated re-expression of E-cadherin through suppression of β-catenin can be inferred from the results on BT-549 cells. As shown in Figure 3.11, PL or PL-NPs did not decrease the protein levels of β-catenin in BT-549 cells. Consequently, E-cadherin expression was not induced by various doses of PL in these cells (Figure 3.15D). In addition, analysis of NDRG1 expression further supports the inhibitory effects of PL on the Wnt/β-catenin pathway. NDRG1 is a tumor metastasis suppressor, which inhibits EMT and the Wnt/β-catenin pathway through inhibition of LRP6, reactivation of GSK-3β, and subsequent degradation of cytoplasmic β-catenin (149). As shown in Figure 3.14, low doses of PL and PL-NPs significantly upregulated the expression of NDRG1 mRNA and protein by 2-8-fold in MDA-MB-231 cells. Restoration of NDRG1 by PL would therefore seem to be a plausible mechanism for the prevention of EMT and metastasis.

Along with the Wnt/β-catenin pathway, TGF-β/Smad signaling has also been implicated in the induction of EMT and tumor progression. In a recent study, Sengupta

and colleagues (2013) suggested that exposure of MDA-MB-231 cells to TGF-β increases their proliferation rate, and also induces EMT through increased expression of Snail, fibronectin, and N-cadherin, as well as reduced expression of E-cadherin (121). However, an older study suggests that TGF-β-induced EMT is a rare event in vitro (297). In fact, MDA-MB-231 cells, although still sensitive to TGF-β signaling, do not become more mesenchymal in appearance following treatment with TGF-β (297). Regardless, in this study, I showed that, in the absence of TGF-β, PL and PL-NPs decreased the protein levels of Smad3, an important component of TGF-β signaling, in MDA-MB-231 cells. Moreover, the induction of NDRG1 by PL and PL-NPs (Figure 3.14), is also consistent with inhibition of TGF-β signaling because NDRG1 is known to reduce levels of Smad2 and inhibit phosphorylation of Smad3 (150). These findings highlight the potential promotion by PL of an epithelial phenotype in mesenchymal-like breast cancer cells, while inhibiting EMT. PL can reverse the cadherin balance of MDA-MB-231 cells by inhibiting the Wnt/β-catenin and TGF-β/Smad pathways, as well as the EMT-TFs. This is first report on the EMT inhibitory effects of PL on breast cancer cells.

Although, the protein levels of N-cadherin were decreased, the mRNA expression of E-cadherin was increased in the presence of PL and PL-NPs. N-cadherin mRNA expression was also increased by PL by 2-3-fold (Figure 3.13). One possible explanation for these effects involves PL-mediated epigenetic reactivation of N-cadherin that is independent of its anti-EMT effects, while post-translational modification or N-cadherin turnover because of PL-induced MET is predicted to reduce N-cadherin protein levels. The role of epigenetics modifications in the expression of N-cadherin has been studied before (298, 299). Also, the expression of Wnt/β-catenin pathway target genes, Slug and c-Myc, remain largely unchanged in the presence of PL, despite the inhibitory effect of PL on Wnt/β-catenin signaling pathway (Figure 3.15B and C). Ultimately, the complex transcriptional regulation of these genes along with the convoluted nature of EMT signaling networks requires further investigation.

The ability of PL to reverse mesenchymal characteristics while promoting a more epithelial phenotype may have a huge clinical implication. PL could very well interfere with the mesenchymal state of invasive cancer cells in the primary tumor or within the circulation and prevent their metastatic dissemination and colonization (300). The process

of EMT is described as a spectrum of reversible cellular characteristics that lie between a complete epithelial state and a complete mesenchymal state. Therefore, further investigation is needed to determine how much MDA-MB-231 cells move towards the epithelial end of the spectrum following multiple exposures to low doses of PL.

Some studies have indicated that the exposure of MCF-10A human mammary epithelial cells to low doses of TGF-β results in their mesenchymal transition (272, 297). Indeed, I found that treatment of these cells with 5 ng/mL TGF-β resulted in a mesenchymal morphology and enhanced expression of mesenchymal markers such as N-cadherin and vimentin, as well as MMP-2, MMP-9, and MMP-13 (Figures 3.17-3.19). These results are consistent with previous reports of the effects of TGF-β on MCF-10A cells (272, 297). However, pre-treatment of MCF-10A cells with PL did not interfere with TGF-β signaling, and expression of N-cadherin and vimentin remained elevated in these cells in the presence of both PL and TGF-β (Figure 3.17). Interestingly, PL alone did not affect the expression of N-cadherin, β-catenin, Slug, and vimentin in MCF-10A cells. The inability of PL to modulate endogenous β-catenin in these cells is also consistent with absence of any change in E-cadherin mRNA expression by PL-treated MCF-10A cells (Figure 3.18B). These results suggest that the anti-EMT effects of PL could be specific to cancer cells.

As expected, expression of several MMPs such as MMP-2, MMP-9, and MMP-13 was upregulated in TGF-β-treated MCF-10A cells. While PL decreased TGF-β-induced MMP-2 expression in MCF-10A cells, it did not affect TGF-β-induced MMP-9 and MMP-13 expression by these cells (Figure 3.19), which resembles the effects of PL in MDA-MB-231 cells, and also reflects the differential regulation of MMP expression (292). Interestingly, PL alone did not affect the endogenous expression of MMPs in these cells, which is further evidence of a cancer-cell specific mechanism of PL-mediated suppression of the mesenchymal phenotype. Ultimately, analysis of MMP protein levels, as well MMP activity, is required to make a more conclusive interpretation on the effects of PL on MCF-10A cells in the absence or presence of TGF-β.

4.5 PL-NPs Target the Epigenetic Machinery in TNBC and MCF-10A Cells

Epigenetic regulations play a crucial role during EMT and metastasis (273). For example, E-cadherin promoter methylation and deacetylation is involved in E-cadherin (*CDH1*) silencing during EMT (72–74, 164, 301). Indeed, *CDH1* promoter hypermethylation in MDA-MB-231 and BT-549 cells is associated with EMT in these cell lines (301). Snail-mediated recruitment of HDAC-1 and HDAC-2 to the *CDH1* promoter, and its subsequent transcriptional silencing has also been investigated (74). In addition, ZEB1-mediated recruitment of HDAC-1 and HDAC-2 to the *CDH1* promoter and *E-cadherin* gene silencing also occurs in pancreatic cancer (75). These discoveries, along with my observations that PL mediated E-cadherin re-expression in MDA-MB-231 cells but not in BT-549 cells, encouraged further investigation of the effects of PL on the epigenetic machinery of TNBC cells. As shown in Figure 3.20, PL decreased the protein levels of HDAC-1, -4, and -6, while leaving HDAC-2, and HDAC-3 protein levels unaffected. Similar results were observed with protein levels of HDACs in BT-549 cells; however, HDAC-1 protein levels were not changed in PL-treated BT-549 cells. In addition, DNMT-1 protein levels were significantly downregulated in PL-treated MDA-MB-231 cells, but not in PL-treated BT-549 cells (Figure 3.22A-D). Therefore, I hypothesized that PL-mediated re-expression of E-cadherin in MDA-MB-231 cells could be mediated through inhibition of HDAC-1 and DNMT-1.

Surprisingly, overexpression of HDAC-1 or DNMT-1 by transient transfection in MDA-MB-231 cells did not reduce the effects of PL on E-cadherin expression in these cells. As shown in Figure 3.23, it appears that PL-mediated E-cadherin induction was similar among HDAC-1-, DNMT-1-, and EV-transfected cells. Although the fold changes in E-cadherin mRNA levels were not statistically significant (p value = 0.13), multiple repeats of this experiments showed a trend towards a modest upregulation of E-cadherin following PL treatment, which appears independent of the HDAC-1 or DNMT-1 abundance. These findings might be due to the minimal effects of PL seen on HDAC-1 and DNMT-1. Although PL increased E-cadherin expression by up to 4-fold in MDA-MB-231 cells, HDAC-1 protein levels was only modestly decreased by PL, and a significant decrease in DNMT-1 protein levels was achieved with 5.0 μM PL in these cells. However, these results must be evaluated cautiously, given that E-cadherin

overexpression following PL treatment was not to the same extent as seen previously with un-transfected MDA-MB-231 cells (Figures 3.15A and 3.16). This lack of responsiveness to PL could be due to unintended cellular stress and changes in gene expression patterns during transfection with Lipofectamine® 2000 reagent (302). Furthermore, cells overexpressing HDAC-1 or DNMT-1 were not selected for use in this experiment; therefore, a low transfection efficiency and the presence of many un-transfected cells could mask the inability of PL to induce E-cadherin, and show an effect on mRNA expression that was comparable to EV-transfected cells. Overall, despite previous reports on the roles of HDAC-1 and DNMT-1 in E-cadherin suppression (72, 74), the results of this study suggests that induction of E-cadherin in PL-treated MDA-MB-231 cells may be independent of the epigenetic effects of PL. Indeed, transcription factors such as β-catenin, Snail, Slug, ZEB1, and Twist are also involved in transcriptional suppression of E-cadherin (67, 97, 99, 123, 126, 129). Overexpression of these transcription factors, or simultaneous overexpression of HDAC-1 and DNMT-1 in MDA-MB-231 cells could further shed light on the mechanism of PL-mediated epithelialization.

PL and PL-NP treatment also decreased HDAC-4, and HDAC-6 protein levels in MDA-MB-231 and BT-549 cells. MCF-10A cells also experienced a modest decrease in HDAC-4, HDAC-6, and DNMT-1 proteins (Figures 3.21 and 3.22E-F), suggesting that the epigenetic effects of PL in this case are not cancer cell-specific. However, both HDAC-4 and HDAC-6 have been implicated in cancer, since HDAC-4 downregulates p21 and promotes growth of colon cancer (303), and HDAC-1, -6, and -8 are known to regulate expression of MMP-9 and promote invasiveness by MDA-MB-231 TNBC cells (163). HDAC-3 is induced by hypoxia inducible factor-1α (HIF-1α), a transcription factor produced in cancer cells under hypoxic conditions, which can promote the expression of N-cadherin and vimentin during hypoxia-induced EMT (299, 304). The role of HDAC-3 in regulating N-cadherin, and the inability of PL to decrease HDAC-3 protein levels in MDA-MB-231 cells (Figure 3.20D) is consistent with the increase in N-cadherin mRNA levels following PL treatment (Figure 3.13). Epigenetic silencing of NDRG1 through DNA methylation and histone deacetylation is also observed in human breast and colon cancer cells (146, 147). Therefore, PL-mediated overexpression of

NDRG1 (Figure 3.14) could also be attributed to the effect of PL on HDACs and DNMT-1. These epigenetic enzymes are ubiquitously expressed in cells, and are highly dysregulated in many cancers (154). Although this is the first study to show the potential inhibitory effects of PL on the epigenetic machinery, previous studies have examined the effects of other dietary phytochemicals on the epigenome. For examples, EGCG inhibits DNMT activity by forming a hydrogen bond with its active site, which results in the re-expression of several tumor suppressor genes in human esophageal, colon, and prostate cancer cells (305). EGCG also reduces DNMT-3A and HDAC-3 protein levels in HCT 116 colorectal cancer cells by targeting these proteins for degradation (306). Other phytochemicals such as sulforaphane, curcumin, resveratrol, and genistein are also known for modulating expression, protein levels, or activity of the epigenetic effectors as part of their anti-cancer mechanism (193).

The results on this study provide solid evidence for the potent inhibitory effects of PL on HDACs and DNMTs. These effects could be mediated through degradation of these enzymes, or PL-mediated reduction in their mRNA expression. Other than DNMT-1, DNMT-3A and DNMT-3B are also implicated in cancer. *De novo* methyltransferases, such as DNMT-3B, are also involved in the maintenance of DNA methylation in cancer (158, 307). Interestingly, DNMT-3A and -3B are known for their tumor suppressive effects, as loss of these enzymes promotes cellular transformation and tumorigenesis (307, 308). Further analysis of the effects of PL on the expression and/or activity of HDACs and DNMTs, including DNMT-3A and -3B, is needed if these dietary phytochemicals are to be used as anti-cancer drugs. Ultimately, combination of PL with conventional epigenetic inhibitors could lead to a more effective treatment regimen against a wide range of malignancies, including solid/epithelial tumors.

4.6 Limitations of the Study

Today, as the search for more effective cancer therapeutic continues, the use of effective drug delivery methods continues to attract research interest for cancer therapy. In this study, we set out to develop a feasible method for encapsulating PIP and PL, two very potent pepper-derived anti-cancer phytochemicals into NPs made from synthetic polymers, which would result in a proper encapsulation of these dietary compounds and

an ideal size and shape for effective tumor delivery. However, one of the limitations of this study was based on the human cell lines used for investigating the anti-metastatic properties of PIP-NPs and PL-NPs.

For this investigation, only human TNBC cell lines were used rather than breast tumor samples obtained directly from patients. Despite the tremendous impact of cell culture-based studies on our understanding of human health, two-dimensional growth of cancer cell monolayers does not properly reflect tumor growth in humans. In addition, long-term culture of cells has been associated with changes in DNA methylation patterns which could skew study results (309). Furthermore, monolayer cell culture experiments often results in inaccurate data that are not reproducible in xenograft models or clinical trials (310). As mentioned earlier, the tumor microenvironment, which is not represented in tissue culture studies, plays a central role in many aspects of tumor development and metastasis (56, 57). Although, my study showed the cytotoxic potential of PL and PL-NPs on MCF-7 mammospheres grown in vitro, further in vivo confirmation of the anti-cancer and anti-metastatic properties of PIP-NPs and PL-NPs is needed to render these alkaloids as attractive therapeutic alternatives to conventional treatment. Furthermore, the dose-limiting toxicities of PIP-NPs and PL-NPs must be examined on several other normal cells lines, including MCF-10A cells, and HMECs, as well as TNBC cell lines at different time points. For this study, the comparisons between encapsulated and free PIP or PL were made at a single time-point, which may not fully capture the delayed time-course of NP formulation due to NP uptake by cells and subsequent drug release.

The in vitro experiments described in this thesis also require further confirmation to make a more indisputable conclusion about the anti-EMT effect of PL. For some experiments, multiple doses of 5.0 μM PL were used instead of a single dose of 2.5 μM PL. Therefore, these experiments need to be further confirmed with a single 2.5 μM dose of PL, and the possible toxicity of 5.0 μM PL also needs to be evaluated. Ultimately, the mRNA and protein levels of genes do not always match. Therefore, confirming the effects of PL on MMP protein levels and activity using western blotting and gelatin zymography, respectively, is necessary. Similarly, PL-induced E-cadherin expression in MDA-MB-231 cells is only seen at the mRNA level. Further confirmation on the effects of PL on E-cadherin protein levels in MDA-MB-231 cells should also be considered

using western blotting and/or flow cytometry. Also, the toxicity of ARP-100, an MMP inhibitor, was not investigated in this study. Although ARP-100 appeared to decrease the invasiveness of MDA-MB-231 cells through a gelatin-coated membrane, its effects on cell viability must also be tested using Annexin-V-FLUOS/PI apoptosis assay, to ensure that the invasion inhibitory effect of ARP-100 is solely based on inhibition of MMP activity and not a reduction in cell number due to apoptosis/necrosis. Furthermore, the results of the transfection experiment were largely inconclusive. Optimization of the transfection process using perhaps a more efficient transfecting agent that causes less cellular stress, or using knockdown instead of transient expression could enhance our understanding of the inhibitory role of PL in EMT.

4.7 Future Directions

The present study provides considerable evidence for the potential use of PIP-NPs and PL-NPs in cancer therapy. Despite their cytotoxic effects on TNBC cells and MCF-7 mammospheres, the mechanism of cellular uptake and intracellular processing of PIP-NPs and PL-NPs is not fully elucidated. Understanding the mechanism of uptake of NPs is important, especially for NPs that are not targeted for a particular ligand, to fully appreciate their subcellular activity. Several studies have hinted at the role of clathrin-mediated endocytosis as possible mechanism for uptake of PEG-PLA-NPs and PEG-PLGA-NPs (285). Encapsulation of fluorescent compounds such as coumarin-6 or FITC, along with cellular uptake inhibitors can be used to examine and compare the uptake of mPEG-PLGA NPs by cancer cells and normal cells.

This study was also designed to investigate the anti-metastatic effects of PIP and PL on TNBC cells. Given the potency of PL, the effects of this phytochemical were further investigated in the context of EMT regulation and epigenetic modification. However, PIP also exhibited strong anti-cancer and anti-metastatic effects, both in vitro and in vivo (218, 233). Therefore, future studies should also examine the anti-EMT potential of PIP, perhaps using the PIP-NPs introduced in this study as a delivery method. Furthermore, previous studies have attributed many of the pharmacological effects of PL to its ability to induce cellular ROS (201, 203, 204, 206), which play a vital role as signaling molecule in cell survival and proliferation but can also damage cellular

components and lead to cell death. The effect of ROS on the anti-metastatic properties of PL was not investigated in this study. Future study should incorporate ROS scavengers, N-acetyl-L-cysteine or reduced glutathione, to determine if the effects of PL on EMT in TNBC cells is dependent on ROS. In addition to measuring MMP protein levels and activity following PL treatment, the effects of PL on MDA-MB-231 cells could be further investigated using exogenous expression of MMPs, knockdown of MMPs or selective MMP inhibitors. For instance, MMP-2 and/or MMP-9 overexpressing MDA-MB-231 cells could be treated with non-cytotoxic doses of PL and placed in chemotaxis chambers against fibronectin or gelatin coated membranes, to determine their invasion rates. These experiments would further shed light on the inhibitory effects of PL on cancer cell invasion and MMP expression.

Finally, this study was solely based on the preliminary in vitro effects of PIP and PL on the metastatic properties or breast cancer cells. Given the successful encapsulation of these phytochemicals into NPs, future studies should deliver PIP-NPs and PL-NPs in vivo using mouse models of breast cancer. Due to the improved efficacy and bioavailability that is usually reported with encapsulation of phytochemicals or anti-cancer drugs, the PIP-NPs and PL-NPs generated in this study are predicted to exhibit better efficacy compared to free PIP and PL, when administered intra-venously or intra-tumorally.

4.8 Summary and Conclusions

This study shows that PIP and PL can be successfully encapsulated into mPEG-PLGA NPs using the thin-film hydration method, without weakening their bioactivity. PIP-NPs and PL-NPs decreased the growth of and induced apoptosis in TNBC cells to the same extend as free PIP and PL. At non-cytotoxic doses, PIP-NPs and PL-NPs decreased the migration and invasiveness of MDA-MB-231 breast cancer cells. Both PL and PL-NPs showed suppressive effects on the metastasis-associated EMT, through inhibition of EMT-TFs, such as ZEB1, β-catenin, and Slug, upregulation of epithelial marker E-cadherin and metastasis suppressor NDRG1, and downregulation of mesenchymal marker N-cadherin. The anti-EMT effects of PL and PL-NPs could be mediated through their

effects on epigenetic regulators. A proposed model for the effects PL on TNBC cell growth and metastatic activity is summarized in Figure 4.1.

PIP and PL are two pepper-derived natural compounds that may have a promising future in cancer therapy. The conventional treatment for cancer, particularly TNBC, is associated with unintended side effects; hence, alternative therapeutic approaches with higher tumor selectivity are urgently needed. The findings of this study provide further insight into the anti-metastatic and EMT regulatory potential of PIP and PL, both of which inhibited the migration and invasion of MDA-MB-231 cells in vitro. Low doses of PL inhibited EMT, modulated cancer epigenome, and promoted an epithelial phenotype in MDA-MB-231 cells. Targeting EMT interferes with the metastatic potential of tumor cells and that have the potential to cause relapse. The use NPs as a drug delivery approach improved the solubility of PIP and PL, and sets the stage for a more effective therapeutic delivery of these compounds in vivo.

PIP and PL could complement other anti-cancer therapeutics in the destruction of primary tumor and metastases, when administered as a combination therapy, due to their broad anti-cancer effects and their ability to inhibit drug-metabolizing CYP450 enzymes (207, 311). However, PIP and PL could also antagonize the effects of immunotherapy, as these phytochemicals also possess immunomodulatory effects. For example, PIP exhibits inhibitory effects on both innate and adaptive immune cells (211–213), while PL prevents dendritic cell maturation (312). The use of ligand-modified NPs that actively target PIP and PL into tumor cells is essential when these phytochemicals are combined with immunotherapy in order to avoid unwanted effects on immune cells. Further analysis of the anti-tumor and anti-metastatic potential of PIP and PL will help determine the population of breast cancer patients that would benefit most from these compounds. Certainly, the results presented in this study will be a helpful guide to future in vivo and clinical studies involving PIP- and PL-NPs.

Figure 4.1 Schematic diagram of the effects of PL-NPs, at cytotoxic and non-cytotoxic doses, on MDA-MB-231 breast cancer cells.

Although at high doses, PL-NPs induced cancer cell death, low-dose PL-NPs suppressed Wnt/β-catenin and TGF-β/Smad signaling pathways, and decreased the protein levels of ZEB1, β-catenin, and Slug, while increasing the expression of the epithelial marker, E-cadherin, and tumor suppressor NDRG1. PL-mediated inhibition of EMT and promotion of an epithelial phenotype in MDA-MB-231 cells may be mediated through effects of PL on the epigenetic machinery.

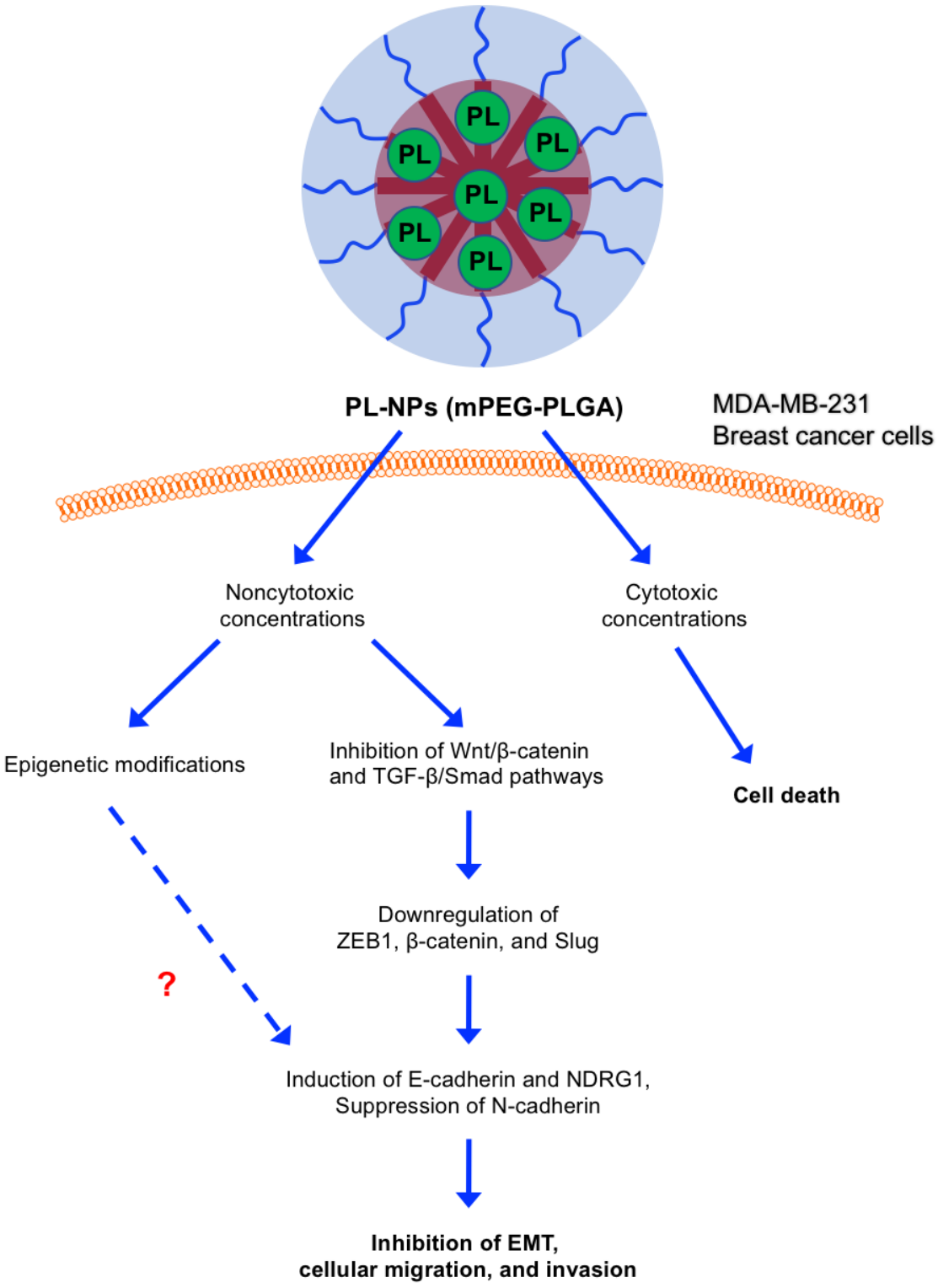
PL
PL
PL
PL
PL
PL
PL
PL-NPs (mPEG-PLGA)
MDA-MB-231
Breast cancer cells
Noncytotoxic
concentrations
Cytotoxic
concentrations
Epigenetic modifications
Inhibition of Wnt/β-catenin
and TGF-β/Smad pathways
Cell death
Downregulation of
ZEB1, β-catenin, and Slug
?
Induction of E-cadherin and NDRG1,
Suppression of N-cadherin
Inhibition of EMT,
cellular migration, and invasion

Figure 4.1

References

1. Canadian Cancer Society's Advisory Committee on Cancer Statistics, *Canadian Cancer Statistics 2016*. Toronto, ON: Available at: cancer.ca/Canadian-Cancer-Statistics-2016-EN.pdf.(2016).
2. Ferlay, J., I. Soerjomataram, R. Dikshit, S. Eser, C. Mathers, M. Rebelo, D. M. Parkin, D. Forman, and F. Bray, Cancer incidence and mortality worldwide: sources, methods and major patterns in GLOBOCAN 2012. *Int J Cancer* **136** (5): E359-86 (2015).
3. Hanahan, D., and R. A. Weinberg, The hallmarks of cancer. *Cell* **100** (1): 57–70 (2000).
4. Hanahan, D., and R. a Weinberg, Hallmarks of cancer: the next generation. *Cell* **144** (5): 646–74 (2011).
5. Weigelt, B., and J. S. Reis-Filho, Histological and molecular types of breast cancer: is there a unifying taxonomy? *Nat Rev Clin Oncol* **6** (12): 718–30 (2009).
6. The world Health Organization Histological Typing of Breast Tumors--Second Edition. The World Organization. *Am J Clin Pathol* **78** (6): 806–16 (1982).
7. Schnitt, S. J., Classification and prognosis of invasive breast cancer: from morphology to molecular taxonomy. *Mod Pathol* **23 Suppl 2** (S2): S60-4 (2010).
8. Maughan, K. L., M. A. Lutterbie, and P. S. Ham, Treatment of breast cancer. *Am Fam Physician* **81** (11): 1339–46 (2010).
9. Perou, C. M., T. Sørlie, M. B. Eisen, M. van de Rijn, S. S. Jeffrey, C. A. Rees, J. R. Pollack, D. T. Ross, H. Johnsen, L. A. Akslen, O. Fluge, A. Pergamenschikov, C. Williams, S. X. Zhu, P. E. Lønning, A. L. Børresen-Dale, P. O. Brown, and D. Botstein, Molecular portraits of human breast tumours. *Nature* **406** (6797): 747–52 (2000).
10. Sørlie, T., C. M. Perou, R. Tibshirani, T. Aas, S. Geisler, H. Johnsen, T. Hastie, M. B. Eisen, M. van de Rijn, S. S. Jeffrey, T. Thorsen, H. Quist, J. C. Matese, P. O. Brown, D. Botstein, P. E. Lønning, and A. L. Børresen-Dale, Gene expression patterns of breast carcinomas distinguish tumor subclasses with clinical implications. *Proc Natl Acad Sci U S A* **98** (19): 10869–74 (2001).
11. Eroles, P., A. Bosch, J. A. Pérez-Fidalgo, and A. Lluch, Molecular biology in breast cancer: intrinsic subtypes and signaling pathways. *Cancer Treat Rev* **38** (6): 698–707 (2012).
12. Herschkowitz, J. I., K. Simin, V. J. Weigman, I. Mikaelian, J. Usary, Z. Hu, K. E. Rasmussen, L. P. Jones, S. Assefnia, S. Chandrasekharan, M. G. Backlund, Y. Yin, A. I. Khramtsov, R. Bastein, J. Quackenbush, R. I. Glazer, P. H. Brown, J. E. Green, L. Kopelovich, P. A. Furth, J. P. Palazzo, O. I. Olopade, P. S. Bernard, G. A. Churchill, T. Van Dyke, and C. M. Perou, Identification of conserved gene expression features between murine mammary carcinoma models and human breast tumors. *Genome Biol* **8** (5): R76 (2007).
13. Prat, A., J. S. Parker, O. Karginova, C. Fan, C. Livasy, J. I. Herschkowitz, X. He, and C. M. Perou, Phenotypic and molecular characterization of the claudin-low intrinsic subtype of breast cancer. *Breast Cancer Res* **12** (5): R68 (2010).
14. Sorlie, T., R. Tibshirani, J. Parker, T. Hastie, J. S. Marron, A. Nobel, S. Deng, H. Johnsen, R. Pesich, S. Geisler, J. Demeter, C. M. Perou, P. E. Lønning, P. O.

Brown, A.-L. Børresen-Dale, and D. Botstein, Repeated observation of breast tumor subtypes in independent gene expression data sets. *Proc Natl Acad Sci U S A* **100** (14): 8418–23 (2003).
15. Carey, L. A., C. M. Perou, C. A. Livasy, L. G. Dressler, D. Cowan, K. Conway, G. Karaca, M. A. Troester, C. K. Tse, S. Edmiston, S. L. Deming, J. Geradts, M. C. U. Cheang, T. O. Nielsen, P. G. Moorman, H. S. Earp, and R. C. Millikan, Race, breast cancer subtypes, and survival in the Carolina Breast Cancer Study. *JAMA* **295** (21): 2492–502 (2006).
16. Sorlie, T., Molecular portraits of breast cancer: tumour subtypes as distinct disease entities. *Eur J Cancer* **40** (18): 2667–2675 (2004).
17. Dent, R., M. Trudeau, K. I. Pritchard, W. M. Hanna, H. K. Kahn, C. A. Sawka, L. A. Lickley, E. Rawlinson, P. Sun, and S. A. Narod, Triple-Negative Breast Cancer: Clinical Features and Patterns of Recurrence. *Clin Cancer Res* **13** (15): 4429–4434 (2007).
18. Berry, D. A., C. Cirrincione, I. C. Henderson, M. L. Citron, D. R. Budman, L. J. Goldstein, S. Martino, E. A. Perez, H. B. Muss, L. Norton, C. Hudis, and E. P. Winer, Estrogen-receptor status and outcomes of modern chemotherapy for patients with node-positive breast cancer. *JAMA* **295** (14): 1658–67 (2006).
19. Oakman, C., G. Viale, and A. Di Leo, Management of triple negative breast cancer. *The Breast* **19** (5): 312–21 (2010).
20. Petrelli, F., A. Coinu, K. Borgonovo, M. Cabiddu, M. Ghilardi, V. Lonati, and S. Barni, The value of platinum agents as neoadjuvant chemotherapy in triple-negative breast cancers: a systematic review and meta-analysis. *Breast Cancer Res Treat* **144** (2): 223–32 (2014).
21. Alli, E., V. B. Sharma, P. Sunderesakumar, and J. M. Ford, Defective repair of oxidative dna damage in triple-negative breast cancer confers sensitivity to inhibition of poly(ADP-ribose) polymerase. *Cancer Res* **69** (8): 3589–96 (2009).
22. O'Shaughnessy, J., C. Osborne, J. E. Pippen, M. Yoffe, D. Patt, C. Rocha, I. C. Koo, B. M. Sherman, and C. Bradley, Iniparib plus Chemotherapy in Metastatic Triple-Negative Breast Cancer. *N Engl J Med* **364** (3): 205–214 (2011).
23. O'Shaughnessy, J., L. Schwartzberg, M. A. Danso, K. D. Miller, H. S. Rugo, M. Neubauer, N. Robert, B. Hellerstedt, M. Saleh, P. Richards, J. M. Specht, D. A. Yardley, R. W. Carlson, R. S. Finn, E. Charpentier, I. Garcia-Ribas, and E. P. Winer, Phase III study of iniparib plus gemcitabine and carboplatin versus gemcitabine and carboplatin in patients with metastatic triple-negative breast cancer. *J Clin Oncol* **32** (34): 3840–7 (2014).
24. Turner, N., M. B. Lambros, H. M. Horlings, A. Pearson, R. Sharpe, R. Natrajan, F. C. Geyer, M. van Kouwenhove, B. Kreike, A. Mackay, A. Ashworth, M. J. van de Vijver, and J. S. Reis-Filho, Integrative molecular profiling of triple negative breast cancers identifies amplicon drivers and potential therapeutic targets. *Oncogene* **29** (14): 2013–23 (2010).
25. Jia, L. Y., M. K. Shanmugam, G. Sethi, and A. Bishayee, Potential role of targeted therapies in the treatment of triple-negative breast cancer. *Anticancer Drugs* **27** (3): 147–55 (2016).
26. Vousden, K. H., and C. Prives, Blinded by the Light: The Growing Complexity of p53. *Cell* **137** (3): 413–431 (2009).

27. Bykov, V. J. N., N. Issaeva, A. Shilov, M. Hultcrantz, E. Pugacheva, P. Chumakov, J. Bergman, K. G. Wiman, and G. Selivanova, Restoration of the tumor suppressor function to mutant p53 by a low-molecular-weight compound. *Nat Med* **8** (3): 282–8 (2002).
28. Synnott, N. C., A. Murray, P. M. McGowan, M. Kiely, P. A. Kiely, N. O'Donovan, D. P. O'Connor, W. M. Gallagher, J. Crown, and M. J. Duffy, Mutant p53: a novel target for the treatment of patients with triple-negative breast cancer? *Int J Cancer* **140** (1): 234–246 (2017).
29. Lehmann, S., V. J. N. Bykov, D. Ali, O. Andrén, H. Cherif, U. Tidefelt, B. Uggla, J. Yachnin, G. Juliusson, A. Moshfegh, C. Paul, K. G. Wiman, and P.-O. Andersson, Targeting p53 in vivo: a first-in-human study with p53-targeting compound APR-246 in refractory hematologic malignancies and prostate cancer. *J Clin Oncol* **30** (29): 3633–9 (2012).
30. Nakano, K., and K. H. Vousden, PUMA, a novel proapoptotic gene, is induced by p53. *Mol Cell* **7** (3): 683–94 (2001).
31. Thornborrow, E. C., S. Patel, A. E. Mastropietro, E. M. Schwartzfarb, and J. J. Manfredi, A conserved intronic response element mediates direct p53-dependent transcriptional activation of both the human and murine bax genes. *Oncogene* **21** (7): 990–9 (2002).
32. Wu, Y., J. W. Mehew, C. A. Heckman, M. Arcinas, and L. M. Boxer, Negative regulation of bcl-2 expression by p53 in hematopoietic cells. *Oncogene* **20** (2): 240–51 (2001).
33. Kerr, J. F., A. H. Wyllie, and A. R. Currie, Apoptosis: a basic biological phenomenon with wide-ranging implications in tissue kinetics. *Br J Cancer* **26** (4): 239–57 (1972).
34. Fadok, V. A., D. L. Bratton, S. C. Frasch, M. L. Warner, and P. M. Henson, The role of phosphatidylserine in recognition of apoptotic cells by phagocytes. *Cell Death Differ* **5** (7): 551–62 (1998).
35. Vermes, I., C. Haanen, and C. Reutelingsperger, Flow cytometry of apoptotic cell death. *J Immunol Methods* **243** (1–2): 167–90 (2000).
36. Ashkenazi, A., and V. M. Dixit, Death receptors: signaling and modulation. *Science* **281** (5381): 1305–8 (1998).
37. Long, J. S., and K. M. Ryan, New frontiers in promoting tumour cell death: targeting apoptosis, necroptosis and autophagy. *Oncogene* **31** (49): 5045–5060 (2012).
38. Degterev, A., M. Boyce, and J. Yuan, A decade of caspases. *Oncogene* **22** (53): 8543–67 (2003).
39. Korsmeyer, S. J., M. C. Wei, M. Saito, S. Weiler, K. J. Oh, and P. H. Schlesinger, Pro-apoptotic cascade activates BID, which oligomerizes BAK or BAX into pores that result in the release of cytochrome c. *Cell Death Differ* **7** (12): 1166–73 (2000).
40. Saelens, X., N. Festjens, L. Vande Walle, M. van Gurp, G. van Loo, and P. Vandenabeele, Toxic proteins released from mitochondria in cell death. *Oncogene* **23** (16): 2861–74 (2004).
41. Cain, K., S. B. Bratton, C. Langlais, G. Walker, D. G. Brown, X. M. Sun, and G. M. Cohen, Apaf-1 oligomerizes into biologically active approximately 700-kDa

and inactive approximately 1.4-MDa apoptosome complexes. *J Biol Chem* **275** (9): 6067–70 (2000).
42. Vandenabeele, P., L. Galluzzi, T. Vanden Berghe, and G. Kroemer, Molecular mechanisms of necroptosis: an ordered cellular explosion. *Nat Rev Mol Cell Biol* **11** (10): 700–714 (2010).
43. Hockenbery, D., G. Nuñez, C. Milliman, R. D. Schreiber, and S. J. Korsmeyer, Bcl-2 is an inner mitochondrial membrane protein that blocks programmed cell death. *Nature* **348** (6299): 334–6 (1990).
44. Fulda, S., E. Meyer, and K.-M. Debatin, Inhibition of TRAIL-induced apoptosis by Bcl-2 overexpression. *Oncogene* **21** (15): 2283–94 (2002).
45. Frenzel, A., F. Grespi, W. Chmelewskij, and A. Villunger, Bcl2 family proteins in carcinogenesis and the treatment of cancer. *Apoptosis* **14** (4): 584–596 (2009).
46. Harris, C. C., p53 tumor suppressor gene: from the basic research laboratory to the clinic--an abridged historical perspective. *Carcinogenesis* **17** (6): 1187–98 (1996).
47. Fecker, L. F., C. C. Geilen, G. Tchernev, U. Trefzer, C. Assaf, B. M. Kurbanov, C. Schwarz, P. T. Daniel, and J. Eberle, Loss of proapoptotic Bcl-2-related multidomain proteins in primary melanomas is associated with poor prognosis. *J Invest Dermatol* **126** (6): 1366–71 (2006).
48. Ghavami, S., M. Hashemi, S. R. Ande, B. Yeganeh, W. Xiao, M. Eshraghi, C. J. Bus, K. Kadkhoda, E. Wiechec, A. J. Halayko, and M. Los, Apoptosis and cancer: mutations within caspase genes. *J Med Genet* **46** (8): 497–510 (2009).
49. Hueber, A. O., M. Zörnig, D. Lyon, T. Suda, S. Nagata, and G. I. Evan, Requirement for the CD95 receptor-ligand pathway in c-Myc-induced apoptosis. *Science* **278** (5341): 1305–9 (1997).
50. Cragg, M. S., C. Harris, A. Strasser, and C. L. Scott, Unleashing the power of inhibitors of oncogenic kinases through BH3 mimetics. *Nat Rev Cancer* **9** (5): 321–6 (2009).
51. Merino, D., S. W. Lok, J. E. Visvader, and G. J. Lindeman, Targeting BCL-2 to enhance vulnerability to therapy in estrogen receptor-positive breast cancer. *Oncogene* **35** (15): 1877–1887 (2016).
52. Kennecke, H., R. Yerushalmi, R. Woods, M. C. U. Cheang, D. Voduc, C. H. Speers, T. O. Nielsen, and K. Gelmon, Metastatic behavior of breast cancer subtypes. *J Clin Oncol* **28** (20): 3271–7 (2010).
53. Talmadge, J. E., and I. J. Fidler, AACR centennial series: the biology of cancer metastasis: historical perspective. *Cancer Res* **70** (14): 5649–69 (2010).
54. Chambers, A. F., A. C. Groom, and I. C. MacDonald, Dissemination and growth of cancer cells in metastatic sites. *Nat Rev Cancer* **2** (8): 563–72 (2002).
55. Valastyan, S., and R. A. Weinberg, Tumor Metastasis: Molecular Insights and Evolving Paradigms. *Cell* **147** (2): 275–292 (2011).
56. Bissell, M. J., and W. C. Hines, Why don't we get more cancer? A proposed role of the microenvironment in restraining cancer progression. *Nat Med* **17** (3): 320–9 (2011).
57. Joyce, J. A., and J. W. Pollard, Microenvironmental regulation of metastasis. *Nat Rev Cancer* **9** (4): 239–52 (2009).
58. Brooks, S. A., H. J. Lomax-Browne, T. M. Carter, C. E. Kinch, and D. M. S. Hall, Molecular interactions in cancer cell metastasis. *Acta Histochem* **112** (1): 3–25

(2010).
59. Yoshida, S., M. Ono, T. Shono, H. Izumi, T. Ishibashi, H. Suzuki, and M. Kuwano, Involvement of interleukin-8, vascular endothelial growth factor, and basic fibroblast growth factor in tumor necrosis factor alpha-dependent angiogenesis. *Mol Cell Biol* **17** (7): 4015–23 (1997).
60. Rundhaug, J. E., Matrix metalloproteinases and angiogenesis. *J Cell Mol Med* **9** (2): 267–85 (2005).
61. Duffy, M. J., The urokinase plasminogen activator system: role in malignancy. *Curr Pharm Des* **10** (1): 39–49 (2004).
62. Bachelder, R. E., M. A. Wendt, and A. M. Mercurio, Vascular endothelial growth factor promotes breast carcinoma invasion in an autocrine manner by regulating the chemokine receptor CXCR4. *Cancer Res* **62** (24): 7203–6 (2002).
63. Price, D. J., T. Miralem, S. Jiang, R. Steinberg, and H. Avraham, Role of vascular endothelial growth factor in the stimulation of cellular invasion and signaling of breast cancer cells. *Cell Growth Differ* **12** (3): 129–35 (2001).
64. Campbell, I. D., and M. J. Humphries, Integrin Structure, Activation, and Interactions. *Cold Spring Harb Perspect Biol* **3** (3): a004994–a004994 (2011).
65. Angst, B. D., C. Marcozzi, and A. I. Magee, The cadherin superfamily: diversity in form and function. *J Cell Sci* **114** (Pt 4): 629–41 (2001).
66. Frisch, S. M., and H. Francis, Disruption of epithelial cell-matrix interactions induces apoptosis. *J Cell Biol* **124** (4): 619–26 (1994).
67. Onder, T. T., P. B. Gupta, S. a Mani, J. Yang, E. S. Lander, and R. a Weinberg, Loss of E-cadherin promotes metastasis via multiple downstream transcriptional pathways. *Cancer Res* **68** (10): 3645–54 (2008).
68. Nieman, M. T., R. S. Prudoff, K. R. Johnson, and M. J. Wheelock, N-cadherin promotes motility in human breast cancer cells regardless of their E-cadherin expression. *J Cell Biol* **147** (3): 631–44 (1999).
69. Nagi, C., M. Guttman, S. Jaffer, R. Qiao, R. Keren, A. Triana, M. Li, J. Godbold, I. J. Bleiweiss, and R. B. Hazan, N-cadherin expression in breast cancer: correlation with an aggressive histologic variant--invasive micropapillary carcinoma. *Breast Cancer Res Treat* **94** (3): 225–35 (2005).
70. Strathdee, G., Epigenetic versus genetic alterations in the inactivation of E-cadherin. *Semin Cancer Biol* **12** (5): 373–9 (2002).
71. David, J. M., and A. K. Rajasekaran, Dishonorable Discharge: The Oncogenic Roles of Cleaved E-Cadherin Fragments. *Cancer Res* **72** (12): 2917–2923 (2012).
72. Graff, J. R., E. Gabrielson, H. Fujii, S. B. Baylin, and J. G. Herman, Methylation patterns of the E-cadherin 5' CpG island are unstable and reflect the dynamic, heterogeneous loss of E-cadherin expression during metastatic progression. *J Biol Chem* **275** (4): 2727–32 (2000).
73. Corn, P. G., B. D. Smith, E. S. Ruckdeschel, D. Douglas, S. B. Baylin, and J. G. Herman, E-Cadherin Expression Is Silenced by 5 ′ CpG Island Methylation in Acute Leukemia E-Cadherin Expression Is Silenced by 5 CpG Island Methylation in. **6** (November): 4243–4248 (2000).
74. Peinado, H., E. Ballestar, M. Esteller, and A. Cano, Snail Mediates E-Cadherin Repression by the Recruitment of the Sin3A/Histone Deacetylase 1 (HDAC1)/HDAC2 Complex. *Mol Cell Biol* **24** (1): 306–319 (2003).

75. Aghdassi, a., M. Sendler, a. Guenther, J. Mayerle, C.-O. Behn, C.-D. Heidecke, H. Friess, M. Buchler, M. Evert, M. M. Lerch, and F. U. Weiss, Recruitment of histone deacetylases HDAC1 and HDAC2 by the transcriptional repressor ZEB1 downregulates E-cadherin expression in pancreatic cancer. *Gut* **61** (3): 439–448 (2012).
76. Garg, M., Epithelial-mesenchymal transition - activating transcription factors - multifunctional regulators in cancer. *World J Stem Cells* **5** (4): 188–95 (2013).
77. Gravdal, K., O. J. Halvorsen, S. a Haukaas, and L. a Akslen, A switch from E-cadherin to N-cadherin expression indicates epithelial to mesenchymal transition and is of strong and independent importance for the progress of prostate cancer. *Clin Cancer Res* **13** (23): 7003–11 (2007).
78. Duffy, M. J., The role of proteolytic enzymes in cancer invasion and metastasis. *Clin Exp Metastasis* **10** (3): 145–155 (1992).
79. Tester, A. M., N. Ruangpanit, R. L. Anderson, and E. W. Thompson, MMP-9 secretion and MMP-2 activation distinguish invasive and metastatic sublines of a mouse mammary carcinoma system showing epithelial-mesenchymal transition traits. *Clin Exp Metastasis* **18** (7): 553–60 (2000).
80. Balduyck, M., F. Zerimech, V. Gouyer, R. Lemaire, B. Hemon, G. Grard, C. Thiebaut, V. Lemaire, E. Dacquembronne, T. Duhem, A. Lebrun, M. J. Dejonghe, and G. Huet, Specific expression of matrix metalloproteinases 1, 3, 9 and 13 associated with invasiveness of breast cancer cells in vitro. *Clin Exp Metastasis* **18** (2): 171–8 (2000).
81. Radisky, E. S., and D. C. Radisky, Matrix metalloproteinase-induced epithelial-mesenchymal transition in breast cancer. *J Mammary Gland Biol Neoplasia* **15** (2): 201–12 (2010).
82. Duffy, M. J., T. M. Maguire, A. Hill, E. McDermott, and N. O'Higgins, Metalloproteinases: role in breast carcinogenesis, invasion and metastasis. *Breast Cancer Res* **2** (4): 252 (2000).
83. Nagase, H., R. Visse, and G. Murphy, Structure and function of matrix metalloproteinases and TIMPs. *Cardiovasc Res* **69** (3): 562–73 (2006).
84. Overall, C. M., and O. Kleifeld, Towards third generation matrix metalloproteinase inhibitors for cancer therapy. *Br J Cancer* **94** (7): 941–6 (2006).
85. Vincenti, M. P., and C. E. Brinckerhoff, Transcriptional regulation of collagenase (MMP-1, MMP-13) genes in arthritis: integration of complex signaling pathways for the recruitment of gene-specific transcription factors. *Arthritis Res* **4** (3): 157–164 (2002).
86. Boire, A., L. Covic, A. Agarwal, S. Jacques, S. Sherifi, and A. Kuliopulos, PAR1 Is a Matrix Metalloprotease-1 Receptor that Promotes Invasion and Tumorigenesis of Breast Cancer Cells. *Cell* **120** (3): 303–313 (2005).
87. Liu, H., Y. Kato, S. A. Erzinger, G. M. Kiriakova, Y. Qian, D. Palmieri, P. S. Steeg, and J. E. Price, The role of MMP-1 in breast cancer growth and metastasis to the brain in a xenograft model. *BMC Cancer* **12** (1): 583 (2012).
88. Kubiatowski, T., T. Jang, M. B. Lachyankar, R. Salmonsen, R. R. Nabi, P. J. Quesenberry, N. S. Litofsky, A. H. Ross, and L. D. Recht, Association of increased phosphatidylinositol 3-kinase signaling with increased invasiveness and gelatinase activity in malignant gliomas. *J Neurosurg* **95** (3): 480–8 (2001).

89. Shukla, S., G. T. Maclennan, D. J. Hartman, P. Fu, M. I. Resnick, and S. Gupta, Activation of PI3K-Akt signaling pathway promotes prostate cancer cell invasion. *Int J cancer* **121** (7): 1424–32 (2007).
90. Mendes, O., H.-T. Kim, and G. Stoica, Expression of MMP2, MMP9 and MMP3 in breast cancer brain metastasis in a rat model. *Clin Exp Metastasis* **22** (3): 237–46 (2005).
91. Zhang, B., X. Cao, Y. Liu, W. Cao, F. Zhang, S. Zhang, H. Li, L. Ning, L. Fu, Y. Niu, R. Niu, B. Sun, and X. Hao, Tumor-derived matrix metalloproteinase-13 (MMP-13) correlates with poor prognosis of invasive breast cancer. *BMC Cancer* **8** (1): 83 (2008).
92. Flores-Pliego, A., A. Espejel-Nuñez, M. Castillo-Castrejon, N. Meraz-Cruz, J. Beltran-Montoya, V. Zaga-Clavellina, S. Nava-Salazar, M. Sanchez-Martinez, F. Vadillo-Ortega, and G. Estrada-Gutierrez, Matrix Metalloproteinase-3 (MMP-3) Is an Endogenous Activator of the MMP-9 Secreted by Placental Leukocytes: Implication in Human Labor. *PLoS One* **10** (12): e0145366 (2015).
93. Lochter, A., A. Srebrow, C. J. Sympson, N. Terracio, Z. Werb, and M. J. Bissell, Misregulation of Stromelysin-1 Expression in Mouse Mammary Tumor Cells Accompanies Acquisition of Stromelysin-1-dependent Invasive Properties. *J Biol Chem* **272** (8): 5007–5015 (1997).
94. Radisky, D. C., D. D. Levy, L. E. Littlepage, H. Liu, C. M. Nelson, J. E. Fata, D. Leake, E. L. Godden, D. G. Albertson, M. Angela Nieto, Z. Werb, and M. J. Bissell, Rac1b and reactive oxygen species mediate MMP-3-induced EMT and genomic instability. *Nature* **436** (7047): 123–127 (2005).
95. Kalluri, R., and R. A. Weinberg, The basics of epithelial-mesenchymal transition. *J Clin Invest* **119** (6): 1420–8 (2009).
96. Thiery, J. P., H. Acloque, R. Y. J. Huang, and M. A. Nieto, Epithelial-mesenchymal transitions in development and disease. *Cell* **139** (5): 871–90 (2009).
97. Medici, D., E. D. Hay, and B. R. Olsen, Snail and Slug Promote Epithelial-Mesenchymal Transition through -Catenin-T-Cell Factor-4-dependent Expression of Transforming Growth Factor- 3. *Mol Biol Cell* **19** (11): 4875–4887 (2008).
98. Barrallo-Gimeno, A., and M. A. Nieto, The Snail genes as inducers of cell movement and survival: implications in development and cancer. *Development* **132** (14): 3151–61 (2005).
99. Mani, S. a, W. Guo, M.-J. Liao, E. N. Eaton, A. Ayyanan, A. Y. Zhou, M. Brooks, F. Reinhard, C. C. Zhang, M. Shipitsin, L. L. Campbell, K. Polyak, C. Brisken, J. Yang, and R. a Weinberg, The epithelial-mesenchymal transition generates cells with properties of stem cells. *Cell* **133** (4): 704–15 (2008).
100. Fang, X., Y. Cai, J. Liu, Z. Wang, Q. Wu, Z. Zhang, C. J. Yang, L. Yuan, and G. Ouyang, Twist2 contributes to breast cancer progression by promoting an epithelial-mesenchymal transition and cancer stem-like cell self-renewal. *Oncogene* **30** (47): 4707–20 (2011).
101. Aktas, B., M. Tewes, T. Fehm, S. Hauch, R. Kimmig, and S. Kasimir-Bauer, Stem cell and epithelial-mesenchymal transition markers are frequently overexpressed in circulating tumor cells of metastatic breast cancer patients. *Breast Cancer Res* **11** (4): R46 (2009).
102. Kallergi, G., M. A. Papadaki, E. Politaki, D. Mavroudis, V. Georgoulias, and S.

Agelaki, Epithelial to mesenchymal transition markers expressed in circulating tumour cells of early and metastatic breast cancer patients. *Breast Cancer Res* **13** (3): R59 (2011).
103. Kurrey, N. K., S. P. Jalgaonkar, A. V Joglekar, A. D. Ghanate, P. D. Chaskar, R. Y. Doiphode, and S. a Bapat, Snail and slug mediate radioresistance and chemoresistance by antagonizing p53-mediated apoptosis and acquiring a stem-like phenotype in ovarian cancer cells. *Stem Cells* **27** (9): 2059–68 (2009).
104. Beck, B., and C. Blanpain, Unravelling cancer stem cell potential. *Nat Rev Cancer* **13** (10): 727–738 (2013).
105. Al-Hajj, M., M. S. Wicha, A. Benito-Hernandez, S. J. Morrison, and M. F. Clarke, Prospective identification of tumorigenic breast cancer cells. *Proc Natl Acad Sci U S A* **100** (7): 3983–8 (2003).
106. Ginestier, C., M. H. Hur, E. Charafe-Jauffret, F. Monville, J. Dutcher, M. Brown, J. Jacquemier, P. Viens, C. G. Kleer, S. Liu, A. Schott, D. Hayes, D. Birnbaum, M. S. Wicha, and G. Dontu, ALDH1 is a marker of normal and malignant human mammary stem cells and a predictor of poor clinical outcome. *Cell Stem Cell* **1** (5): 555–67 (2007).
107. Marcato, P., C. A. Dean, D. Pan, R. Araslanova, M. Gillis, M. Joshi, L. Helyer, L. Pan, A. Leidal, S. Gujar, C. A. Giacomantonio, and P. W. K. Lee, Aldehyde Dehydrogenase Activity of Breast Cancer Stem Cells Is Primarily Due To Isoform ALDH1A3 and Its Expression Is Predictive of Metastasis. *Stem Cells* **29** (1): 32–45 (2011).
108. Liu, S., G. Dontu, I. D. Mantle, S. Patel, N. Ahn, K. W. Jackson, P. Suri, and M. S. Wicha, Hedgehog signaling and Bmi-1 regulate self-renewal of normal and malignant human mammary stem cells. *Cancer Res* **66** (12): 6063–71 (2006).
109. Chaffer, C. L., N. D. Marjanovic, T. Lee, G. Bell, C. G. Kleer, F. Reinhardt, A. C. D'Alessio, R. A. Young, and R. A. Weinberg, Poised chromatin at the ZEB1 promoter enables breast cancer cell plasticity and enhances tumorigenicity. *Cell* **154** (1): 61–74 (2013).
110. Hwang, W.-L., M.-H. Yang, M.-L. Tsai, H.-Y. Lan, S.-H. Su, S.-C. Chang, H.-W. Teng, S.-H. Yang, Y.-T. Lan, S.-H. Chiou, and H.-W. Wang, SNAIL regulates interleukin-8 expression, stem cell-like activity, and tumorigenicity of human colorectal carcinoma cells. *Gastroenterology* **141** (1): 279–91, 291–5 (2011).
111. Heldin, C.-H., M. Landström, and A. Moustakas, Mechanism of TGF-beta signaling to growth arrest, apoptosis, and epithelial-mesenchymal transition. *Curr Opin Cell Biol* **21** (2): 166–76 (2009).
112. Nawshad, A., D. Lagamba, A. Polad, and E. D. Hay, Transforming growth factor-beta signaling during epithelial-mesenchymal transformation: implications for embryogenesis and tumor metastasis. *Cells Tissues Organs* **179** (1–2): 11–23 (2005).
113. Meulmeester, E., and P. Ten Dijke, The dynamic roles of TGF-β in cancer. *J Pathol* **223** (2): 205–18 (2011).
114. Munoz, N. M., M. Upton, A. Rojas, M. K. Washington, L. Lin, A. Chytil, E. G. Sozmen, B. B. Madison, A. Pozzi, R. T. Moon, H. L. Moses, and W. M. Grady, Transforming growth factor beta receptor type II inactivation induces the malignant transformation of intestinal neoplasms initiated by Apc mutation.

Cancer Res **66** (20): 9837–9844 (2006).
115. Takaku, K., M. Oshima, H. Miyoshi, M. Matsui, M. F. Seldin, and M. M. Taketo, Intestinal tumorigenesis in compound mutant mice of both Dpc4 (Smad4) and Apc genes. *Cell* **92** (5): 645–56 (1998).
116. Zhu, Y., J. a Richardson, L. F. Parada, and J. M. Graff, Smad3 mutant mice develop metastatic colorectal cancer. *Cell* **94** (6): 703–14 (1998).
117. Diaz-Chavez, J., R. Hernandez-Pando, P. F. Lambert, and P. Gariglio, Down-regulation of transforming growth factor-beta type II receptor (TGF-betaRII) protein and mRNA expression in cervical cancer. *Mol Cancer* **7** (Cc): 3 (2008).
118. Oft, M., K.-H. Heider, and H. Beug, TGFβ signaling is necessary for carcinoma cell invasiveness and metastasis. *Curr Biol* **8** (23): 1243–1252 (1998).
119. Yan, Z., X. Deng, and E. Friedman, Oncogenic Ki-ras confers a more aggressive colon cancer phenotype through modification of transforming growth factor-beta receptor III. *J Biol Chem* **276** (2): 1555–63 (2001).
120. Bierie, B., and H. L. Moses, Tumour microenvironment: TGFbeta: the molecular Jekyll and Hyde of cancer. *Nat Rev Cancer* **6** (7): 506–20 (2006).
121. Sengupta, S., S. Jana, S. Biswas, P. K. Mandal, and A. Bhattacharyya, Cooperative involvement of NFAT and SnoN mediates transforming growth factor-β (TGF-β) induced EMT in metastatic breast cancer (MDA-MB 231) cells. *Clin Exp Metastasis* **30** (8): 1019–31 (2013).
122. Vincent, T., E. P. A. Neve, J. R. Johnson, A. Kukalev, F. Rojo, J. Albanell, K. Pietras, I. Virtanen, L. Philipson, P. L. Leopold, R. G. Crystal, A. G. de Herreros, A. Moustakas, R. F. Pettersson, and J. Fuxe, A SNAIL1-SMAD3/4 transcriptional repressor complex promotes TGF-beta mediated epithelial-mesenchymal transition. *Nat Cell Biol* **11** (8): 943–50 (2009).
123. Shirakihara, T., M. Saitoh, and K. Miyazono, Differential regulation of epithelial and mesenchymal markers by deltaEF1 proteins in epithelial mesenchymal transition induced by TGF-beta. *Mol Biol Cell* **18** (9): 3533–44 (2007).
124. Bakin, a V, a K. Tomlinson, N. a Bhowmick, H. L. Moses, and C. L. Arteaga, Phosphatidylinositol 3-kinase function is required for transforming growth factor beta-mediated epithelial to mesenchymal transition and cell migration. *J Biol Chem* **275** (47): 36803–10 (2000).
125. Julien, S., I. Puig, E. Caretti, J. Bonaventure, L. Nelles, F. van Roy, C. Dargemont, A. G. de Herreros, A. Bellacosa, and L. Larue, Activation of NF-κB by Akt upregulates Snail expression and induces epithelium mesenchyme transition. *Oncogene* **26** (53): 7445–7456 (2007).
126. Chua, H. L., P. Bhat-Nakshatri, S. E. Clare, a Morimiya, S. Badve, and H. Nakshatri, NF-kappaB represses E-cadherin expression and enhances epithelial to mesenchymal transition of mammary epithelial cells: potential involvement of ZEB-1 and ZEB-2. *Oncogene* **26** (5): 711–24 (2007).
127. Kumar, M., D. F. Allison, N. N. Baranova, J. J. Wamsley, A. J. Katz, S. Bekiranov, D. R. Jones, and M. W. Mayo, NF-κB regulates mesenchymal transition for the induction of non-small cell lung cancer initiating cells. *PLoS One* **8** (7): e68597 (2013).
128. Yao, H., E. Ashihara, and T. Maekawa, Targeting the Wnt/β-catenin signaling pathway in human cancers. *Expert Opin Ther Targets* **15** (7): 873–87 (2011).

129. Yook, J. I., X.-Y. Li, I. Ota, C. Hu, H. S. Kim, N. H. Kim, S. Y. Cha, J. K. Ryu, Y. J. Choi, J. Kim, E. R. Fearon, and S. J. Weiss, A Wnt-Axin2-GSK3beta cascade regulates Snail1 activity in breast cancer cells. *Nat Cell Biol* **8** (12): 1398–406 (2006).
130. Stemmer, V., B. de Craene, G. Berx, and J. Behrens, Snail promotes Wnt target gene expression and interacts with beta-catenin. *Oncogene* **27** (37): 5075–80 (2008).
131. Hu, T., and C. Li, Convergence between Wnt-β-catenin and EGFR signaling in cancer. *Mol Cancer* **9** 236 (2010).
132. Zhou, B. P., J. Deng, W. Xia, J. Xu, Y. M. Li, M. Gunduz, and M.-C. Hung, Dual regulation of Snail by GSK-3β-mediated phosphorylation in control of epithelial–mesenchymal transition. *Nat Cell Biol* **6** (10): 931–940 (2004).
133. Taki, M., N. Kamata, K. Yokoyama, R. Fujimoto, S. Tsutsumi, and M. Nagayama, Downregulation of Wnt4 and upregulation of Wnt5a expression by epithelialmesenchymal transition in human squamous carcinoma cells. *Cancer Sci* **94** (7): 593–597 (2003).
134. Nishita, M., M. Enomoto, K. Yamagata, and Y. Minami, Cell/tissue-tropic functions of Wnt5a signaling in normal and cancer cells. *Trends Cell Biol* **20** (6): 346–54 (2010).
135. Espinoza, I., R. Pochampally, F. Xing, K. Watabe, and L. Miele, Notch signaling: targeting cancer stem cells and epithelial-to-mesenchymal transition. *Onco Targets Ther* **6** 1249–59 (2013).
136. Liu, L., X. Chen, Y. Wang, Z. Qu, Q. Lu, J. Zhao, X. Yan, H. Zhang, and Y. Zhou, Notch3 is important for TGF-beta-induced epithelial-mesenchymal transition in non-small cell lung cancer bone metastasis by regulating ZEB-1. *Cancer Gene Ther* **21** (9): 364–372 (2014).
137. Leong, K. G., K. Niessen, I. Kulic, A. Raouf, C. Eaves, I. Pollet, and A. Karsan, Jagged1-mediated Notch activation induces epithelial-to-mesenchymal transition through Slug-induced repression of E-cadherin. *J Exp Med* **204** (12): 2935–2948 (2007).
138. Theunissen, J.-W., and F. J. de Sauvage, Paracrine Hedgehog signaling in cancer. *Cancer Res* **69** (15): 6007–10 (2009).
139. Feldmann, G., S. Dhara, V. Fendrich, D. Bedja, R. Beaty, M. Mullendore, C. Karikari, H. Alvarez, C. Iacobuzio-Donahue, A. Jimeno, K. L. Gabrielson, W. Matsui, and A. Maitra, Blockade of hedgehog signaling inhibits pancreatic cancer invasion and metastases: a new paradigm for combination therapy in solid cancers. *Cancer Res* **67** (5): 2187–96 (2007).
140. Varnat, F., A. Duquet, M. Malerba, M. Zbinden, C. Mas, P. Gervaz, and A. Ruiz i Altaba, Human colon cancer epithelial cells harbour active HEDGEHOG-GLI signalling that is essential for tumour growth, recurrence, metastasis and stem cell survival and expansion. *EMBO Mol Med* **1** (6–7): 338–51 (2009).
141. Kothari, A. N., Z. Mi, M. Zapf, and P. C. Kuo, Novel clinical therapeutics targeting the epithelial to mesenchymal transition. *Clin Transl Med* **3** (1): 35 (2014).
142. van Belzen, N., W. N. Dinjens, M. P. Diesveld, N. A. Groen, A. C. van der Made, Y. Nozawa, R. Vlietstra, J. Trapman, and F. T. Bosman, A novel gene which is up-

regulated during colon epithelial cell differentiation and down-regulated in colorectal neoplasms. *Lab Invest* **77** (1): 85–92 (1997).
143. Bandyopadhyay, S., S. K. Pai, S. C. Gross, S. Hirota, S. Hosobe, K. Miura, K. Saito, T. Commes, S. Hayashi, M. Watabe, and K. Watabe, The Drg-1 gene suppresses tumor metastasis in prostate cancer. *Cancer Res* **63** (8): 1731–6 (2003).
144. Bandyopadhyay, S., S. K. Pai, S. Hirota, S. Hosobe, Y. Takano, K. Saito, D. Piquemal, T. Commes, M. Watabe, S. C. Gross, Y. Wang, S. Ran, and K. Watabe, Role of the putative tumor metastasis suppressor gene Drg-1 in breast cancer progression. *Oncogene* **23** (33): 5675–81 (2004).
145. Kovacevic, Z., and D. R. Richardson, The metastasis suppressor, Ndrg-1: a new ally in the fight against cancer. *Carcinogenesis* **27** (12): 2355–2366 (2006).
146. Han, L.-L., L. Hou, M.-J. Zhou, Z. Ma, D.-L. Lin, L. Wu, and Y. Ge, Aberrant NDRG1 methylation associated with its decreased expression and clinicopathological significance in breast cancer. *J Biomed Sci* **20** 52 (2013).
147. Guan, R. J., H. L. Ford, Y. Fu, Y. Li, L. M. Shaw, and A. B. Pardee, Drg-1 as a differentiation-related, putative metastatic suppressor gene in human colon cancer. *Cancer Res* **60** (3): 749–55 (2000).
148. Li, J., and L. Kretzner, The growth-inhibitory Ndrg1 gene is a Myc negative target in human neuroblastomas and other cell types with overexpressed N- or c-myc. *Mol Cell Biochem* **250** (1–2): 91–105 (2003).
149. Liu, W., F. Xing, M. Iiizumi-Gairani, H. Okuda, M. Watabe, S. K. Pai, P. R. Pandey, S. Hirota, A. Kobayashi, Y.-Y. Mo, K. Fukuda, Y. Li, and K. Watabe, N-myc downstream regulated gene 1 modulates Wnt-β-catenin signalling and pleiotropically suppresses metastasis. *EMBO Mol Med* **4** (2): 93–108 (2012).
150. Chen, Z., D. Zhang, F. Yue, M. Zheng, Z. Kovacevic, and D. R. Richardson, The iron chelators Dp44mT and DFO inhibit TGF-β-induced epithelial-mesenchymal transition via up-regulation of N-Myc downstream-regulated gene 1 (NDRG1). *J Biol Chem* **287** (21): 17016–28 (2012).
151. Zheng, X., J. L. Carstens, J. Kim, M. Scheible, J. Kaye, H. Sugimoto, C.-C. Wu, V. S. LeBleu, and R. Kalluri, Epithelial-to-mesenchymal transition is dispensable for metastasis but induces chemoresistance in pancreatic cancer. *Nature* **527** (7579): 525–530 (2015).
152. Fischer, K. R., A. Durrans, S. Lee, J. Sheng, F. Li, S. T. C. Wong, H. Choi, T. El Rayes, S. Ryu, J. Troeger, R. F. Schwabe, L. T. Vahdat, N. K. Altorki, V. Mittal, and D. Gao, Epithelial-to-mesenchymal transition is not required for lung metastasis but contributes to chemoresistance. *Nature* **527** (7579): 472–476 (2015).
153. Wang, J., Q. Wei, X. Wang, S. Tang, H. Liu, F. Zhang, M. K. Mohammed, J. Huang, D. Guo, M. Lu, F. Liu, J. Liu, C. Ma, X. Hu, R. C. Haydon, T.-C. He, and H. H. Luu, Transition to resistance: An unexpected role of the EMT in cancer chemoresistance. *Genes Dis* **3** (1): 3–6 (2016).
154. Sharma, S., T. K. Kelly, and P. A. Jones, Epigenetics in cancer. *Carcinogenesis* **31** (1): 27–36 (2010).
155. Esteller, M., CpG island hypermethylation and tumor suppressor genes: a booming present, a brighter future. *Oncogene* **21** (35): 5427–40 (2002).
156. Szyf, M., Prospects for the development of epigenetic drugs for CNS conditions. *Nat Rev Drug Discov* **14** (7): 461–474 (2015).

157. Kim, M., and J. Costello, DNA methylation: an epigenetic mark of cellular memory. *Exp Mol Med* **49** (4): e322 (2017).
158. Rhee, I., K. E. Bachman, B. H. Park, K.-W. Jair, R.-W. C. Yen, K. E. Schuebel, H. Cui, A. P. Feinberg, C. Lengauer, K. W. Kinzler, S. B. Baylin, and B. Vogelstein, DNMT1 and DNMT3b cooperate to silence genes in human cancer cells. *Nature* **416** (6880): 552–6 (2002).
159. Bannister, A. J., and T. Kouzarides, Regulation of chromatin by histone modifications. *Cell Res* **21** (3): 381–395 (2011).
160. Nandakumar, V., M. Vaid, T. O. Tollefsbol, and S. K. Katiyar, Aberrant DNA hypermethylation patterns lead to transcriptional silencing of tumor suppressor genes in UVB-exposed skin and UVB-induced skin tumors of mice. *Carcinogenesis* **32** (4): 597–604 (2011).
161. Glozak, M. A., and E. Seto, Histone deacetylases and cancer. *Oncogene* **26** (37): 5420–5432 (2007).
162. Tate, C. R., L. V Rhodes, H. C. Segar, J. L. Driver, F. N. Pounder, M. E. Burow, and B. M. Collins-Burow, Targeting triple-negative breast cancer cells with the histone deacetylase inhibitor panobinostat. *Breast Cancer Res* **14** (3): R79 (2012).
163. Park, S. Y., J. A. Jun, K. J. Jeong, H. J. Heo, J. S. Sohn, H. Y. Lee, C. G. Park, and J. Kang, Histone deacetylases 1, 6 and 8 are critical for invasion in breast cancer. *Oncol Rep* **25** (6): 1677–81 (2011).
164. Graff, J. R., J. G. Herman, R. G. Lapidus, H. Chopra, R. Xu, D. F. Jarrard, W. B. Isaacs, P. M. Pitha, N. E. Davidson, and S. B. Baylin, E-cadherin expression is silenced by DNA hypermethylation in human breast and prostate carcinomas. *Cancer Res* **55** (22): 5195–9 (1995).
165. Wright, J. a, J. K. Richer, and G. J. Goodall, microRNAs and EMT in mammary cells and breast cancer. *J Mammary Gland Biol Neoplasia* **15** (2): 213–23 (2010).
166. Tryndyak, V. P., F. a Beland, and I. P. Pogribny, E-cadherin transcriptional down-regulation by epigenetic and microRNA-200 family alterations is related to mesenchymal and drug-resistant phenotypes in human breast cancer cells. *Int J Cancer* **126** (11): 2575–83 (2010).
167. Vrba, L., T. J. Jensen, J. C. Garbe, R. L. Heimark, A. E. Cress, S. Dickinson, M. R. Stampfer, and B. W. Futscher, Role for DNA methylation in the regulation of miR-200c and miR-141 expression in normal and cancer cells. *PLoS One* **5** (1): e8697 (2010).
168. Burk, U., J. Schubert, U. Wellner, O. Schmalhofer, E. Vincan, S. Spaderna, and T. Brabletz, A reciprocal repression between ZEB1 and members of the miR-200 family promotes EMT and invasion in cancer cells. *EMBO Rep* **9** (6): 582–9 (2008).
169. Gregory, P. A., A. G. Bert, E. L. Paterson, S. C. Barry, A. Tsykin, G. Farshid, M. A. Vadas, Y. Khew-Goodall, and G. J. Goodall, The miR-200 family and miR-205 regulate epithelial to mesenchymal transition by targeting ZEB1 and SIP1. *Nat Cell Biol* **10** (5): 593–601 (2008).
170. Müller, A., and M. Florek, 5-Azacytidine/Azacitidine. *Recent Results Cancer Res* **184** 159–70 (2010).
171. Plimack, E. R., H. M. Kantarjian, and J.-P. Issa, Decitabine and its role in the treatment of hematopoietic malignancies. *Leuk Lymphoma* **48** (8): 1472–1481

(2007).
172. Shaker, S., M. Bernstein, L. F. Momparler, and R. L. Momparler, Preclinical evaluation of antineoplastic activity of inhibitors of DNA methylation (5-aza-2'-deoxycytidine) and histone deacetylation (trichostatin A, depsipeptide) in combination against myeloid leukemic cells. *Leuk Res* **27** (5): 437–44 (2003).
173. Yang, X., D. L. Phillips, a T. Ferguson, W. G. Nelson, J. G. Herman, and N. E. Davidson, Synergistic activation of functional estrogen receptor (ER)-alpha by DNA methyltransferase and histone deacetylase inhibition in human ER-alpha-negative breast cancer cells. *Cancer Res* **61** (19): 7025–7029 (2001).
174. Li, Y., Y.-Y. Yuan, S. M. Meeran, and T. O. Tollefsbol, Synergistic epigenetic reactivation of estrogen receptor-alpha (ERalpha) by combined green tea polyphenol and histone deacetylase inhibitor in ERalpha-negative breast cancer cells. *Mol Cancer* **9** (1): 274 (2010).
175. Duenas-Gonzalez, A., M. Candelaria, C. Perez-Plascencia, E. Perez-Cardenas, E. de la Cruz-Hernandez, and L. A. Herrera, Valproic acid as epigenetic cancer drug: Preclinical, clinical and transcriptional effects on solid tumors. *Cancer Treat Rev* **34** (3): 206–222 (2008).
176. Gilan, O., E. Y. N. Lam, I. Becher, D. Lugo, E. Cannizzaro, G. Joberty, A. Ward, M. Wiese, C. Y. Fong, S. Ftouni, D. Tyler, K. Stanley, L. MacPherson, C.-F. Weng, Y.-C. Chan, M. Ghisi, D. Smil, C. Carpenter, P. Brown, N. Garton, M. E. Blewitt, A. J. Bannister, T. Kouzarides, B. J. P. Huntly, R. W. Johnstone, G. Drewes, S.-J. Dawson, C. H. Arrowsmith, P. Grandi, R. K. Prinjha, and M. A. Dawson, Functional interdependence of BRD4 and DOT1L in MLL leukemia. *Nat Struct Mol Biol* **23** (7): 673–681 (2016).
177. Prebet, T., Z. Sun, M. E. Figueroa, R. Ketterling, A. Melnick, P. L. Greenberg, J. Herman, M. Juckett, M. R. Smith, L. Malick, E. Paietta, M. Czader, M. Litzow, J. Gabrilove, H. P. Erba, S. D. Gore, and M. S. Tallman, Prolonged administration of azacitidine with or without entinostat for myelodysplastic syndrome and acute myeloid leukemia with myelodysplasia-related changes: results of the US Leukemia Intergroup trial E1905. *J Clin Oncol* **32** (12): 1242–8 (2014).
178. Issa, J.-P., G. Garcia-Manero, X. Huang, J. Cortes, F. Ravandi, E. Jabbour, G. Borthakur, M. Brandt, S. Pierce, and H. M. Kantarjian, Results of phase 2 randomized study of low-dose decitabine with or without valproic acid in patients with myelodysplastic syndrome and acute myelogenous leukemia. *Cancer* **121** (4): 556–561 (2015).
179. Kong, D., A. Ahmad, B. Bao, Y. Li, S. Banerjee, and F. H. Sarkar, Histone deacetylase inhibitors induce epithelial-to-mesenchymal transition in prostate cancer cells. *PLoS One* **7** (9): e45045 (2012).
180. Jiang, G.-M., H.-S. Wang, F. Zhang, K.-S. Zhang, Z.-C. Liu, R. Fang, H. Wang, S.-H. Cai, and J. Du, Histone deacetylase inhibitor induction of epithelial-mesenchymal transitions via up-regulation of Snail facilitates cancer progression. *Biochim Biophys Acta* **1833** (3): 663–71 (2013).
181. Lee, E., J. Wang, K. Yumoto, Y. Jung, F. C. Cackowski, A. M. Decker, Y. Li, D. Samid *et al.*, DNMT1 Regulates Epithelial-Mesenchymal Transition and Cancer Stem Cells, Which Promotes Prostate Cancer Metastasis. *Neoplasia* **18** (9): 553–566 (2016).

182. Mehta, R. G., G. Murillo, R. Naithani, and X. Peng, Cancer chemoprevention by natural products: how far have we come? *Pharm Res* **27** (6): 950–61 (2010).
183. Weng, C.-J., and G.-C. Yen, Chemopreventive effects of dietary phytochemicals against cancer invasion and metastasis: phenolic acids, monophenol, polyphenol, and their derivatives. *Cancer Treat Rev* **38** (1): 76–87 (2012).
184. Middleton, E., C. Kandaswami, and T. C. Theoharides, The effects of plant flavonoids on mammalian cells: implications for inflammation, heart disease, and cancer. *Pharmacol Rev* **52** (4): 673–751 (2000).
185. Joshipura, K. J., F. B. Hu, J. E. Manson, M. J. Stampfer, E. B. Rimm, F. E. Speizer, G. Colditz, A. Ascherio, B. Rosner, D. Spiegelman, and W. C. Willett, The effect of fruit and vegetable intake on risk for coronary heart disease. *Ann Intern Med* **134** (12): 1106–14 (2001).
186. Reuter, S., S. Eifes, M. Dicato, B. B. Aggarwal, and M. Diederich, Modulation of anti-apoptotic and survival pathways by curcumin as a strategy to induce apoptosis in cancer cells. *Biochem Pharmacol* **76** (11): 1340–51 (2008).
187. Watson, J. L., R. Hill, P. B. Yaffe, A. Greenshields, M. Walsh, P. W. Lee, C. a Giacomantonio, and D. W. Hoskin, Curcumin causes superoxide anion production and p53-independent apoptosis in human colon cancer cells. *Cancer Lett* **297** (1): 1–8 (2010).
188. Sun, C., Y. Hu, X. Liu, T. Wu, Y. Wang, W. He, and W. Wei, Resveratrol downregulates the constitutional activation of nuclear factor-κB in multiple myeloma cells, leading to suppression of proliferation and invasion, arrest of cell cycle, and induction of apoptosis. *Cancer Genet Cytogenet* **165** (1): 9–19 (2006).
189. Wu, H., X. Liang, Y. Fang, X. Qin, Y. Zhang, and J. Liu, Resveratrol inhibits hypoxia-induced metastasis potential enhancement by restricting hypoxia-induced factor-1α expression in colon carcinoma cells. *Biomed Pharmacother* **62** (9): 613–621 (2008).
190. Tang, F.-Y., Y.-C. Su, N.-C. Chen, H.-S. Hsieh, and K.-S. Chen, Resveratrol inhibits migration and invasion of human breast-cancer cells. *Mol Nutr Food Res* **52** (6): 683–691 (2008).
191. Yang, C. S., X. Wang, G. Lu, and S. C. Picinich, Cancer prevention by tea: animal studies, molecular mechanisms and human relevance. *Nat Rev Cancer* **9** (6): 429–439 (2009).
192. Singh, B. N., H. B. Singh, A. Singh, A. H. Naqvi, and B. R. Singh, Dietary phytochemicals alter epigenetic events and signaling pathways for inhibition of metastasis cascade: Phytoblockers of metastasis cascade. *Cancer Metastasis Rev* **33** (1): 41–85 (2014).
193. Shukla, S., S. M. Meeran, and S. K. Katiyar, Epigenetic regulation by selected dietary phytochemicals in cancer chemoprevention. *Cancer Lett* **355** (1): 9–17 (2014).
194. Deng, Y. I., E. Verron, and R. Rohanizadeh, Molecular Mechanisms of Anti-metastatic Activity of Curcumin. *Anticancer Res* **36** (11): 5639–5647 (2016).
195. Khan, M. A., M. Tania, C. Wei, Z. Mei, S. Fu, J. Cheng, J. Xu, and J. Fu, Thymoquinone inhibits cancer metastasis by downregulating TWIST1 expression to reduce epithelial to mesenchymal transition. *Oncotarget* **6** (23): 19580–91 (2015).

196. Jordan, M. A., and L. Wilson, Microtubules as a target for anticancer drugs. *Nat Rev Cancer* **4** (4): 253–265 (2004).
197. Bezerra, D. P., C. Pessoa, M. O. de Moraes, N. Saker-Neto, E. R. Silveira, and L. V Costa-Lotufo, Overview of the therapeutic potential of piplartine (piperlongumine). *Eur J Pharm Sci* **48** (3): 453–63 (2013).
198. Rao, V. R., P. Muthenna, G. Shankaraiah, C. Akileshwari, K. H. Babu, G. Suresh, K. S. Babu, R. S. Chandra Kumar, K. R. Prasad, P. A. Yadav, J. M. Petrash, G. B. Reddy, and J. M. Rao, Synthesis and biological evaluation of new piplartine analogues as potent aldose reductase inhibitors (ARIs). *Eur J Med Chem* **57** 344–61 (2012).
199. Cícero Bezerra Felipe, F., J. Trajano Sousa Filho, L. E. de Oliveira Souza, J. Alexandre Silveira, D. Esdras de Andrade Uchoa, E. Rocha Silveira, O. Deusdênia Loiola Pessoa, and G. S. de Barros Viana, Piplartine, an amide alkaloid from Piper tuberculatum, presents anxiolytic and antidepressant effects in mice. *Phytomedicine* **14** (9): 605–12 (2007).
200. Son, D. J., S. Y. Kim, S. S. Han, C. W. Kim, S. Kumar, B. S. Park, S. E. Lee, Y. P. Yun, H. Jo, and Y. H. Park, Piperlongumine inhibits atherosclerotic plaque formation and vascular smooth muscle cell proliferation by suppressing PDGF receptor signaling. *Biochem Biophys Res Commun* **427** (2): 349–54 (2012).
201. Raj, L., T. Ide, A. U. Gurkar, M. Foley, M. Schenone, X. Li, N. J. Tolliday, T. R. Golub, S. a Carr, A. F. Shamji, A. M. Stern, A. Mandinova, S. L. Schreiber, and S. W. Lee, Selective killing of cancer cells by a small molecule targeting the stress response to ROS. *Nature* **475** (7355): 231–234 (2011).
202. Jyothi, D., P. Vanathi, P. Mangala Gowri, V. Rama Subba Rao, J. Madhusudana Rao, and A. S. Sreedhar, Diferuloylmethane augments the cytotoxic effects of piplartine isolated from Piper chaba. *Toxicol In Vitro* **23** (6): 1085–91 (2009).
203. Shrivastava, S., P. Kulkarni, D. Thummuri, M. K. Jeengar, V. G. M. Naidu, M. Alvala, G. B. Redddy, and S. Ramakrishna, Piperlongumine, an alkaloid causes inhibition of PI3 K/Akt/mTOR signaling axis to induce caspase-dependent apoptosis in human triple-negative breast cancer cells. *Apoptosis* **19** (7): 1148–64 (2014).
204. Makhov, P., K. Golovine, E. Teper, a Kutikov, R. Mehrazin, a Corcoran, a Tulin, R. G. Uzzo, and V. M. Kolenko, Piperlongumine promotes autophagy via inhibition of Akt/mTOR signalling and mediates cancer cell death. *Br J Cancer* **110** (4): 899–907 (2014).
205. Zheng, J., D. J. Son, S. M. Gu, J. R. Woo, Y. W. Ham, H. P. Lee, W. J. Kim, J. K. Jung, and J. T. Hong, Piperlongumine inhibits lung tumor growth via inhibition of nuclear factor kappa B signaling pathway. *Sci Rep* **6** (1): 26357 (2016).
206. Ginzburg, S., K. V Golovine, P. B. Makhov, R. G. Uzzo, A. Kutikov, and V. M. Kolenko, Piperlongumine inhibits NF-κB activity and attenuates aggressive growth characteristics of prostate cancer cells. *Prostate* **74** (2): 177–86 (2014).
207. de Lima Moreira, F., M. D. Habenschus, T. Barth, L. M. M. Marques, A. C. Pilon, V. da Silva Bolzani, R. Vessecchi, N. P. Lopes, and A. R. M. de Oliveira, Metabolic profile and safety of piperlongumine. *Sci Rep* **6** 33646 (2016).
208. Zhou, X. J., M. Martin, M. Placidi, J. P. Cano, and R. Rahmani, In vivo and in vitro pharmacokinetics and metabolism of vincaalkaloids in rat II. Vinblastine and

Vincristine. *Eur J Drug Metab Pharmacokinet* **15** (4): 323–332 (1990).
209. Graham, H. D., Reaction of Piperine with nitric acid. Adaptation to quantitative assay of the piperine content of pepper. *J Pharm Sci* **54** (2): 319–321 (1965).
210. Srinivasan, K., K. 1. Srinivasan, K., Black pepper and its pungent principle-piperine: a review of diverse physiological effects. Crit Rev Food Sci Nutr 47 (8): 735–48 (2007).Srinivasan, and K. Srinivasan, Black pepper and its pungent principle-piperine: a review of diverse physiological effects. *Crit Rev Food Sci Nutr* **47** (8): 735–48 (2007).
211. Doucette, C. D., G. Rodgers, R. S. Liwski, and D. W. Hoskin, Piperine from Black Pepper Inhibits Activation-Induced Proliferation and Effector Function of T Lymphocytes. *J Cell Biochem* (April): n/a-n/a (2015).
212. Pradeep, C. R., and G. Kuttan, Effect of piperine on the inhibition of nitric oxide (NO) and TNF-alpha production. *Immunopharmacol Immunotoxicol* **25** (3): 337–346 (2003).
213. Kumar, S., V. Singhal, R. Roshan, A. Sharma, G. W. Rembhotkar, and B. Ghosh, Piperine inhibits TNF-alpha induced adhesion of neutrophils to endothelial monolayer through suppression of NF-kappaB and IkappaB kinase activation. *Eur J Pharmacol* **575** (1–3): 177–186 (2007).
214. Taqvi, S. I. H., A. J. Shah, and A. H. Gilani, Blood pressure lowering and vasomodulator effects of piperine. *J Cardiovasc Pharmacol* **52** (5): 452–8 (2008).
215. Fu, M., Z. H. Sun, and H. C. Zuo, Neuroprotective effect of piperine on primarily cultured hippocampal neurons. *Biol Pharm Bull* **33** (4): 598–603 (2010).
216. Selvendiran, K., and D. Sakthisekaran, Chemopreventive effect of piperine on modulating lipid peroxidation and membrane bound enzymes in benzo(a)pyrene induced lung carcinogenesis. *Biomed Pharmacother* **58** (4): 264–267 (2004).
217. Yaffe, P. B., M. R. Power Coombs, C. D. Doucette, M. Walsh, and D. W. Hoskin, Piperine, an alkaloid from black pepper, inhibits growth of human colon cancer cells via G1 arrest and apoptosis triggered by endoplasmic reticulum stress. *Mol Carcinog* **54** (October 2013): 1070–85 (2014).
218. Greenshields, A. L., C. D. Doucette, K. M. Sutton, L. Madera, H. Annan, P. B. Yaffe, A. F. Knickle, Z. Dong, and D. W. Hoskin, Piperine inhibits the growth and motility of triple-negative breast cancer cells. *Cancer Lett* **357** (1): 129–140 (2015).
219. Vijayakumar, R. S., D. Surya, and N. Nalini, Antioxidant efficacy of black pepper (Piper nigrum L.) and piperine in rats with high fat diet induced oxidative stress. *Redox Rep* **9** (2): 105–110 (2004).
220. Han, H.-K., The effects of black pepper on the intestinal absorption and hepatic metabolism of drugs. *Expert Opin Drug Metab Toxicol* **7** (6): 721–9 (2011).
221. Faas, L., R. Venkatasamy, R. C. Hider, A. R. Young, and A. Soumyanath, In vivo evaluation of piperine and synthetic analogues as potential treatments for vitiligo using a sparsely pigmented mouse model. *Br J Dermatol* **158** (5): 941–950 (2008).
222. Krishnakumar, N., S. Manoharan, P. R. Palaniappan, P. Venkatachalam, and M. G. A. Manohar, Chemopreventive efficacy of piperine in 7,12-dimethyl benz [a] anthracene (DMBA)-induced hamster buccal pouch carcinogenesis: an FT-IR study. *Food Chem Toxicol* **47** (11): 2813–2820 (2009).
223. Vellaichamy, L., S. Balakrishnan, K. Panjamurthy, S. Manoharan, and L. M. Alias,

Chemopreventive potential of piperine in 7,12-dimethylbenz[a]anthracene-induced skin carcinogenesis in Swiss albino mice. *Environ Toxicol Pharmacol* **28** (1): 11–8 (2009).
224. Pathak, N., and S. Khandelwal, Cytoprotective and immunomodulating properties of piperine on murine splenocytes: an in vitro study. *Eur J Pharmacol* **576** (1–3): 160–170 (2007).
225. Lu, Y., J. Liu, H. Li, and L. Gu, Piperine Ameliorates Lipopolysaccharide-Induced Acute Lung Injury via Modulating NF-κB Signaling Pathways. *Inflammation* **39** (1): 303–8 (2016).
226. Zhang, J., X. Zhu, H. Li, B. Li, L. Sun, T. Xie, T. Zhu, H. Zhou, and Z. Ye, Piperine inhibits proliferation of human osteosarcoma cells via G2/M phase arrest and metastasis by suppressing MMP-2/-9 expression. *Int Immunopharmacol* **24** (1): 50–8 (2015).
227. Lin, Y., J. Xu, H. Liao, L. Li, and L. Pan, Piperine induces apoptosis of lung cancer A549 cells via p53-dependent mitochondrial signaling pathway. *Tumour Biol* **35** (4): 3305–10 (2014).
228. Ouyang, D., L. Zeng, H. Pan, L. Xu, Y. Wang, K. Liu, and X. He, Piperine inhibits the proliferation of human prostate cancer cells via induction of cell cycle arrest and autophagy. *Food Chem Toxicol* **60** 424–30 (2013).
229. Bezerra, D. P., F. O. de Castro, A. P. Alves, C. Pessoa, M. O. de Moraes, E. R. Silveira, M. W. A. Lima, F. J. Elmiro, N. M. de Alencar, R. O. Mesquita, M. W. A. Lima, and L. V Costa-Lotufo, In vitro and in vivo antitumor effect of 5-FU combined with piplartine and piperine. *J Appl Toxicol* **28** (2): 156–163 (2008).
230. Do, M. T., H. G. Kim, J. H. Choi, T. Khanal, B. H. Park, T. P. Tran, T. C. Jeong, and H. G. Jeong, Antitumor efficacy of piperine in the treatment of human HER2-overexpressing breast cancer cells. *Food Chem* **141** (3): 2591–9 (2013).
231. Hwang, Y. P., H. J. Yun, H. G. Kim, E. H. Han, J. H. Choi, Y. C. Chung, and H. G. Jeong, Suppression of phorbol-12-myristate-13-acetate-induced tumor cell invasion by piperine via the inhibition of PKCalpha/ERK1/2-dependent matrix metalloproteinase-9 expression. *Toxicol Lett* **203** (1): 9–19 (2011).
232. Pradeep, C. R., and G. Kuttan, Piperine is a potent inhibitor of nuclear factor-kappaB (NF-kappaB), c-Fos, CREB, ATF-2 and proinflammatory cytokine gene expression in B16F-10 melanoma cells. *Int Immunopharmacol* **4** (14): 1795–1803 (2004).
233. Lai, L., Q. Fu, Y. Liu, K. Jiang, Q. Guo, Q. Chen, B. Yan, Q. Wang, and J. Shen, Piperine suppresses tumor growth and metastasis in vitro and in vivo in a 4T1 murine breast cancer model. *Acta Pharmacol Sin* **33** (4): 523–30 (2012).
234. Doucette, C. D., A. L. Hilchie, R. Liwski, and D. W. Hoskin, Piperine, a dietary phytochemical, inhibits angiogenesis. *J Nutr Biochem* **24** (1): 231–9 (2013).
235. Kakarala, M., D. E. Brenner, H. Korkaya, C. Cheng, K. Tazi, C. Ginestier, S. Liu, G. Dontu, and M. S. Wicha, Targeting breast stem cells with the cancer preventive compounds curcumin and piperine. *Breast Cancer Res Treat* **122** (3): 777–785 (2010).
236. Bajad, S., M. Coumar, R. Khajuria, O. P. Suri, and K. L. Bedi, Characterization of a new rat urinary metabolite of piperine by LC/NMR/MS studies. *Eur J Pharm Sci* **19** (5): 413–421 (2003).

237. Veerareddy, P. R., and V. Vobalaboina, Pharmacokinetics and tissue distribution of piperine lipid nanospheres. *Pharmazie* **63** (5): 352–355 (2008).
238. Jeong, K., C. S. Kang, Y. Kim, Y.-D. Lee, I. C. Kwon, and S. Kim, Development of highly efficient nanocarrier-mediated delivery approaches for cancer therapy. *Cancer Lett* **374** (1): 31–43 (2016).
239. Wicki, A., D. Witzigmann, V. Balasubramanian, and J. Huwyler, Nanomedicine in cancer therapy: Challenges, opportunities, and clinical applications. *J Control Release* **200** 138–157 (2015).
240. Parveen, S., and S. K. Sahoo, Polymeric nanoparticles for cancer therapy. *J Drug Target* **16** (2): 108–23 (2008).
241. Blanco, E., H. Shen, and M. Ferrari, Principles of nanoparticle design for overcoming biological barriers to drug delivery. *Nat Biotechnol* **33** (9): 941–951 (2015).
242. Astete, C. E., and C. M. Sabliov, Synthesis and characterization of PLGA nanoparticles. *J Biomater Sci Polym Ed* **17** (3): 247–89 (2006).
243. Khalil, N. M., T. C. F. do Nascimento, D. M. Casa, L. F. Dalmolin, A. C. de Mattos, I. Hoss, M. A. Romano, and R. M. Mainardes, Pharmacokinetics of curcumin-loaded PLGA and PLGA-PEG blend nanoparticles after oral administration in rats. *Colloids Surf B Biointerfaces* **101** 353–60 (2013).
244. Hobbs, S. K., W. L. Monsky, F. Yuan, W. G. Roberts, L. Griffith, V. P. Torchilin, and R. K. Jain, Regulation of transport pathways in tumor vessels: role of tumor type and microenvironment. *Proc Natl Acad Sci U S A* **95** (8): 4607–12 (1998).
245. Mehta, D., Signaling Mechanisms Regulating Endothelial Permeability. *Physiol Rev* **86** (1): 279–367 (2006).
246. Cabral, H., Y. Matsumoto, K. Mizuno, Q. Chen, M. Murakami, M. Kimura, Y. Terada, M. R. Kano, K. Miyazono, M. Uesaka, N. Nishiyama, and K. Kataoka, Accumulation of sub-100 nm polymeric micelles in poorly permeable tumours depends on size. *Nat Nanotechnol* **6** (12): 815–823 (2011).
247. Choi, H. S., W. Liu, P. Misra, E. Tanaka, J. P. Zimmer, B. I. Ipe, M. G. Bawendi, and J. V Frangioni, Renal clearance of quantum dots. *Nat Biotechnol* **25** (10): 1165–1170 (2007).
248. Owens, D. E., and N. A. Peppas, Opsonization, biodistribution, and pharmacokinetics of polymeric nanoparticles. *Int J Pharm* **307** (1): 93–102 (2006).
249. Barenholz, Y., Doxil®--the first FDA-approved nano-drug: lessons learned. *J Control Release* **160** (2): 117–34 (2012).
250. Mamot, C., R. Ritschard, A. Wicki, G. Stehle, T. Dieterle, L. Bubendorf, C. Hilker, S. Deuster, R. Herrmann, and C. Rochlitz, Tolerability, safety, pharmacokinetics, and efficacy of doxorubicin-loaded anti-EGFR immunoliposomes in advanced solid tumours: a phase 1 dose-escalation study. *Lancet Oncol* **13** (12): 1234–41 (2012).
251. Xin, Y., Q. Huang, J.-Q. Tang, X.-Y. Hou, P. Zhang, L. Z. Zhang, and G. Jiang, Nanoscale drug delivery for targeted chemotherapy. *Cancer Lett* **379** (1): 24–31 (2016).
252. Socinski, M. A., I. Bondarenko, N. A. Karaseva, A. M. Makhson, I. Vynnychenko, I. Okamoto, J. K. Hon, V. Hirsh, P. Bhar, H. Zhang, J. L. Iglesias, and M. F. Renschler, Weekly nab-paclitaxel in combination with carboplatin versus solvent-

based paclitaxel plus carboplatin as first-line therapy in patients with advanced non-small-cell lung cancer: final results of a phase III trial. *J Clin Oncol* **30** (17): 2055–62 (2012).
253. Goel, A., A. B. Kunnumakkara, and B. B. Aggarwal, Curcumin as 'Curecumin': from kitchen to clinic. *Biochem Pharmacol* **75** (4): 787–809 (2008).
254. Sharma, R. A., W. P. Steward, and A. J. Gescher, Pharmacokinetics and pharmacodynamics of curcumin. *Adv Exp Med Biol* **595** 453–70 (2007).
255. Yallapu, M. M., M. C. Ebeling, S. Khan, V. Sundram, N. Chauhan, B. K. Gupta, S. E. Puumala, M. Jaggi, and S. C. Chauhan, Novel curcumin-loaded magnetic nanoparticles for pancreatic cancer treatment. *Mol Cancer Ther* **12** (8): 1471–80 (2013).
256. Majumdar, D., K. H. Jung, H. Zhang, S. Nannapaneni, X. Wang, A. R. M. Ruhul Amin, Z. Chen, Z. G. Chen, and D. M. Shin, Luteolin nanoparticle in chemoprevention: In vitro and in vivo anticancer activity. *Cancer Prev Res* **7** 65–73 (2014).
257. Zhang, Z., and S.-S. Feng, The drug encapsulation efficiency, in vitro drug release, cellular uptake and cytotoxicity of paclitaxel-loaded poly(lactide)-tocopheryl polyethylene glycol succinate nanoparticles. *Biomaterials* **27** (21): 4025–33 (2006).
258. Yang, Q., J. Liao, X. Deng, J. Liang, C. Long, C. Xie, X. Chen, L. Zhang, J. Sun, J. Peng, B. Chu, G. Guo, F. Luo, and Z. Qian, Anti-Tumor Activity and Safety Evaluation of Fisetin-Loaded Methoxy Poly(ethylene glycol)–Poly(ε-Caprolactone) Nanoparticles. *J Biomed Nanotechnol* **10** (4): 580–591 (2014).
259. Xue, B., Y. Wang, X. Tang, P. Xie, Y. Wang, F. Luo, C. Wu, and Z. Qian, Biodegradable Self-Assembled MPEG-PCL Micelles for Hydrophobic Oridonin Delivery In Vitro. *J Biomed Nanotechnol* **8** (1): 80–89 (2012).
260. Liu, Y., Y. Chang, C. Yang, Z. Sang, T. Yang, W. Ang, W. Ye, Y. Wei, C. Gong, and Y. Luo, Biodegradable nanoassemblies of piperlongumine display enhanced anti-angiogenesis and anti-tumor activities. *Nanoscale* **6** 4325–37 (2014).
261. Fessi, Curt; Devissaguet, Jean-Philippe; Puisieux, Francis; Thies, C., Precipitation of film-forming material and biologically active substance from solvent-non-solvent mixture. United States: Available at: http://www.google.com/patents/US5118528.(1992).
262. Lim Soo, P., J. Liu, C. Allen, H. Lee, and M. Butler, *Polymeric Micelles for Formulation of Anti-Cancer Drugs*. in *Nanotechnology for Cancer Therapy*, CRC Press (2006), pp.317–355.
263. Stockert, J. C., A. Blázquez-Castro, M. Cañete, R. W. Horobin, and Á. Villanueva, MTT assay for cell viability: Intracellular localization of the formazan product is in lipid droplets. *Acta Histochem* **114** (8): 785–796 (2012).
264. Yang, T. T., P. Sinai, and S. R. Kain, An acid phosphatase assay for quantifying the growth of adherent and nonadherent cells. *Anal Biochem* **241** (1): 103–8 (1996).
265. Bustin, S. A., V. Benes, J. A. Garson, J. Hellemans, J. Huggett, M. Kubista, R. Mueller, T. Nolan, M. W. Pfaffl, G. L. Shipley, J. Vandesompele, and C. T. Wittwer, The MIQE guidelines: minimum information for publication of quantitative real-time PCR experiments. *Clin Chem* **55** (4): 611–22 (2009).

266. Emiliani, S., W. Fischle, C. Van Lint, Y. Al-Abed, and E. Verdin, Characterization of a human RPD3 ortholog, HDAC3. *Proc Natl Acad Sci U S A* **95** (6): 2795–800 (1998).
267. Li, H., T. Rauch, Z.-X. Chen, P. E. Szabó, A. D. Riggs, and G. P. Pfeifer, The histone methyltransferase SETDB1 and the DNA methyltransferase DNMT3A interact directly and localize to promoters silenced in cancer cells. *J Biol Chem* **281** (28): 19489–500 (2006).
268. Do, M. T., H. G. Kim, J. H. Choi, T. Khanal, B. H. Park, T. P. Tran, T. C. Jeong, and H. G. Jeong, Antitumor efficacy of piperine in the treatment of human HER2-overexpressing breast cancer cells. *Food Chem* **141** (3): 2591–9 (2013).
269. Manuel Iglesias, J., I. Beloqui, F. Garcia-Garcia, O. Leis, A. Vazquez-Martin, A. Eguiara, S. Cufi, A. Pavon, J. A. Menendez, J. Dopazo, and A. G. Martin, Mammosphere Formation in Breast Carcinoma Cell Lines Depends upon Expression of E-cadherin. *PLoS One* **8** (10): 1–12 (2013).
270. Cioce, M., S. Gherardi, G. Viglietto, S. Strano, G. Blandino, P. Muti, and G. Ciliberto, Mammosphere-forming cells from breast cancer cell lines as a tool for the identification of CSC-like- and early progenitor-targeting drugs. *Cell Cycle* **9** (14): 2878–87 (2010).
271. Wang, Y., and B. P. Zhou, Epithelial-mesenchymal transition in breast cancer progression and metastasis. *Chin J Cancer* **30** (9): 603–11 (2011).
272. Liang, Q., L. Li, J. Zhang, Y. Lei, L. Wang, D.-X. Liu, J. Feng, P. Hou, R. Yao, Y. Zhang, B. Huang, and J. Lu, CDK5 is essential for TGF-β1-induced epithelial-mesenchymal transition and breast cancer progression. *Sci Rep* **3** 2932 (2013).
273. Tam, W. L., and R. A. Weinberg, The epigenetics of epithelial-mesenchymal plasticity in cancer. *Nat Med* **19** (11): 1438–1449 (2013).
274. Sak, K., Chemotherapy and Dietary Phytochemical Agents. *Chemother Res Pract* **2012** 1–11 (2012).
275. Yokoyama, M., P. Opanasopit, T. Okano, K. Kawano, and Y. Maitani, Polymer Design and Incorporation Methods for Polymeric Micelle Carrier System Containing Water-insoluble Anti-cancer Agent Camptothecin. *J Drug Target* **12** (6): 373–384 (2004).
276. Lapinski, M. M., A. Castro-Forero, A. J. Greiner, R. Y. Ofoli, and G. J. Blanchard, Comparison of Liposomes Formed by Sonication and Extrusion: Rotational and Translational Diffusion of an Embedded Chromophore. *Langmuir* **23** (23): 11677–11683 (2007).
277. Pachauri, M., E. D. Gupta, and P. C. Ghosh, Piperine loaded PEG-PLGA nanoparticles: Preparation, characterization and targeted delivery for adjuvant breast cancer chemotherapy. *J Drug Deliv Sci Technol* **29** 269–282 (2015).
278. Gan, M., W. Zhang, S. Wei, and H. Dang, The influence of mPEG-PCL and mPEG-PLGA on encapsulation efficiency and drug-loading of SN-38 NPs. *Artif Cells, Nanomedicine, Biotechnol* **45** (2): 389–397 (2017).
279. Li, R., X. Li, L. Xie, D. Ding, Y. Hu, X. Qian, L. Yu, Y. Ding, X. Jiang, and B. Liu, Preparation and evaluation of PEG-PCL nanoparticles for local tetradrine delivery. *Int J Pharm* **379** (1): 158–66 (2009).
280. Alexis, F., E. Pridgen, L. K. Molnar, and O. C. Farokhzad, Factors affecting the clearance and biodistribution of polymeric nanoparticles. *Mol Pharm* **5** (4): 505–

515 (2008).
281. Gao, C., J. Pan, W. Lu, M. Zhang, L. Zhou, and J. Tian, In-vitro evaluation of paclitaxel-loaded MPEG-PLGA nanoparticles on laryngeal cancer cells. *Anticancer Drugs* **20** (9): 807–14 (2009).
282. Bezerra, D. P., F. O. Castro, A. P. N. N. Alves, C. Pessoa, M. O. Moraes, E. R. Silveira, M. A. S. Lima, F. J. M. Elmiro, and L. V. Costa-Lotufo, In vivo growth-inhibition of Sarcoma 180 by piplartine and piperine, two alkaloid amides from Piper. *Brazilian J Med Biol Res* **39** (6): 801–807 (2006).
283. Hanley, C., J. Layne, A. Punnoose, K. M. Reddy, I. Coombs, A. Coombs, K. Feris, and D. Wingett, Preferential killing of cancer cells and activated human T cells using ZnO nanoparticles. *Nanotechnology* **19** (29): 295103 (2008).
284. Costa, E. C., V. M. Gaspar, J. G. Marques, P. Coutinho, and I. J. Correia, Evaluation of nanoparticle uptake in co-culture cancer models. *PLoS One* **8** (7): e70072 (2013).
285. Yameen, B., W. Il Choi, C. Vilos, A. Swami, J. Shi, and O. C. Farokhzad, Insight into nanoparticle cellular uptake and intracellular targeting. *J Control Release* **190** 485–499 (2014).
286. Friedl, P., and K. Wolf, Tumour-cell invasion and migration: diversity and escape mechanisms. *Nat Rev Cancer* **3** (5): 362–374 (2003).
287. Zhao, X., and J.-L. Guan, Focal adhesion kinase and its signaling pathways in cell migration and angiogenesis. *Adv Drug Deliv Rev* **63** (8): 610–5 (2011).
288. Henderson, V., B. Smith, L. J. Burton, D. Randle, M. Morris, and V. A. Odero-Marah, Snail promotes cell migration through PI3K/AKT-dependent Rac1 activation as well as PI3K/AKT-independent pathways during prostate cancer progression. *Cell Adh Migr* **9** (4): 255–264 (2015).
289. Ribeiro, A. S., A. Albergaria, B. Sousa, A. L. Correia, M. Bracke, R. Seruca, F. C. Schmitt, and J. Paredes, Extracellular cleavage and shedding of P-cadherin: a mechanism underlying the invasive behaviour of breast cancer cells. *Oncogene* **29** (3): 392–402 (2010).
290. Borghaei, R. C., P. L. Rawlings, M. Javadi, and J. Woloshin, NF-κB binds to a polymorphic repressor element in the MMP-3 promoter. *Biochem Biophys Res Commun* **316** (1): 182–188 (2004).
291. Sanchavanakit, N., W. Saengtong, J. Manokawinchoke, and P. Pavasant, TNF-α stimulates MMP-3 production via PGE2 signalling through the NF-kB and p38 MAPK pathway in a murine cementoblast cell line. *Arch Oral Biol* **60** (7): 1066–74 (2015).
292. Xue, M., L. March, P. N. Sambrook, and C. J. Jackson, Differential regulation of matrix metalloproteinase 2 and matrix metalloproteinase 9 by activated protein C: Relevance to inflammation in rheumatoid arthritis. *Arthritis Rheum* **56** (9): 2864–2874 (2007).
293. Xu, J., J. R. Prosperi, N. Choudhury, O. I. Olopade, and K. H. Goss, β-Catenin Is Required for the Tumorigenic Behavior of Triple-Negative Breast Cancer Cells. *PLoS One* **10** (2): e0117097 (2015).
294. Wu, Z.-Q., X.-Y. Li, C. Y. Hu, M. Ford, C. G. Kleer, and S. J. Weiss, Canonical Wnt signaling regulates Slug activity and links epithelial-mesenchymal transition with epigenetic Breast Cancer 1, Early Onset (BRCA1) repression. *Proc Natl Acad*

Sci **109** (41): 16654–16659 (2012).
295. Yook, J. I., X.-Y. Li, I. Ota, E. R. Fearon, and S. J. Weiss, Wnt-dependent Regulation of the E-cadherin Repressor Snail. *J Biol Chem* **280** (12): 11740–11748 (2005).
296. Chao, Y. L., C. R. Shepard, and A. Wells, Breast carcinoma cells re-express E-cadherin during mesenchymal to epithelial reverting transition. *Mol Cancer* **9** 179 (2010).
297. Brown, K. A., M. E. Aakre, A. E. Gorska, J. O. Price, S. E. Eltom, J. A. Pietenpol, and H. L. Moses, Induction by transforming growth factor-β1 of epithelial to mesenchymal transition is a rare event in vitro. *Breast Cancer Res* **6** (3): R215 (2004).
298. Malouf, G. G., J. H. Taube, Y. Lu, T. Roysarkar, S. Panjarian, M. R. Estecio, J. Jelinek, J. Yamazaki, N. J.-M. Raynal, H. Long, T. Tahara, A. Tinnirello, P. Ramachandran, X.-Y. Zhang, S. Liang, S. A. Mani, and J.-P. J. Issa, Architecture of epigenetic reprogramming following Twist1-mediated epithelial-mesenchymal transition. *Genome Biol* **14** (12): R144 (2013).
299. Serrano-Gomez, S. J., M. Maziveyi, and S. K. Alahari, Regulation of epithelial-mesenchymal transition through epigenetic and post-translational modifications. *Mol Cancer* **15** (1): 18 (2016).
300. Yeung, K. T., and J. Yang, Epithelial-mesenchymal transition in tumor metastasis. *Mol Oncol* **11** (1): 28–39 (2017).
301. Lombaerts, M., T. van Wezel, K. Philippo, J. W. F. Dierssen, R. M. E. Zimmerman, J. Oosting, R. van Eijk, P. H. Eilers, B. van de Water, C. J. Cornelisse, and a-M. Cleton-Jansen, E-cadherin transcriptional downregulation by promoter methylation but not mutation is related to epithelial-to-mesenchymal transition in breast cancer cell lines. *Br J Cancer* **94** (5): 661–671 (2006).
302. Fiszer-Kierzkowska, A., N. Vydra, A. Wysocka-Wycisk, Z. Kronekova, M. Jarząb, K. M. Lisowska, and Z. Krawczyk, Liposome-based DNA carriers may induce cellular stress response and change gene expression pattern in transfected cells. *BMC Mol Biol* **12** (1): 27 (2011).
303. Wilson, A. J., D.-S. Byun, S. Nasser, L. B. Murray, K. Ayyanar, D. Arango, M. Figueroa, A. Melnick, G. D. Kao, L. H. Augenlicht, and J. M. Mariadason, HDAC4 Promotes Growth of Colon Cancer Cells via Repression of p21. *Mol Biol Cell* **19** (10): 4062–4075 (2008).
304. De Craene, B., and G. Berx, Regulatory networks defining EMT during cancer initiation and progression. *Nat Rev Cancer* **13** (2): 97–110 (2013).
305. Fang, M. Z., Y. Wang, N. Ai, Z. Hou, Y. Sun, H. Lu, W. Welsh, and C. S. Yang, Tea polyphenol (-)-epigallocatechin-3-gallate inhibits DNA methyltransferase and reactivates methylation-silenced genes in cancer cell lines. *Cancer Res* **63** (22): 7563–70 (2003).
306. Moseley, V. R., J. Morris, R. W. Knackstedt, and M. J. Wargovich, Green tea polyphenol epigallocatechin 3-gallate, contributes to the degradation of DNMT3A and HDAC3 in HCT 116 human colon cancer cells. *Anticancer Res* **33** (12): 5325–33 (2013).
307. Fernandez, A. F., C. Huidobro, and M. F. Fraga, De novo DNA methyltransferases: oncogenes, tumor suppressors, or both? *Trends Genet* **28** (10):

474–479 (2012).
308. Rinaldi, L., A. Avgustinova, M. Martín, D. Datta, G. Solanas, N. Prats, and S. A. Benitah, Loss of Dnmt3a and Dnmt3b does not affect epidermal homeostasis but promotes squamous transformation through PPAR-γ. *Elife* **6** (2017).
309. Bork, S., S. Pfister, H. Witt, P. Horn, B. Korn, A. D. Ho, and W. Wagner, DNA methylation pattern changes upon long-term culture and aging of human mesenchymal stromal cells. *Aging Cell* **9** (1): 54–63 (2010).
310. Pishas, K. I., and S. L. Lessnick, Recent advances in targeted therapy for Ewing sarcoma. *F1000Research* **5** 2077 (2016).
311. Bhardwaj, R. K., H. Glaeser, L. Becquemont, U. Klotz, S. K. Gupta, and M. F. Fromm, Piperine, a major constituent of black pepper, inhibits human P-glycoprotein and CYP3A4. *J Pharmacol Exp Ther* **302** (2): 645–650 (2002).
312. Xiao, Y., M. Shi, Q. Qiu, M. Huang, S. Zeng, Y. Zou, Z. Zhan, L. Liang, X. Yang, and H. Xu, Piperlongumine Suppresses Dendritic Cell Maturation by Reducing Production of Reactive Oxygen Species and Has Therapeutic Potential for Rheumatoid Arthritis. *J Immunol* **196** (12): 4925–4934 (2016).